The University Of Sheffield.

Department Of Mechanical Engineering

A STUDY OF TRIBOLOGICAL PROCESSES DURING THE MILLING OF RICE

Alexander J. Baker

January 2014

Thesis submitted for the Degree of Doctor of Philosophy

Summary

This thesis is concerned with the wear of machinery during the rice milling process. Two machines have been studied in detail (which combined constitute “milling”). Background literature has been studied and further added to such that machine improvements can be made relating to both capacity and component wear life.

The first part of the work undertaken considers material properties of rice grains in their various forms and machine components with which contact is made. Dimension measurements and SEM imagery have highlighted the organic nature of rice grains as an abrasive, and observations of the change in properties from pre to post process made. Mass change, grain profiles, coefficient of friction, grain hardness and compressive strength have all been measured.

Wear observations of husking and polishing components has revealed similarities with known wear mechanisms. Microscopy and profilometry have shown the areas which are susceptible to increased wear rates whilst measurement of scratch angles has illustrated the motion of grains through the polisher.

Small scale testing has been a key part of the research due to the impractically high capacity of full scale machines. Husking tests have established that the shear stress required to achieve a given husked ratio is constant suggesting that a harder rubber with the same coefficient of friction as a softer rubber will husk more efficiently. Fast capture camera footage of husking experiments has shown that grains rotate between the rubber counterfaces before husking which effectively creates a region of high pressure at either end of the grain. It has also revealed that grains maintain their initial contact with the slow roller whilst sliding against the fast roller once husked. Probable mechanisms for this effect have been determined and experiments have been conducted showing that the uneven wear created by the effect could be minimised by axial vibration of the slow roller.

Small scale polishing experiments have been used to reveal the locations of the highest wear (through paint test) which have a pattern consistent with an uneven fill by the grains entering the polishing chamber or a resonance of the screens caused by cage spacing. High wear was noted at inlet thought to be a result of rapid scattering of grains on entry from the feed screw. Pressure sensitive paper has been used to determine contact pressure profiles for various stages and conditions in the polishing chamber and laser vibrometry has been used to observe the effect of loading on machine vibration. Computer simulations have been developed to simulate grain flow and have shown good compatibility with the physical experiments. This leads to the potential to use such methods for future machine design.

Finally, this thesis covers the potential for further work along with how the work is best suited for industrial implementation.

Nomenclature

l	mm	Grain length (longitudinal dimension)
w	mm	Grain width (dorsoventral dimension)
t	mm	Grain thickness (lateral dimension)
H	HV	Hardness
ν		Poisson's Ratio
φ	rad	Angle of internal friction
a	m	Radius of contact area
P	N	Load
E	Pa	Elastic modulus
R'	m	Reduced radius
E^*	Pa	Reduced modulus
Q	KJ/Kg	Specific husking energy
μ		Coefficient of friction
p	N/kg	Specific normal force
ϕ_n	m/s	Peripheral velocity difference
l_d	m	Contact distance
R_{ay}	m	Radius of curvature
b	m	Contact half width
p_m	Pa	Mean contact pressure
τ_m	Pa	Mean shear stress
δ	m	Roller separation
r	m	Polisher blade radius
ω	rad s^{-1}	Angular velocity
U	m/s	Grain velocity
θ	rad	Blade tip angle
V	m/s	Blade velocity
x	%	% fill
ρ	kg/m³	Bulk density

V_b	m^3	Feed volume (between two blades)
N		Number of blade passes per hour
m	tonnes/hr	Feed rate

Contents

1 INTRODUCTION

Rice (Oryza sativa) is the staple food for more than half the world's population [1]. Though normally considered a semi-aquatic, annual grass plant it can grow in a wide range of conditions from flooded land to arid and hilly climates, from 53° north to 40° south and from sea level to over 3000m. Various production methods are adopted to cultivate and process the grain, generally depending on scale and wealth of the producer, but ranging from very primitive to highly mechanised. [2]

Mechanical milling technology was first developed in the UK around 1860 [3], spreading to Burma where the machines became power driven. Since then, the technologies involved in milling rice have developed, particularly in material improvements, with machine design alterations generally made on a trial and improvement basis. Improvement is measured in terms of quality of product and machine capacity, but also in terms of machine wear life, since in processing progressively larger volumes of grain, components are likely to fail more rapidly.

1.1 Aims and Objectives

The aim of this thesis is to develop an understanding of the tribological mechanisms involved in the milling process so that technological advancement can be made without recourse to trial and improvement.

The objectives of the work were as follows:

- Identify the wear patterns present on major machine components in both rubber roll huskers and rice polishers (which together constitute "milling")

- Use of "lab scale" milling machines to analyse wear and processing mechanisms

- Conventional and bespoke tribological testing to identify the behaviour of the current milling machine materials and their resistance to wear in order that a benchmark be set from which to measure alternative materials.

- Using the understanding of the tribological processes to determine what improvements can be made to machine design to improve wear life of components

1.2 Thesis Layout

Chapter 1 gives a brief overview of the thesis and the aims and objectives upon which it is based. An analysis of rice grains as a material is given in Chapter 2 along with details on the milling process, its historical development and an introduction to the machines which are to be studied in detail. Cases relating to the wear of materials by particulates are discussed in Chapter 3 along with various known processes which affect the manner in which a surface can be worn. These include various particle properties such as hardness, shape and size and the effect of each on the solid particle erosion of a surface is discussed.

In Chapter 4, rice grains as an abrasive material are studied and various properties measured. This section includes the study of how the grains composition and nature changes through the milling process, in terms of hardness, density, dimensions and coefficient of friction. This is followed by an analysis of the mill materials in Chapter 5, both in observation of the wear (through microscopy and profilometry) and in relation to the mechanisms by which the grains move.

Chapter 6 discusses findings based on the tribology of rice husking, observed by means of fast capture imaging and coupon testing, and how the various rubber properties relate to the efficiency of rubber roll husking. Wear tests are presented as

a means of determining superior husking rubbers. Chapter 7 advances these theories of husking mechanisms and efficiencies through the use of a laboratory scale husker, which has been used observe true grain motion through the rollers. A theory is presented on the improvement of efficiency through the addition of a complimentary mechanism.

The tribology of rice polishing is discussed in Chapter 8, including a novel method for determining the pressure profile within the polishing chamber, the mechanics of the screen materials along with a computer simulation based method of analysing the performance of a polisher.

Conclusions and references are presented through chapters 9 and 10 respectively.

2 RICE AND RICE MILLING

This chapter covers the key aspects concerning rice grains both as an agricultural product and by the millers who process the grains. An introduction is given to the biological nature of rice grains and the technologies involved in processing it for human consumption.

In 1972 the Food and Agriculture Organisation of the United Nations formulated a "Recommended Model Grading System for Rice in International Trade"[4]. This specification details the classification and grading terms currently in operation, providing a good basis for conformity between different areas of research. This standardisation covers all aspects of the grain and milling process such as size, shape and weight and rice grain form. The terms are laid out in this chapter and are the basis for grain description throughout this study.

2.1 Rice Overview

2.1.1 Grain Makeup

Rice grains are made up of four main parts. The kernel of the grain is botanically known as the caryopsis which consists of both a seed and tightly adherent fruit coat or pericarp [5]. There are two parts to the husk (lemma and palea) which give protection to the grain as it develops. The rachilla attaches the grain to the plant stem. The other parts of the grain include the embryo (or germ) and leaf like structures known as glumes – which are like the lemma and palea but do not extend up the grain (see figure 1).

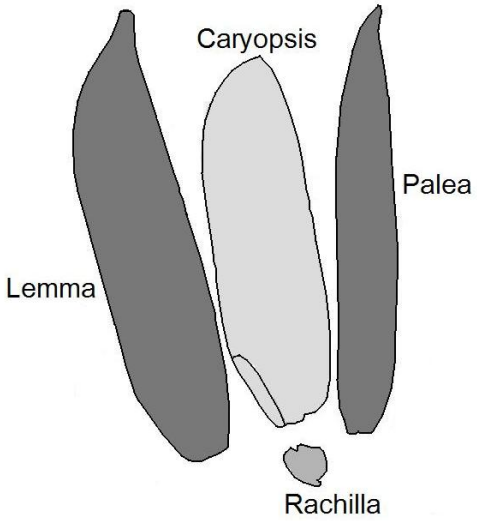

Figure 1 Parts of a Rice Kernel

The kernel is made up of various layers surrounding a starchy endosperm and the embryo as shown in figure 2.

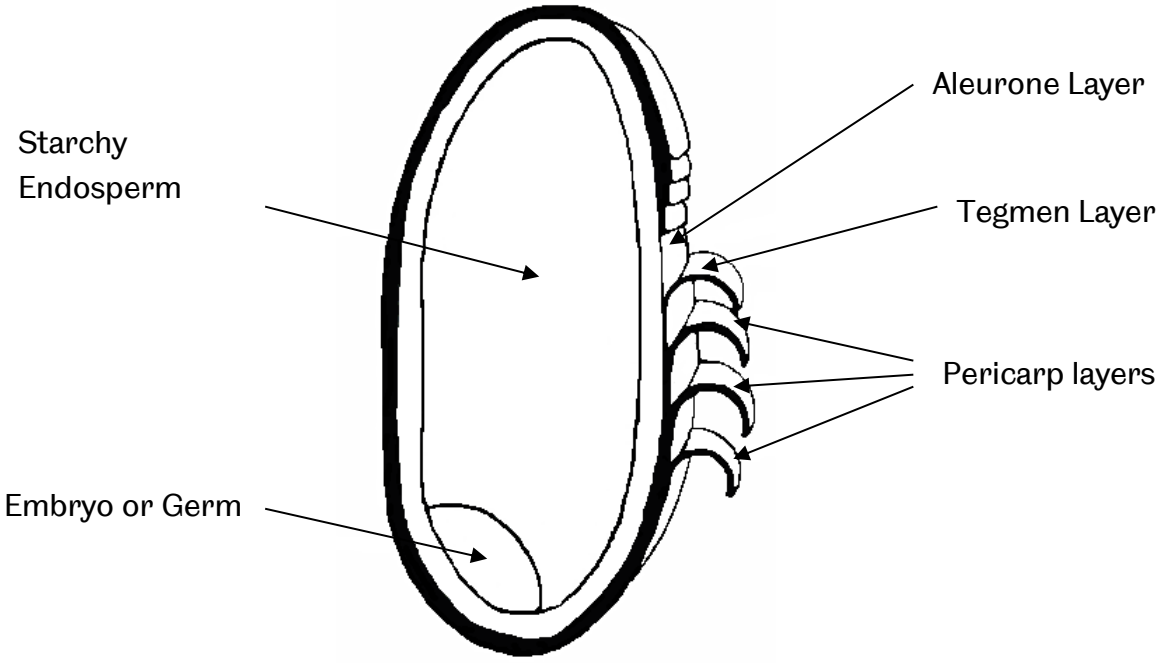

Figure 2 Layers of a Rice Kernel [6]

Bran is the name given to the combination of the aleurone, tegmen and pericarp layers. Commercial bran (consisting bran layers plus the embryo) accounts for around 10-15% of the rough rice and provides a source of protein (12-15%) and lipids (15-20%)[1].

2.1.2 Global Usage

Rice forms the staple diet for over 50 percent of the world's population. The global usage of rice is increasing more rapidly than the population [7], [8] (see Figure 3) which demonstrates the importance of the grain as a foodstuff. It is thought that the increased demand for rice is due in part to the adoption of high-yielding varieties in many parts of Asia and increased plantings of hybrid rice in china [1]. Figure 3 shows the rice usage figures compared with global population and how they have changed over time.

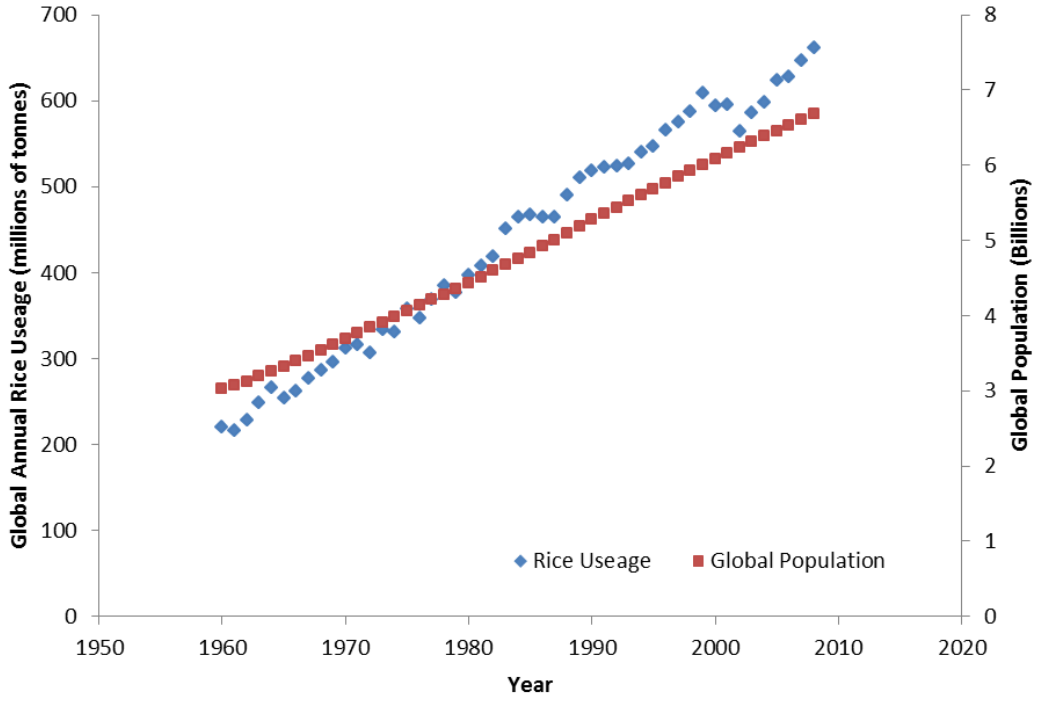

Figure 3 Rice Usage Figures Compared with Global Population

2.1.3 Rice Variety

2.1.3.1 Number of Varieties

The number of different grain varieties is very difficult to define[8]. There could, depending on definition of "variety" be anywhere between zero and 500,000 types of Oryza sativa (Asian cultivated rice)[9]. Cultivated varieties (or "cultivars") add another dimension to the potential number of varieties to be considered and many countries maintain an official list of recognised varieties. The International Rice Information System has classified around 5,000, however there may be greater or

fewer than this since no-one has brought together the lists of every country. Including traditional varieties then the number of varieties could be in the hundreds of thousands. India alone claims to have over 100,000 varieties whilst the International Rice Gene Bank, maintained by the International Rice Research Institute holds over 117,000 types of rice[10]. Counting the number of varieties is very difficult since traditional varieties are named for convenience rather than for legal purposes. This means that there is not one name per variety, and many names are just generic like “black rice” or “glutinous rice”.

2.1.3.2 Grain distinctions

Rice grains are described by indicating the following[4]:

a) The size, shape and weight (class)
b) The degree of milling, parboiling and extra processing (other than milling)
c) Acquired characteristics such as broken, damaged, foreign materials, moisture, immature grains etc.

Grains are classified as either long, medium or short grain. This distinction is made based on the ratio of the length and the width of the grain (as defined in figure 4).

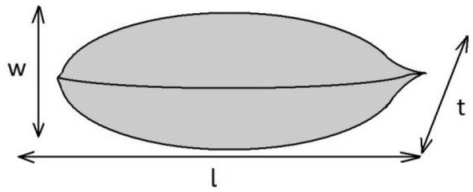

Figure 4 Paddy Grain Dimensions where l = length or longitudinal dimension, w = width or dorsoventral dimension and t = thickness or lateral dimension

Distinctions are also classified by size and weight. The FAO committee’s recommended model describes the grains as below in tables 1, 2 and 3:

Description	Also known as	Whole milled kernel length/width ratio
Long grain	Slender	Over 3.0
Medium grain	Bold	2.0 to 3.0
Short grain	Round	Less than 2.0

Table 1 Grain descriptions based on shape

Description	80 percent or more of whole milled kernel length
Extra-long	7.0mm and above
Long	6.0mm to 6.99mm
Medium	5.0mm to 5.99mm
Short	Less than 5.0mm

Table 2 Grain descriptions based on size

Description	Whole milled 1000 kernels with 14% moisture weight
Extra heavy	Over 25 grams
Heavy	20 to 25 grams
Moderately heavy	Less than 20 grams

Table 3 Grain descriptions based on weight

2.1.4 Grain Variation

Since rice grains are organic in nature, grain properties (including grain size, shape, hardness and strength) vary greatly within the same variety. This variation occurs for a number of reasons including the quality of the soil, the climate of that season and the location of the grain on the plant. This does yield problems when trying to deal with rice grains in laboratory conditions, and requires that results be carefully considered. Grain variation is also apparent between the many varieties meaning that generalisations are difficult to make. Theoretical and analytical models are therefore generally limited to specific varieties and operate within margins of error.

2.1.5 Rice forms

Generally, rice arrives at the mill as paddy, i.e. the kernel wrapped in its inedible protective husk. This is often called unhusked or rough rice, but more commonly "paddy" rice which will be the term used in this thesis (see figure 5).

Figure 5 Paddy Rice

Once the husks have been removed from the grain the grains are referred to as "brown" rice. The name is derived from the colour of the bran layers which generally remain intact during husk removal shown in figure 6.

Figure 6 Brown Rice

"White" rice is the name given to grains from which husks and bran layers have been removed (see figure 7). It is sometimes known as polished or milled rice. The higher the degree of bran removal, the smoother and glossier the appearance of the grains.

Figure 7 White Rice

Often rice undergoes a second stage of polishing to give an even, pearl like lustre. Rice processed in this manner is often referred to as polished, whitened rice (figure 8).

Figure 8 Polished, Whitened Rice

2.2 Milling Process Overview

The processing of rice involves a number of discrete operations the efficiency of each affecting the quality and hence market value of the finished product. The whole process involves cleaning and drying, husking, polishing, whitening, grading and sorting of which husking and polishing constitute “milling”. The other processes can be seen to influence the quality of the product but have not been studied in detail in the course of this project since milling losses and milling machine damage present a much larger issue. An overview of the process is shown in Figure 9.

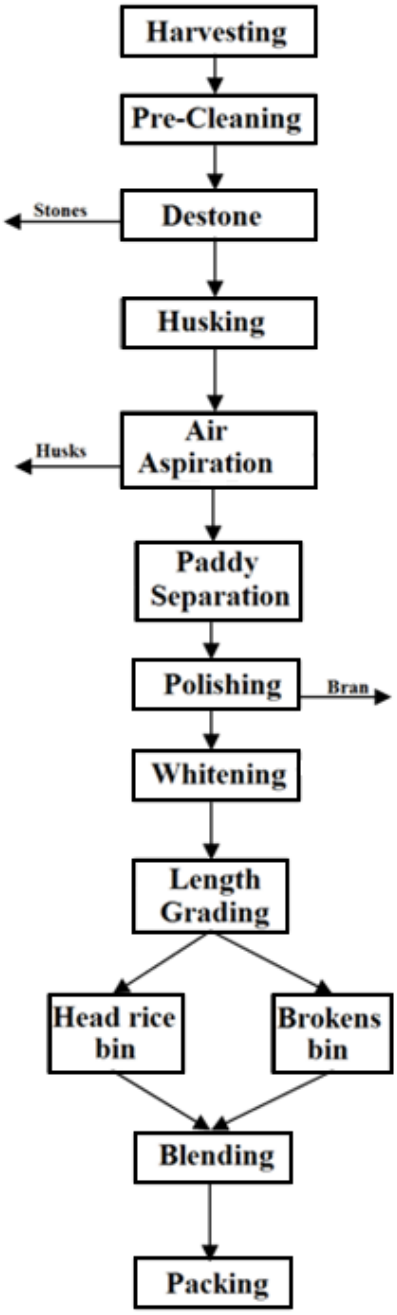

Figure 9 Rice Processing[11]

2.2.1 Paddy cleaning

Paddy rice direct from harvest will include various foreign bodies which must first be removed. A magnetic separator is used for the removal of metal particles such as nails, wire, screws etc. A permanent magnetic core installed within a drum provides continuous self-cleaning of metal contaminants.

Destoners are employed for the removal of high density foreign bodies such as stones and glass. It works by vibrating the bulk material so that different densities

separate into layers allowing unwanted material to be removed. An air recycling system can be used to remove dust from the bulk material.

2.2.2 Paddy drying

Rice processing generally includes some degree of initial paddy drying [12]. When harvested, paddy rice has a moisture content between 24 and 26% (wet basis). Ineffective drying can lead to discolouration, reduced yields and issues with mould and insect activities. The moisture content is reduced to different levels depending on usage, and is carried out by various methods. If paddy is to be used immediately then a moisture content of 18% is attained, later reduced to 14%. For 8-12 month storage grains are generally dried to 13% or less, and for storage exceeding 1 year, to 9%.

Various methods are used for the drying of paddy rice. Sun-drying, used through much of Asia because of its low cost, is labour intensive and control of grain temperature is difficult. In-store drying can be used to dry paddy with moisture content below 18%. Slightly pre-heated air can be used to slowly dry and aerate over a period of days or weeks to desired levels. Heated air drying can be adopted to reduce drying times to around 6-8 hours and increase capacity although this method is capital intensive.

Paddy rice is often subjected to hot water or steam treatment known as parboiling before milling. Parboiled paddy gives increased milling yield and reduces nutrient losses by filling cracks which developed within the grain during maturity [13]. Rice is parboiled by soaking, steaming and drying in a manner which achieves a quick and uniform water absorption [14].

2.2.3 Husking and Polishing (Milling)

In order to process rice into a form which can be consumed, the inedible husk must be removed and to give a higher quality of product, the grains are polished to remove the bran layers from the kernels. This removal of materials from the grain is collectively known as “Milling”.

Traditionally rice husking and polishing would be carried out as a one stage process using a large wooden pestle and mortar. In this instance the polishing of the grain is largely a side effect of the method, with the primary aim being to remove the husk This method inevitably leads to a large percentage of grains breaking which lowers the market value of the product. A two-pass process was adopted with the development of higher capacity milling technology to improve efficiency and reduce the number of broken grains. These two stages are discussed in detail below including the development of the technologies involved and the current milling machine features.

2.2.3.1 Paddy husking

Paddy husking, also known as hulling, defines the removal of the outer protective shell (or husk) of the grains. There are a number of methods which can be adopted to remove the husk from a grain of rice and these are described in detail below.

2.2.3.2 Rice Polishing

Rice polishing is defined as the transformation of brown rice to white rice. In mechanical terms, this equates to the removal of the bran layers and the smoothing and rounding of the grain surface.

2.2.4 Post Processes

2.2.4.1 Enriching

During processing grains lose a good deal of their nutritional value (particularly that found in the bran layer). White rice is often enriched by mixing with an assortment of vitamins and nutrients. This is especially true in developing nations where it is important for the grains to maintain their nutritional value.

2.2.4.2 Storage and Packaging

The storage and handling of grains is important to be undertaken efficiently. Rice grains are often stored for a long time, meaning that storage conditions must suitably meet the requirements to prevent grain loss caused by moisture, adverse weather, rodents, birds, insects and micro-organisms such as fungi. Even during processing, storage must be carefully considered. For instance, if grains are stored unhusked, the husks will offer some protection against insects, however more space will be required to hold the same number of grains. Careful packaging of grains also offers protection and ensures that the product quality remains high until required for usage.

2.3 Rice Husking

2.3.1 The Husking Process

Husking the grain is a process which falls before the majority of procedures. It also represents the beginning of the milling of the grain. There are various methods of husk removal, each with pros and cons. Arguably the most simple method is to peel the grain by hand, removing the lemma and palea from the awn. This would obviously be an impractical method to husk even enough rice for personal use. Therefore the bulk husking of paddy involves either impact of grains or shearing of grains. These two governing mechanisms have been the driving force behind bulk husking technology.

2.3.2 Historical Development

Traditional husking of grains was carried out using a pestle and mortar. Often this would simply be a hollowed log and large stick to beat the grains[15]. The husks would be removed and to some extent the grains would be polished, however this method would produce a lot of broken and cracked grains. It is also very energy intensive and only small quantities of rice can be processed at one time.
Two methods were practised during early mass milling technology development. Namely, rubber roll husking and impeller husking.

2.3.2.1 Rubber Roll Husking

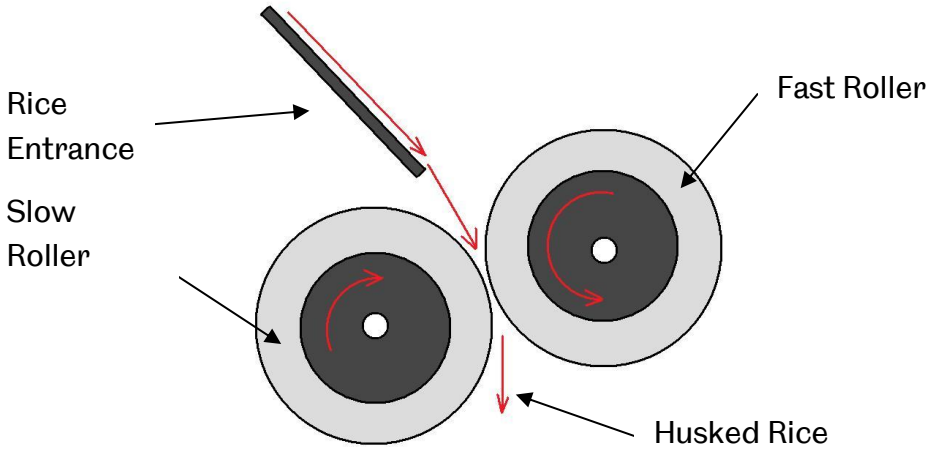

Figure 10 Schematic of Rubber Roll husker

Although some designs vary slightly, for the rubber roll type approach, all use the same fundamental concept (as shown in Figure 10). Rice flows down a chute and is entrained between the two rubber coated rollers. One roller rotates more quickly than the other (typically 950 rpm and 1300 rpm, a ratio of around 1:1.35). The husk is separated into two (or more) parts and the rice falls out freely. Flow rates can be between 3 and 8 tonnes per hour depending on variety of rice. One roller is loaded using a lever arm whilst the other remains stationary. The loading is altered depending on the quality of the product being expelled (increased if husks are being left on, decreased if a large proportion of the rice kernels are breaking during husking). The gap between the two rollers is set so that they do not touch when there is no rice flowing between them. Inevitably this differential slip process leads to frictional heating and the rubber layer on the rollers is subject to high wear rates. The operating parameters (load, gap, roller speeds, and speed differential) of such huskers are largely set experimentally on examining the processed product. The selection of the most appropriate rubber material is frequently chosen on the basis of past experience.

Rubber roll huskers of this type have been in use since the 1920s [3]. Developments since then have been made mostly by trial and improvement, such as wear resistance of the rubber material, optimization of roller speeds and clearances. Modern designs now incorporate automatic adjustment of feed rate and roll clearance, the latter allowing adjustment as the rollers wear.

2.3.2.2 Impeller Husking

In impeller type husking machines the rice is scattered radially and husked by the impact of collision with an external surround. A typical impeller husker is shown schematically in figure 11.

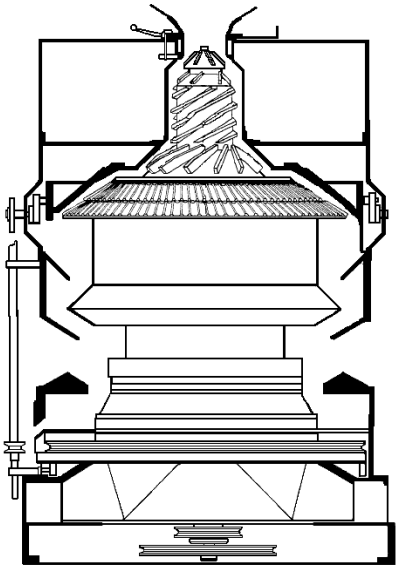

Figure 11 Impeller Husker Schematic[16]

2.3.2.3 Rubber Roll vs Impeller Husking

According to Garibaldi [6], there are a number of advantages to using rubber roller type husking. Firstly, it reduces the risk of breaking grains since pressure is applied more uniformly across grains, and husks are pulled off almost at once. Rubber rollers do not remove the germ and the internal epidermis of the husk which helps to protect the grains against scratches and helps them to keep for longer. Takekura et al. [17] found that using impeller huskers was not suitable if the rice was to be stored since germination rate, whiteness and translucency were found to be poorer than with rubber roll husking and storing for the same length of time. Sieving for recovery of the germ is therefore not required (this is often done for impeller husking). Rollers also reduce the risk of damage to grains caused by unskilled or careless operators since the spring loading in the system provides some degree of automatic control. Finally, for grain varieties which have an awn, extra machining to remove it are not required when using rubber roll husking.

The disadvantage of using rubber rolls for husking is that the rubber sheaths wear rapidly and must be replaced frequently. The rollers also tend to wear unevenly

which can lead to low husking efficiency, or the replacement of just one roller at a time – resulting in more machine down time. Capacity of these huskers is primarily dependant on the width of the rollers which in turn is limited by the necessity of maintaining parallelism. Despite these disadvantages, rubber roll huskers have become the dominant method for large scale husking, primarily due to developments in rubber technology, allowing the rollers to wear more slowly.
Progress tends to be made by trial and error and little is documented on the fundamental mechanisms which govern the behaviour of the rice through the machine. Developments since the early rubber roll huskers have led to improvement of the rubber material, peripheral speed and speed ratio of rollers optimisation, grain feed direction control and improvement of the automatic adjustment for feed rate [3]. In addition to this, focus on three factors has driven development; durability, roller shaft parallelism and automatic adjustment of roller clearance.
Husker durability was improved post World War II by remodelling the husker body into a sturdy metal structure, mounting one roller onto the solid body and one onto a moveable shaft which controls the roller clearance.

2.3.2.4 Other Husking Methods

Various other husking methods have been developed (although none widely adopted).
Under-runner huskers (or "shellers") involve the rotation of a mortar against a stationary abrasive stone (which can be composed of anything from rubber to wood or clay). Often upper and lower disks were coated with emery on their inner surfaces using magnesia cement. A typical under-runner husker is shown in figure 12.

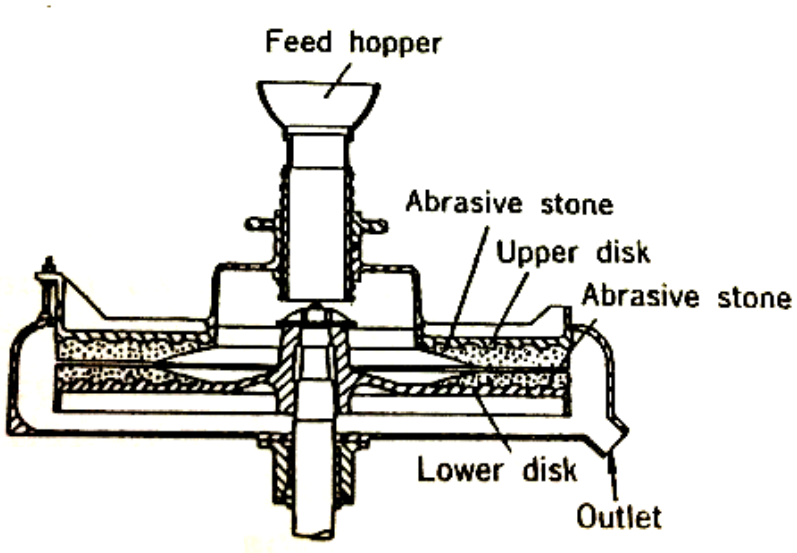

Figure 12 Under-runner Husker[3]

The feed is located above the stationary upper disk and husks and paddy are expelled circumferentially through an outlet. This kind of device however generates a significant percentage of broken grains.

There are a number of variations on the centrifugal husker theme. The Iwata centrifugal paddy husker scatters grains which are then husked on collision with a rubber ring surface (see figure 13).

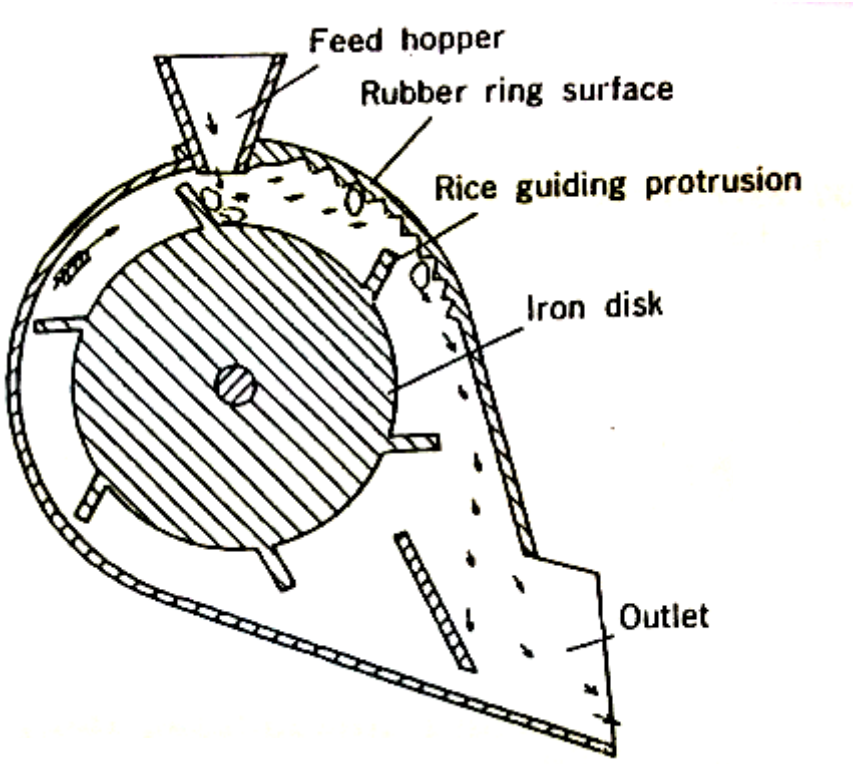

Figure 13 Iwata Centrifugal Paddy Husker[3]

This particular husker was largely abandoned since at the time of its invention husked grains were generally sold on volume rather than weight. Since this husking method resulted in rice with unscratched surfaces if operated correctly, the rice obtained had lower volume than other methods, meaning sales of this husker declined rapidly as other variations became available.

2.3.3 Modern Husking Technology

The modern husking machine (figure 14) incorporates a number of features which improve its husking efficiency and the machine wear life.

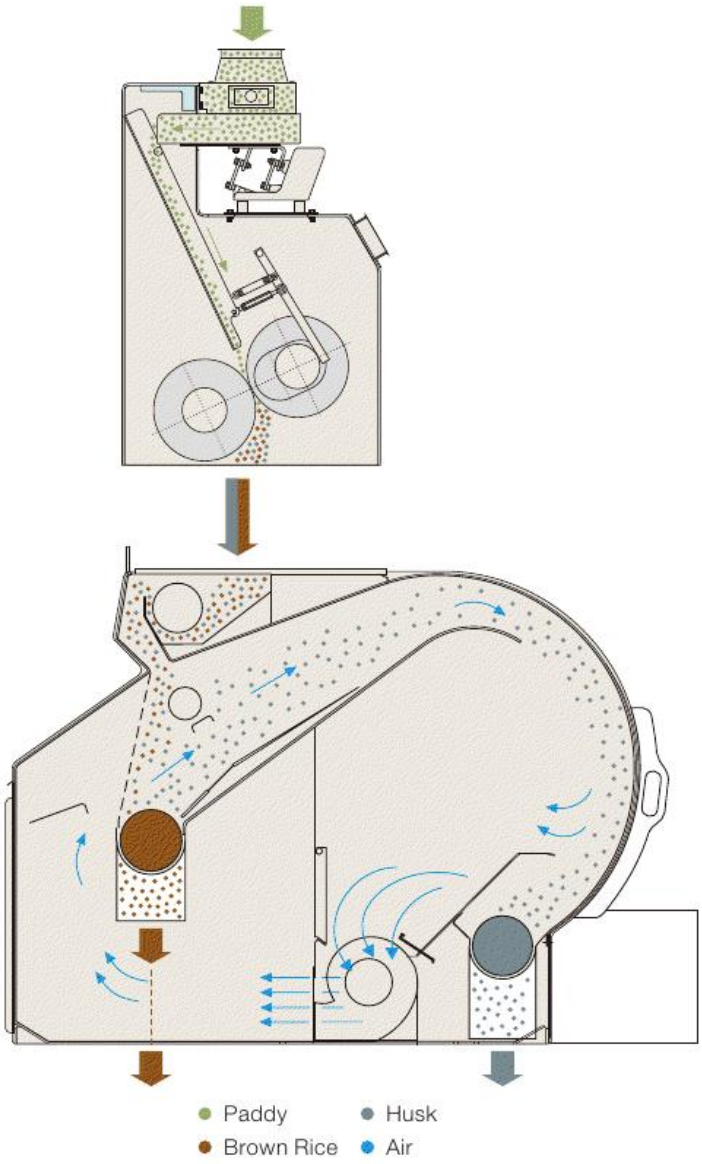

Figure 14 Rice husking technology [18]

The angle of feed can be controlled to ensure that the gains enter at the optimum angle.

Design of the transmission system was developed around 1975 to address the issue of parallelism. The previous cantilever design created the problem of roller clearance enlargement at the ends of the rollers. Positioning accuracy was increased by locating the fulcrum bearings at the sides of the body.

Automatic roller adjustment is achieved by supplying a constant pressure to the moveable arm, normally using a hydraulic cylinder. A solenoid valve releases the pressure when no paddy is passing through the rollers.

Aspirators are typically used to discharge the lighter husks from the heavier kernel once the grains have passed through the rollers.

2.3.4 Husking Materials

The rubbers currently used in roller huskers are generally synthetic rubbers. The rubbers are selected based on their resistance to wear and their suitability for use with foodstuffs. The process of rubber selection is generally based around the knowledge of the manufacturer who has control over the various rubber properties during production. The exact composition and manufacturing method varies between roller producers but generally, rubber is applied to a steel cylinder whose internal form hosts the machine mountings. The rubber is layered up to the desired thickness and hardened whilst rotating to ensure an even coating.
The requirements for successful husking eventually reduce to questions of efficiency, both in terms of husked ratio and in terms of roller life.

2.4 Rice Polishing

2.4.1 Polisher Development

Rice can be polished most simply by rubbing grains together by hand. Applying pressure, the polishing action of grains abrading against each other can occur easily. To process the volumes of rice consumed globally at present in this manner would be highly impractical and inefficient, and so machines have been developed to mechanically carry out the polishing process.
The first vertical abrasive rice-milling machine was developed in the UK around 1860 [3] (figure 15).

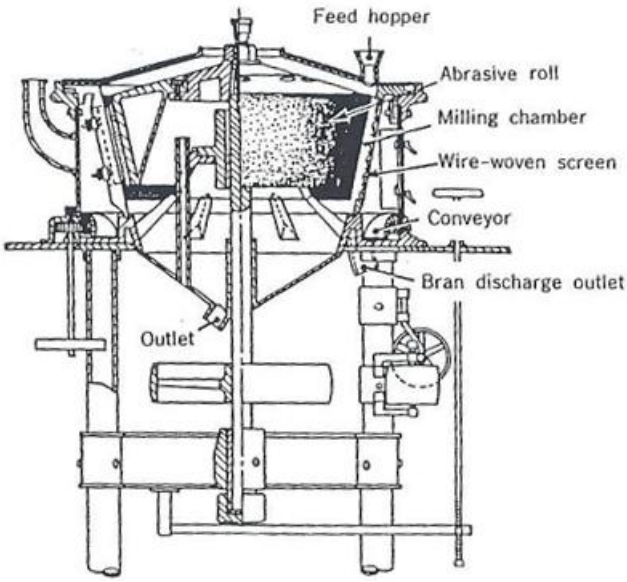

Figure 15 Douglas and Grant Milling Machine [3]

These machines incorporate a milling chamber of wire-woven screen with an abrasive roll. Brown rice enters at the upper inlet and milled rice exits from the lower outlet. Bran is discharged through the wire-woven screen.
The technology soon spread to Burma since the London based company Steel Brothers Inc. owned 80% of the rice milling plants there (having established Burma's first rice mill in 1871 [19]) and employed the British technology. By the time of the

World War II, Burma had the most advanced rice milling operations in the tropical region [3].
In the 1870s, mortar-type rice milling was developed in the USA (shown in figure 16).

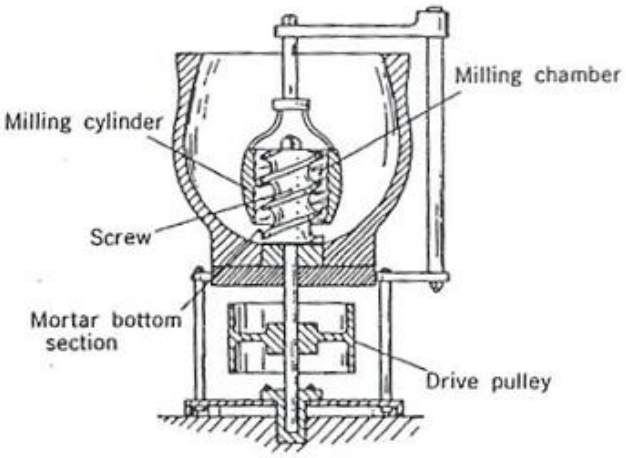

Figure 16 Mortar Milling Machine[3]

This process was an attempt to develop powered mortar whilst avoiding repetitious pestle pounding. Grains are milled by contact occurring as the grains are drawn downwards.
Low speed horizontal milling technology, shown in figure 17, was developed in the USA around 1890, originally designed for removing the pericarp from coffee beans.

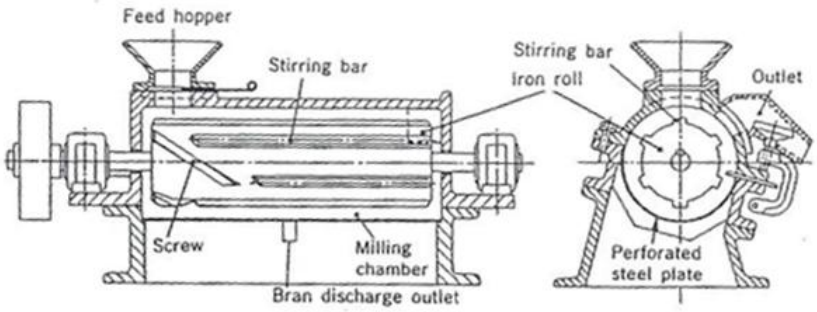

Figure 17 Engleberg Milling Machine[3]

It represents the beginnings of modern polishing technology, however it was inefficient and resulted in a large percentage of broken grains. Progress with this technology was made in Japan around 1920 by focussing on load stability, so that the machines could operate at a higher capacity. The clearance between milling rotor and cylinder was increased since mesh screens could not be produced reliably and hence bran removal required the extra volume. Supplementary stone powder would often be added to improve the machine efficiency. Variable milling action was achieved by resisting the rice at the outlet of the machine:

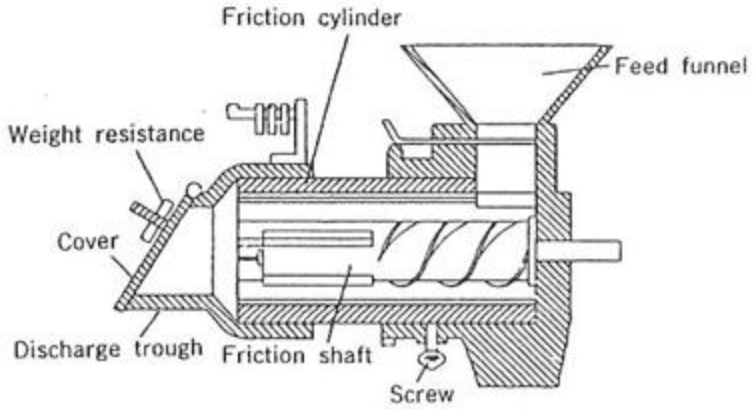

Figure 18 Shimizu type paddy husker[3]

In 1955 a new machine appeared in Japan with a steel perforated milling cylinder and ventilation function (shown in figure 18). Modern polishing technology has developed around this concept.

2.4.2 Modern polishing technology

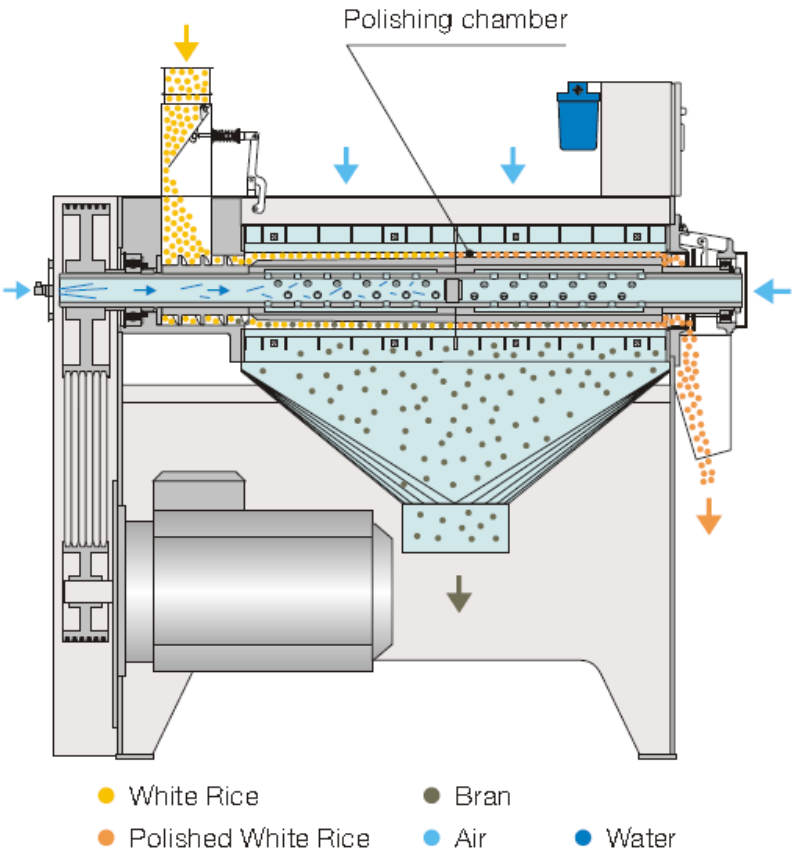

Figure 19 Modern Polisher Design – Buhler Sortex DRPF [20]

Figure 19 shows the modern humidifying polishing machine, invented in 1975. It removes dust, bran and the aleurone layer from a grains longitudinal groove much more effectively than in dry processing.

Rice is polished in two stages on the same shaft. Firstly, the rice passed into the chamber by a feed screw is humidified by water misting. The level of humidification

can be set by the machine operator based on the quality of the product exiting the machine. Flow rates can vary up to around 40l/hr depending on the rice variety being processed and the desired level of humidification. Over humidifying can lead to degradation of the surface of the grain. Once humidified, the rice achieves a pearl-like lustre by abrasion as the rotating cam shaft moves the kernels.
The cam roll is separated into two parts. At the first stage, the four blades are angled slightly to ease the transition of the grains (figure 20).

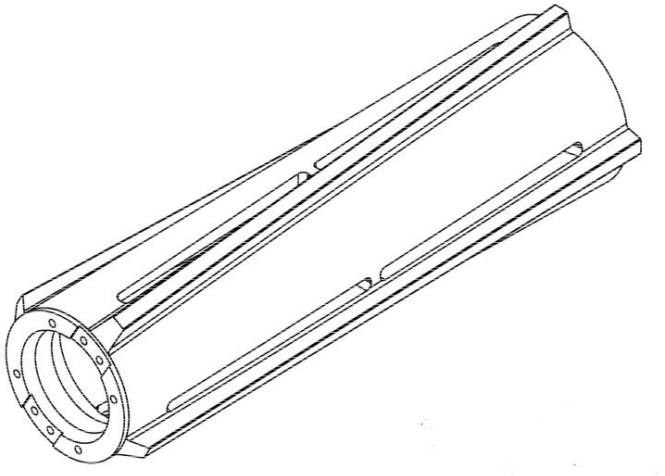

Figure 20 First stage cam roll

In the second half of the machine, the blades run parallel to the shaft in an attempt to generate a more aggressive polishing action (figure 21).

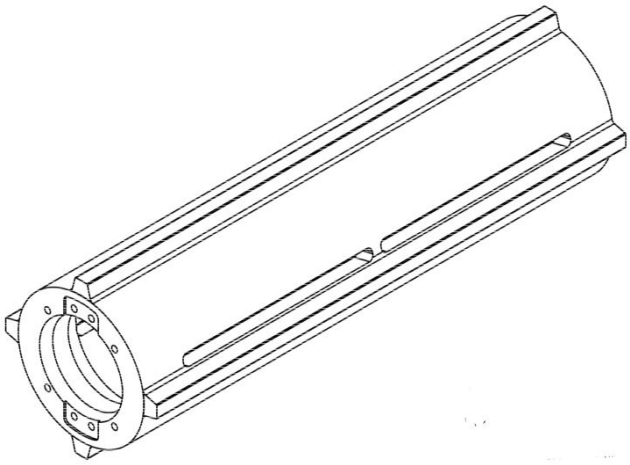

Figure 21 Second stage cam roll

Air aspiration is provided through holes in the cam roll. This is done to assist with the removal of the bran, which, without aspiration would simply remain inside and clog the machine. A secondary function of the air aspiration is a cooling effect, since grains heat up through the friction action, and high temperature fluctuation can result in cracked grains.

2.4.3 Degree of polishing

During polishing grains become smoother in texture and glossier in appearance. No method exists to describe a true degree of polishing, relying instead on the experience of the miller to ensure that the quality of the product is high.
There have however, been some attempts to quantify specific milled properties, such as whiteness. Kett for instance[21], produce analysis machines which utilise light reflectance as a means of determining the whiteness of the grain. Whilst this is useful in some regards, the rice must still be removed from the flow to be tested and the polisher adjusted to attempt to improve product quality if required. This method also fails to take into account the texture of the grain which is considered important to the millers.

2.4.4 Polishing materials

Polishing machines use some replaceable components in order that the machine life be maximised. The primary component which is regularly replaced is the perforated milling cylinder (screen) shown in figure 22.

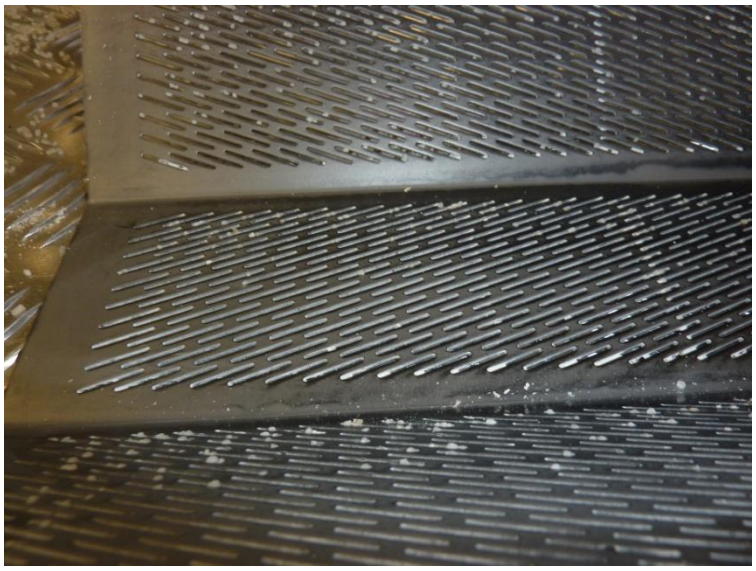

Figure 22 Perforated milling screen

Two screens together form an octagonal cylinder completely surrounding the central rotating blades. The two halves are installed on either side and folded up towards each other to allow for a more rapid replacement (see figure 23).

Figure 23 Perforated Screens in Replacement Position

Recent developments have led to the use of a treated steel plate for the perforated screens. Nitrocarburising the steel generates a much harder surface than the steel offers.

Nitriding is a process which was first developed in the early 1900s [22]. It involves the case hardening of ferrous metals by diffusion of nitrogen into the surface thermochemically. Nitrocarburising is an extension of this process involving the diffusion of both nitrogen and carbon into the surface in order that the hardness of the steel is increased. In addition to increased abrasion resistance, the treated surfaces offer improved fatigue properties and corrosion resistance. Nitrocarburising has also been found to increase friction coefficient and wear resistance of tool steels along with surface roughness and hardness in studies by Chiu et al. [23]

2.4.5 Polishing Control

Flow into the polishing chamber is controlled by altering the inlet spacing through which the rice flows. There is also a shut off valve pre-inlet in order to stop the flow completely. In modern milling automatic load control can be achieved by regulating the output of the machine. The flow is resisted by a weighted plate covering the outlet so that pressure builds through the machine.

The flow is monitored by observing the current drawn by the motor (normally between 40A and 70A for a full chamber), This is not a direct measurement of flow as

the current drawn also varies based various rice properties, bulk properties and the addition of water misting.
The degree of polishing can be altered in two ways. Firstly, in resisting the outflow of the grains, grains are thought to remain in the polishing chamber for longer resulting in a greater degree of polishing, although risks a higher broken grain percentage. Secondly, the addition of water misting greatly enhances the degree of polishing, although over misting can reduce grain quality and, in extreme cases create blockages within the machine.

2.4.6 Summary of Milling Actions

Arguably the most comprehensive documentation of rice milling technology to date comes from the Japanese inventor and developer Toshihiko Satake[3]. Having spent over sixty years since 1928 developing, designing and improving milling machines, in 1990 he documented the current nature of milling technology.
Regarding polishing technology, Satake lists four main actions which contribute to the smoothing and whitening of grains. These are friction action, cutting action, impact action and grinding action. Each is said to occur in varying degrees and can be identified by the nature of the bran removed. These actions have been listed but it has not been shown how these actions have been determined, nor has it been shown how these ratios can be best combined to improve the milling efficiency both in terms of energy used against bran removed, or in terms of the effect of each action on the milling machines.

2.4.6.1 Friction Action

Satake states “Above a certain level, the kinetic friction created in rice milling shows its effect as a large frictional force tearing the rice, but below that level friction evidences itself as heat”. That is to say, that friction action can effectively be separated into effective friction (tearing) or ineffective friction (heating). It is tearing action which is the basic action in low speed milling and is extremely inefficient. Tearing occurs at an average pressure of 100g/cm^2 or more and a speed of 600m/min or less and produces a deep, long cut to the bran.

2.4.6.2 Cutting Action

Cutting is another action typical in low speed milling machines, usually occurring in combination with tearing action. It occurs at 100g/cm^2 or more average pressure and a speed of 600m/min or less. It involves the removal of bran using an edge or blade, such as the slot edges in a polisher screen. In a low speed system, bran is cut long and deeply resulting in large pieces of bran.

2.4.6.3 Grinding Action

Grinding is a high speed action occurring at speeds over 600m/min and pressures lower than 50g/cm^2. In grinding action, the bran is cut shallowly and ground into short pieces. It is a shearing action combining impact and friction and changes to

impact at higher speeds. Grinding efficiency increases when the pressure is low and the speed is high, and is more efficient than low speed action, except for with viscoelastic materials which makes grinding not suitable for low-whiteness milling in which the coefficient of friction is large.

2.4.6.4 Impact Action

Impact is a high speed action which occurs at speeds of 600m/min or more. Lower speeds cause ineffective impact. It is difficult to experiment on impact action since the secondary action during impact often becomes the effective action.

2.4.6.5 Stirring

Stirring is needed for even milling. Bran is not removed from the entire surface of a grain in one motion, so stirring is necessary to ensure that the bran is removed and smoothed across the whole grain. In low speed milling, the ribs on the cam roll alter the density of the grains during motion, which causes the stirring of the grain. In high speed milling, rice not touching the abrasive does not polish and rice must be constantly circulated. Impact with the milling roll or screen creates stirring.

2.4.7 Other polishing technologies

2.4.7.1 Whitening

To achieve a higher gloss to the grains than obtained in standard polishing, a whitening machine (figure 24) can be employed to buff the grains to a smooth, pearl like finish.

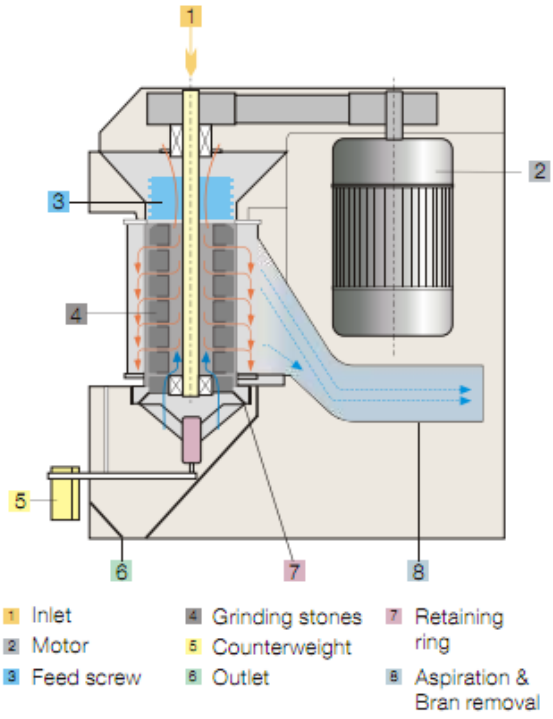

Figure 24 Modern Whitening Technology (Vertical Milling Machine)[24]

The above example of a rice whitener is a vertical abrasive top to bottom milling machine. It operates using similar principals to a rice polisher however, rather than a cam roll, abrasive stones are used. The vertical whitener has a cylindrical milling chamber comprising mesh screens with slots in similar configuration to those in a polisher. Air aspiration helps to ensure efficient bran removal.
The rice is fed in by means of a feed screw, and the whitening intensity is controlled by means of a counterweight and retaining ring which can be used to increase the pressure in the chamber.

2.5 Milling Cost

The milling of grains is a relatively cheap process, considering the quantities produced, however the requirement of replaceable components due to their rapid wear can elevate the financial cost to the miller. This can lead to millers seeking cheaper alternatives than replacing components like for like which can result in the premature failure of components. Whilst this is a known problem, cost is always the major driver and so the trade of cheaper and poorer quality components will continue. This does, however, highlight the need to develop an independent analysis of the milling machines rather than rely on anecdotal evidence from the millers.

2.6 Conclusions

This chapter has covered the key aspects of rice and rice milling technology. The grains composition has been shown along with the structure of the bran layers in a general sense. Since the number of varieties is potentially extremely large (hundreds of thousands) and since the mechanical properties of each could be very different, it is difficult to make general assertions about the nature of rice grains as a whole. Not only can properties differ between varieties, but since grains are organic and their growth dependant on a number of factors (soil conditions, weather conditions etc.) variation occurs within the same variety (plant to plant and year to year).
The milling process history has been discussed and two technologies have been selected for detailed study, namely rubber roll huskers and humidifying polishers, since minimising the wear of these machines is of particular interest to the millers. The combination of milling actions leads to the rapid wear of various machine components which has associated economic costs. Though the underlying physical mechanisms involved in milling are generally not well understood, significant improvement to the machines has been made through a trial and error approach. This highlights the need for a more rigorous approach in order that grain behaviour be understood, along with the underlying mechanisms causing wear of components in order to improve the efficiency of the machines (both in terms of product quality and machine life).

3 WEAR MECHANISMS AND WEAR BY FOODSTUFFS, PARTICLES AND GRAINS

Wear is defined as a loss of material and can present itself in many different forms. Each form of wear has its own development requirements and its own characteristics. It is also the case that the wear of a material is not limited to one single mechanism, but can incorporate many, potentially making determination of the dominant mechanism tricky.

The various mechanisms of wear in general are well documented and act, either in isolation or, more often, in combination. This chapter considers the known wear mechanisms and how they evidence themselves within the scope of food stuff production. Particular attention is paid to granular/particulate wear since this is the nature of rice grains as an abrasive.

3.1 Wear

Tribology, the study of contact, which encompasses "wear" is an area of research which is developing rapidly with ever increasing drive, notably from industry, to enhance understanding of fundamental mechanisms and to develop means of lengthening the life of components.

Different mechanisms of wear tend to evidence themselves on the component in different ways. Some of the various types of wear scar are shown below in figures 25-29:

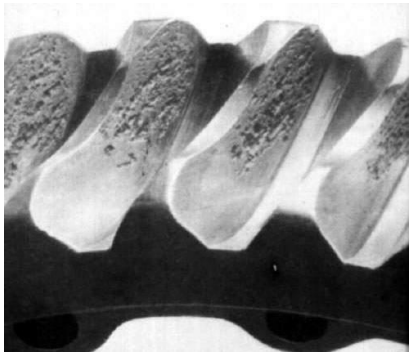

Figure 25 Pitting wear of gear teeth[25]

Figure 26 Surface fatigue of rail wheel[26]

Figure 27 Surface cracking of brake disk[27]

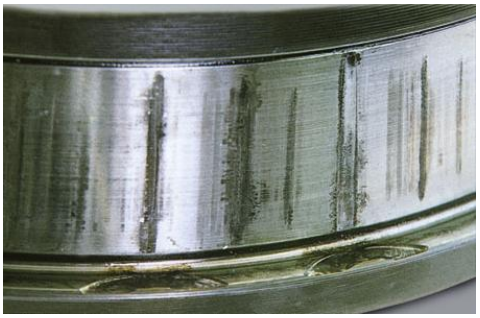

Figure 28 Fretting wear of bearing inner race[28]

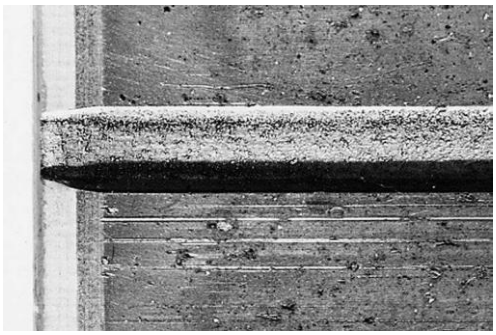

Figure 29 Scoring wear of a journal bearing[29]

Each of the above wear scars have been caused by different mechanisms which are discussed below. Simple observation often gives a good indication of the manner in which wear has been produced.

3.1.1 Mechanisms of Wear

When two bodies in contact slide relative to each other, there are many physical and chemical processes that can interact. Adhesion is an important consideration when surfaces slide, as is abrasion. These are discussed below.

3.1.1.1 Adhesive wear

When two surfaces come into contact, the area of material touching is much smaller than the apparent contact area. It is the tips of asperities that contact and the relatively high pressures cause local deformation and adhesion of the surfaces. This "welding" of the asperities causes material loss when the surfaces begin to move against one another. The junction formed must be sheared for the surfaces to slide and the force to cause this is approximately equal to the frictional resistance (see figure 30).

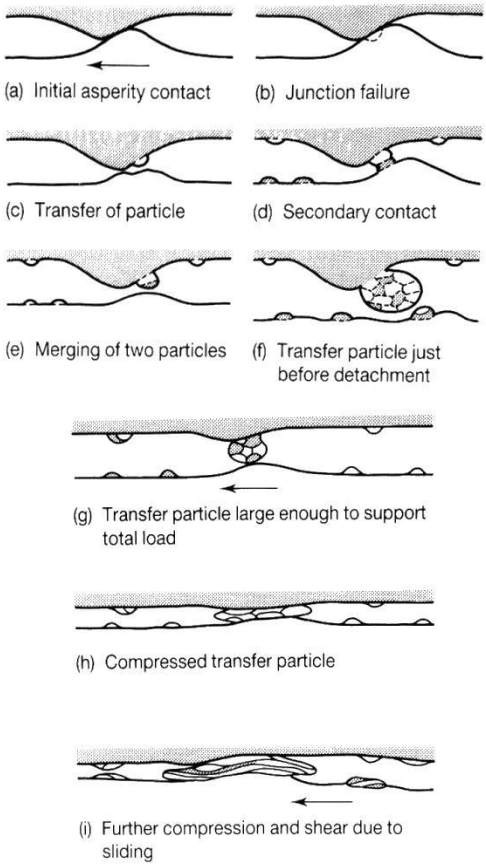

Figure 30 Formation of a transfer particle by asperity rupture and aggregation[30]

If the junction is weaker than the shear strength of the materials then the interface itself will shear resulting in very little transfer of material from one surface to the other and hence very little wear.

3.1.1.2 Abrasive wear

In abrasive wear, as hard particles or protuberances on a counterface slide along a surface material is removed. This can be identified as two-body or three-body abrasive wear depending on the exact nature of the interface, shown in figures 31 and 32.

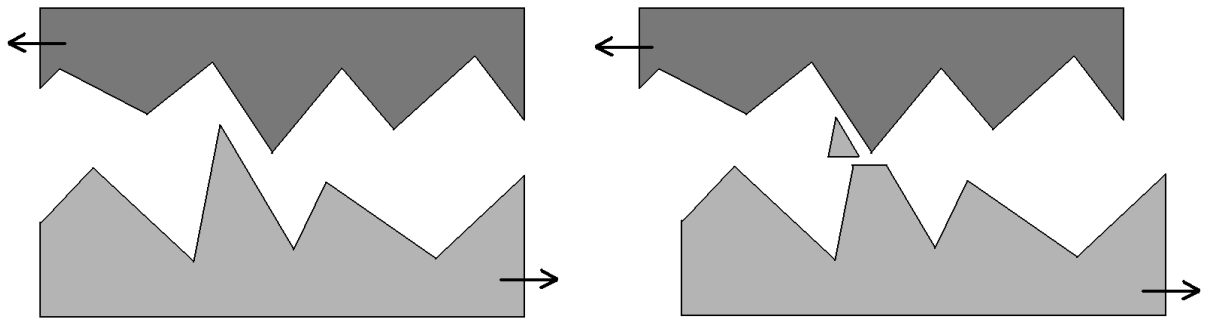

Figure 31 Two body abrasive wear

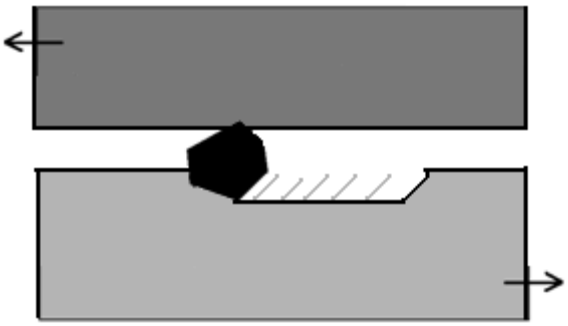

Figure 32 Three body abrasive wear

3.1.1.3 Delamination wear

Delamination wear involves plastic deformation of the surface layer, crack nucleation and crack propagation. It is an extension of surface fatigue wear in which stress hardening can cause sub-surface deformation which would ultimately result in cracking (see figure 33).

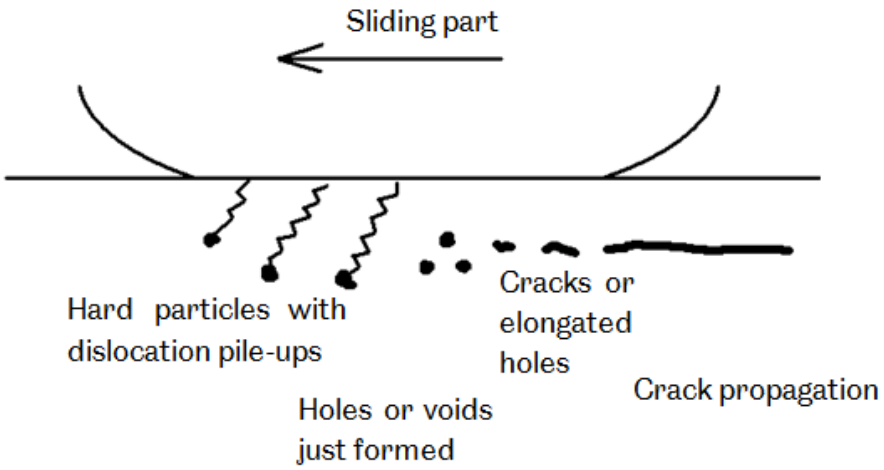

Figure 33 Mechanism of subsurface crack formation and delamination wear[31]

With the addition of further adhesive wear, eventually flat fragments can be lifted from the surfaces affected as in figure 34.

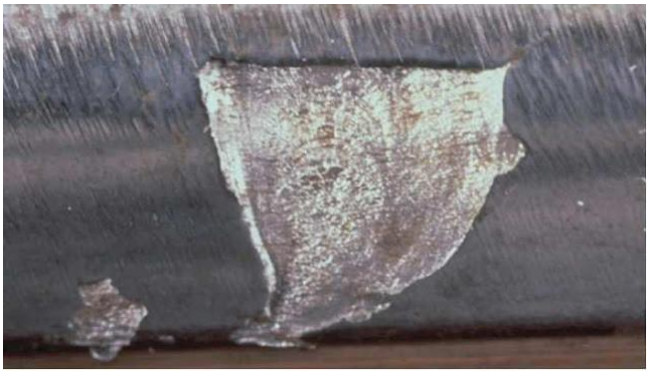

Figure 34 Delamination of a gear tooth[32]

3.2 Particulate Wear

Granular materials is the term used to describe any bulk material with grain size above approximately 1 micrometer (since granular materials must be large enough that they are not subject to thermal motion fluctuations)[33]. Particles tend to behave in a unique manner, sometimes exhibiting the properties of a fluid or gas or solid depending on the energy with which they move[34]. Zhu et al. suggest that the core of particle research lies in the understanding of the relationships between macroscopic and microscopic properties of particulate matter, and that this state of matter is widely encountered but poorly understood[35]. Macroscopically, particle behaviour is controlled by the interactions between individual particles and the fluid through which they move. Microscopically it is the interaction forces which are key to understanding the mechanisms of particulate motion and it is the microscopic behaviour that leads to results that can be generally used. The study of the microdynamic actions is achieved through an understanding of the forces and trajectories of individual particles in a system.

There are two chief mechanisms by which particulates generate wear of a surface[30], namely abrasion and erosion. Abrasion has been discussed above, and occurs in the same way between surfaces and particulates (since even at the scale of particulates, asperities are very small).

Erosion is caused by hard particles striking the surface resulting in a loss of material. It is often qualified as solid particle erosion to distinguish it from the wear caused by the impact of liquid jets or drops (as in figure 35).

Figure 35 Erosive wear of a pump casing[36]

Particulate wear by both abrasion and erosion can be employed usefully, for instance in polishing or grinding processes, however within the context of this thesis both are undesirable effects relating to the wear of various mechanical components. There

are several experimental reports of erosive wear in literature along with some attempts to study the mechanism by simulation[37].

3.2.1 Particulate properties

In order to understand the wear caused by particles, it is important to identify the effect on wear rate by property variation, in terms of material properties of the particulates, but also by their bulk properties. Ian M Hutchings has compiled various aspects relating to wear by particulates in his work "Tribology – Friction and Wear of Engineering Materials"[30], the key aspects of which are discussed below. A 1972 paper by Finnie[38] also notes various aspects influencing the erosion of ductile metals. These include, angle of contact, particle rotation at contact, particle velocity at contact, particle size and shape, surface properties (such as shape and strength) stress level in the surface and particle concentration.

3.2.2 Particle Hardness

In general, the particles involved in abrasion or erosion of a surface generate a more rapid rate of wear as the particle hardness increases. Particles which have a lower hardness than the surface generate much lower wear rates. As the ratio of particle hardness to the surface hardness ($H_{particle}$ / $H_{surface}$) becomes less than around 1, the wear rate becomes much more sensitive to the abrasive hardness[30] as shown in figure 36.

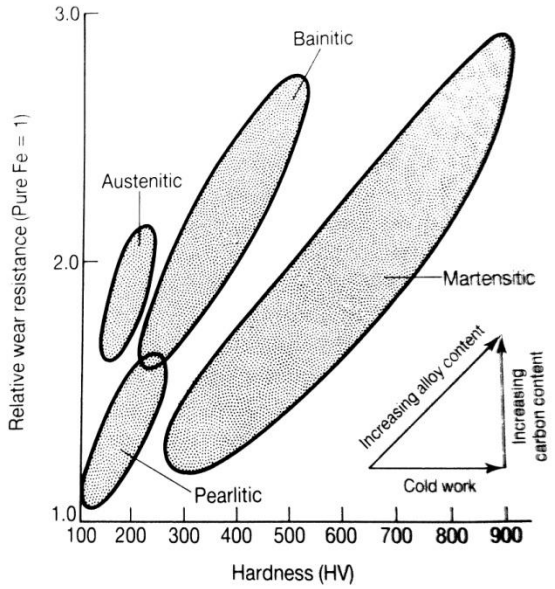

Figure 36 Hardness vs relative wear resistance[30]

In 1824, German mineralogist Frederich Mohs devised a scale based on the observation that there is a certain minimum ratio of hardness needed for one material to be able to scratch another. The rate of wear by erosion or abrasion is

dependent on the plastic indentation of a surface such that when particles have 1.2 times the hardness of the surface wear rates are much faster[39].

3.2.3 Particle Shape

The shape of particles is important when studying their interaction with a surface. The degree of angularity can have a strong influence on the wear rate, with rounded particles having less effect than angular particles. Angularity can be difficult to define however since identifying and defining the features of a complex three dimensional shape is not simple. Whilst a roundness factor can be defined to compare the perimeter and area of a two dimensional projection of the particle with a circle with the same perimeter, in the case of large and non-equiaxed particles this is difficult to determine. Currently "roundness factor" only provides a crude measure of the deviation of the particle from a perfect sphere and whilst some success has been achieved in correlating this with wear rates, the model has much room for improvement.

3.2.4 Particle Size

Whilst the majority of particles responsible for abrasive and erosive wear are between 5 and 500μm, gouging wear may involve hard particles with much larger diameters. Laboratory studies have consistently shown the pattern of size effect for erosive and abrasive wear of metals [40]–[42], a behaviour which is thought to be due to a size effect in the metal strength as shown below in figure 37.

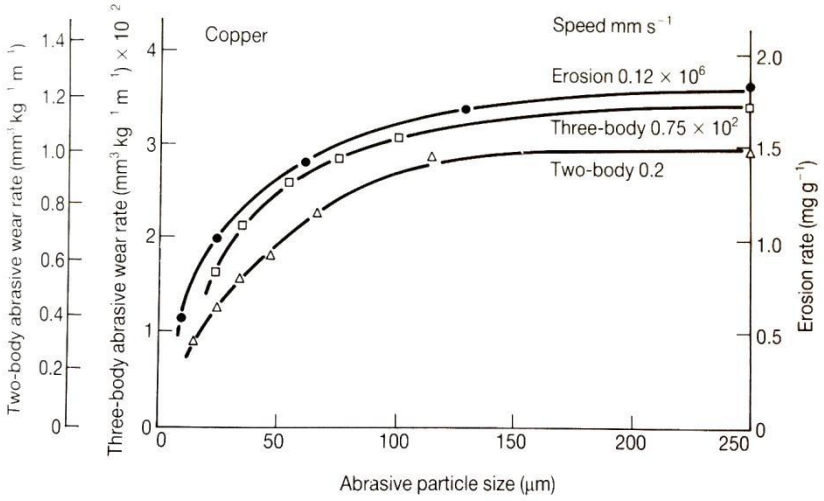

Figure 37 Wear rates of copper under conditions of two-body abrasion, three-body abrasion and erosion by silicon carbide particles of different sizes[30]

Also found in scratching and indentation experiments, it is thought to be due to the relative difficulty of moving dislocations in a small volume of the metal. Regardless of the dominant mechanism, it is consistently observed that larger particles cause proportionately higher wear than small particles.

In addition to particle hardness and size, the particles ability to break down into smaller particles (friability) can have a significant influence on the wear rate of the surface. Particles which break down more easily are in general less likely to remove material from the surface.

3.2.5 Bulk properties

Whilst a knowledge of individual particle properties is essential in the understanding of their relationship to wear rate, it is equally important to understand how the particulates behave in relation to each other. “Bulk” properties are those which define the behaviour of the collective particles together and include parameters such as density and particle interlocking. In certain cases, most notably for powders, electro-static effects and other particle attractions are also of interest.

3.2.6 Other Effects of Solid Particle Erosion

3.2.6.1 Momentum Effect

The effect of erosion is different to three body abrasion in that particles have a larger freedom of movement. Several forces may act on a particle in contact with a surface as shown in figure 38.

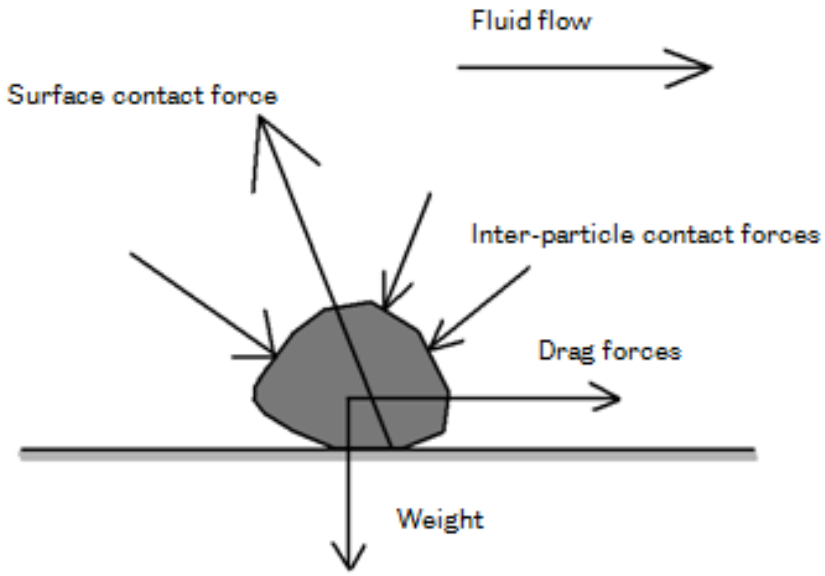

Figure 38 Forces that can act on a particle in contact with a solid surface

The dominant force responsible for decelerating the particles from their initial velocity is the contact force with the surface. The wear rate is dependent on the momentum with which the particles impact the surface, and is therefore a function of particle mass and velocity.

3.2.6.2 Angle Effect

The angle of impact with the surface can have a large effect on the wear rate of the surface (see figure 39).

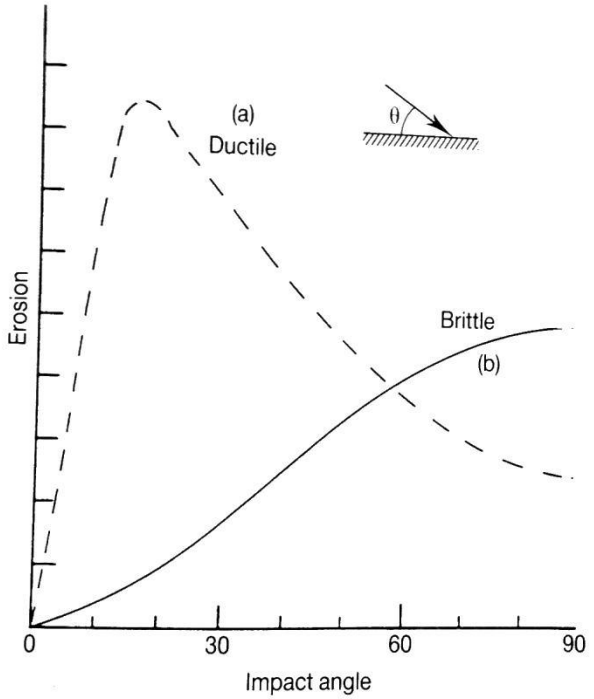

Figure 39 Effect of impact angle on erosion rate[30]

Finnie[43] noticed that there is a dramatic difference in response between brittle and ductile materials when the wear rate is measured as a function of angle of impact.

3.2.6.3 Ductility Effect

Erosive wear can involve either brittle fracture or plastic deformation of the surface. In each case, the mechanism of wear is slightly different.
In the erosion of ductile surfaces Finnie[44] suggested that when abrasive particles strike the surface, some will displace the material and others will remove the material. Erosion by plastic deformation mechanisms vary slightly by angle of impact. Studies of the impact on metals of single particles at 30° angles have shown three dominant mechanisms[30] (as shown in figure 40).

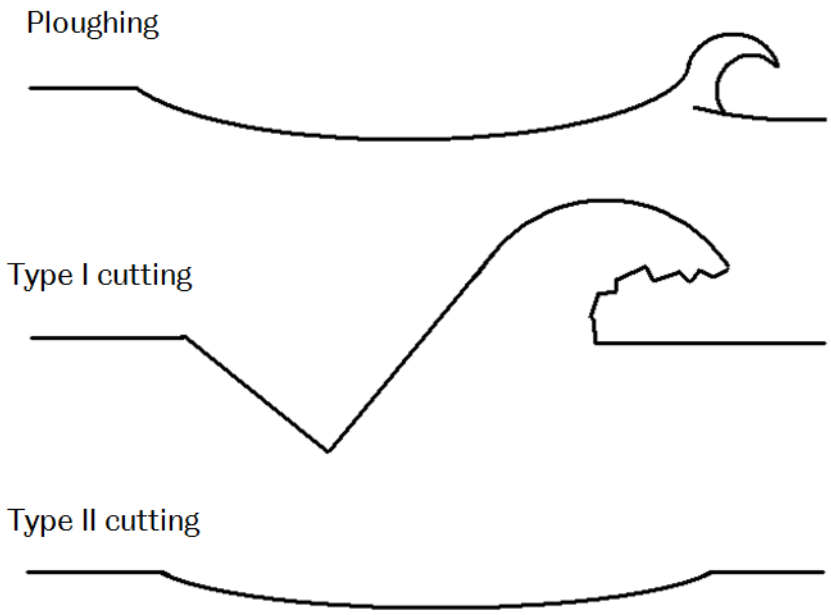

Figure 40 Erosive wear distinctions

Ploughing occurs when a sphere impacts the surface. Type I cutting occurs when an angular particle rotates forwards during impact whilst type II cutting occurs when the particle rotates backwards. Whilst this presents a very simplified classification which becomes more complex when randomly oriented, irregularly shaped particles impact with roughened surfaces, distinctions can be made when observing a surface.

When the impacted material is brittle, the erosive particles cause the formation and intersection of cracks which lead to material loss. There is often some plastic flow around the point of contact. Various models for erosion by brittle fracture have been developed, the majority focussing on impact at 90° since the rate of erosion falls for lower incidence angles. Figure 41 shows the mechanism of material removal of a brittle surface under particle impacts.

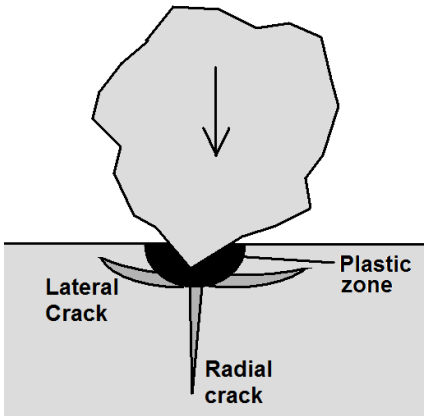

Figure 41 Erosive wear of brittle surfaces[45]

3.2.7 Particulate motion

A number of studies of granular flow have been conducted and some models determined to understand the flow characteristics [46]–[49]. Many of these studies are based on the assumption that under certain conditions, it is the particle collisions which provide the principal mechanism for properties such as momentum and energy being transported. This is analogous with the Chapman-Enskog kinetic theory of dense gases [50]. Lun et al. [51] in 1983 developed theories for an idealised granular material consisting of smooth, uniform, inelastic spherical particles for Couette flow with arbitrary coefficients of restitution.

Despite these developments, predicting the motion of particulates is nearly impossible when the particles are of irregular shapes and sizes. A new approach however is becoming ever more advanced and looks to provide opportunities for discrete particle modelling. Computing power increases mean that simulating individual collisions between particles is progressively less time consuming. The power to calculate and process particulate collisions in a closed system has great potential to improve our understanding of particulate motions and hence how they interact with other particles and boundaries. Whilst full and complex systems are often still beyond current computing capabilities, the trend in computing power suggests that this field will continue to grow strongly.

3.3 Wear Caused by Foodstuffs

There are many other foodstuffs which have similar processing requirements to rice. Many grains and pulses require some degree of shelling or polishing and much of this is done using comparable machinery. In addition, wear is a common occurrence in many other food sorting and processing operations. Although in most situations, wear of components is undesirable, in food processing wear can create the additional problem of contamination of the foodstuff. This not only restricts the choice of materials used on the basis of functionality, but also because it must comply with regulation based on products for human consumption. This often limits the use of lubricants to reduce wear.
Some aspects of wear caused by other foodstuffs are discussed below.

3.3.1.1 Wear in Wheat Processing

During the processing of wheat, the grain is passed between large iron or ceramic rollers to reduce it into flour (see Figure 42).

Figure 42 Iron rollers used in wheat milling[52]

Various studies have been conducted to examine the roller wear [53], [54] many of which use a rubber wheel abrasion test to study the nature of the wear. This method involves simulating the grain using a hard particle and monitoring the effect of material change and particulate variation.

Zhang et al. [55] found that the primary factor affecting the wear properties of the rollers is the particle size, followed by the roller separation as a secondary factor. Rotational speed was found to be a tertiary factor affecting the wear of the rollers. They also determined the optimum of these characteristics required to minimise the wear rate.

Other studies by Zhu and Xie[54] have found that the rollers worn by the soft abrasive wheat have maximum shear stress both on and beneath the surface. This leads to the wear of the rollers by plastic fatigue and multiple impact fatigue in the matrix with brittle spalling in the carbides.

3.3.1.2 Wear in Sugar Cane Processing

Various aspects of sugar cane processing have been investigated with regards to wear regime.

Seabra et al. [56] looked at the use of food grade polymers against stainless steel for use in a sugar worm conveyor where crystals enter the interface between shaft and supporting bushings and cause abrasion (see Figure 43).

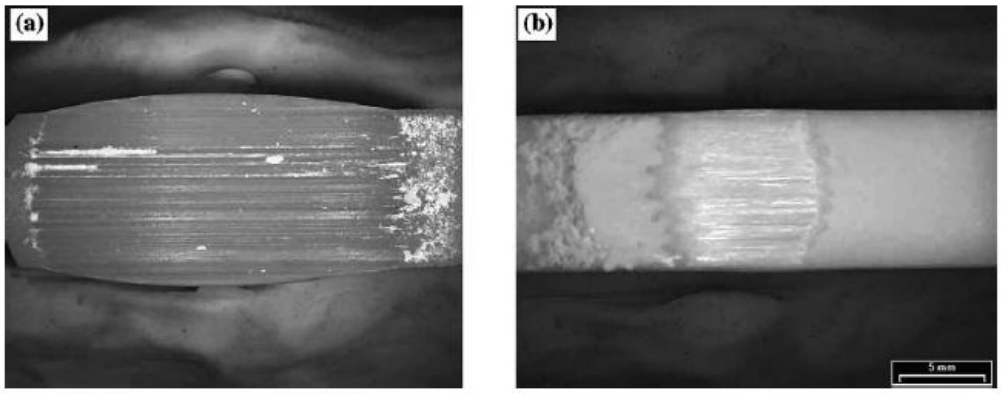

Figure 43 Abraded polymer surfaces using sugar crystals (a) UHMW-PE green, and (b) PETP[56]

Bearings and shafts in particular tend to experience high wear rates in sugar processing. During milling operations, extraneous matter enters the bearing as the shafts move up and down during their operation. This matter usually contains fibres and minerals which degrade the lubricants used and performance is affected. The extraneous matter also is found to degrade the rollers used for compressing the shredded sugar cane (see Figure 44).

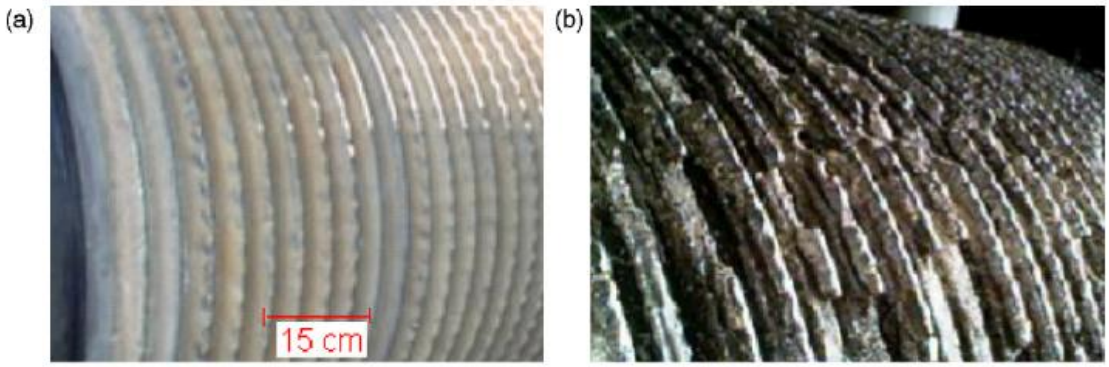

Figure 44 Unworn (a) and worn (b) rollers used to process sugar cane[57]

3.3.1.3 Corrosive and oxidative wear

Corrosive and oxidative wear are mechanisms by which a surface degrades by chemical reaction with its environment. In iron based materials this commonly evidences itself as rust as oxygen molecules bond with the iron molecules. This leads to a change in material properties, and quite often, a degradation of the surface. Oxidation is a common mechanism in many metals leading to changes in surface characteristics. Corrosion, similarly is used to describe a chemical reaction leading to material property changes (and often material loss).

3.4 Conclusions

Wear mechanisms evidence themselves primarily through observation of the worn surfaces. As material is lost from a surface in a variety of ways, sometimes in a

combination of ways, the surface is scarred macroscopically and/or microscopically. The various mechanisms of wear applicable to particulates have been described above.

In addition to the wear mechanisms, particular attention has been paid to research conducted into other milling operations such as sugar and wheat. These are particulates processed using rollers and as such have similarities with the wear observed in rice mills.

Particulate wear is also considered and the various properties of particles which affect wear rate of contacting surfaces are discussed. These include hardness, shape and size. Similarly, the other effects of solid particle erosion are covered above including momentum effect and the difference in effect of impact angle between ductile and brittle surfaces.

Finally, the motions of particulates have been considered and methods employed to model particulate behaviours noted. Modern computing power offers the ability to simulate the relative motions and impacts of individual particles in a closed system. Whilst it is still time consuming to model entire flows (since each motion and impact must be calculated for every particle at every timestep) it does provide a means of observing the forces and pressures expected in a system, which ultimately relates to the wear rate of the materials. There are a number of limitations in computational simulation, such as particles must be simplified (uniform, heterogeneous spheres), however it has been demonstrated to be an important growing technology which offers many advantages over traditional experimentation (chiefly cost and time).

4 MECHANICAL PROPERTIES OF RICE

It is important that the mechanical properties of rice grains are well understood so that the manner in which they interact with the machines can be considered fully. Various properties are of interest, including shape and size, hardness, compressive strength, coefficient of friction and bulk density. Properties vary not only between grains of the same type, but more so between varieties. From size aspects to moisture content and hardness, properties can vary drastically. For this reason, one variety of long grain paddy has been selected to be used in any experiments, chosen since it is both a common variety and convenient to acquire.

4.1 Rice Grain Imaging

A scanning electron microscope has been used to image the long grain paddy, brown and polished grains. Looking in detail at the grain surface can help to reveal the physical changes undergone during the polishing process. It also gives a much greater understanding of the organic nature of the grains and their structure.

The process of scanning electron microscopy requires that samples are electrically conductive at the surface and grounded to prevent a build up of electrostatic charge at the surface of the sample which results in scanning faults and other image artefacts. Since rice grains are not naturally electrically conductive, it can be difficult to obtain clear images through electron microscopy. To alleviate this problem, an ultrathin gold coating has been applied to the rice samples using the vacuum coating method (see Figure 45). The gold coating is thin enough to not distort the features of the grain yet is significant enough to allow good conductivity resulting in clear images.

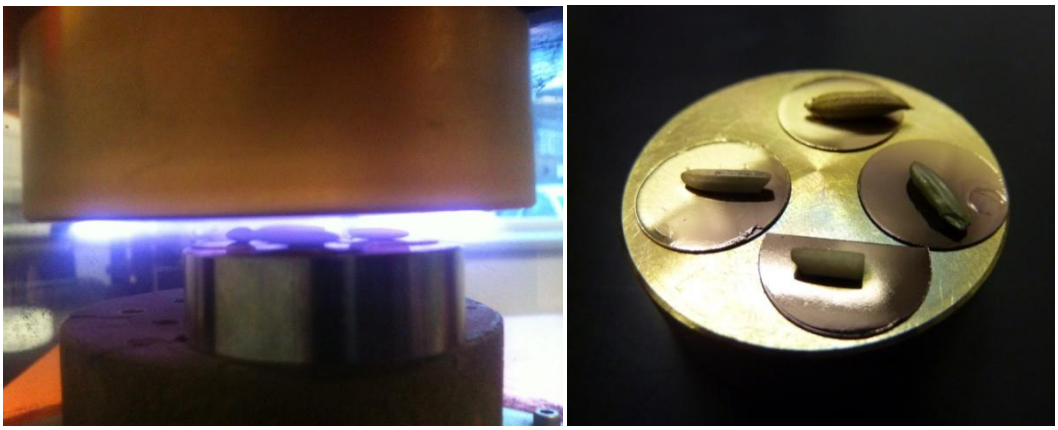

Figure 45 Gold coating of samples

Samples are then placed into the vacuum chamber of the SEM (Figure 46) and an electron beam fired at the sample. The electrons in the sample interact with the beam so that the beams position can be compared with the detected signal to infer topography.

Figure 46 Scanning electron microscope

Rice grains are relatively large compared to the capabilities of the SEM, so for full size images of grains, several images must be combined. Below (Figure 47) is a composite image of a single paddy grain.

Figure 47 SEM Image of rice paddy

Magnifying the image shows the nature of the husk on the micro level. The grain husk consists of ridges and bumps which assist in protecting the grain within (see Figure 48below).

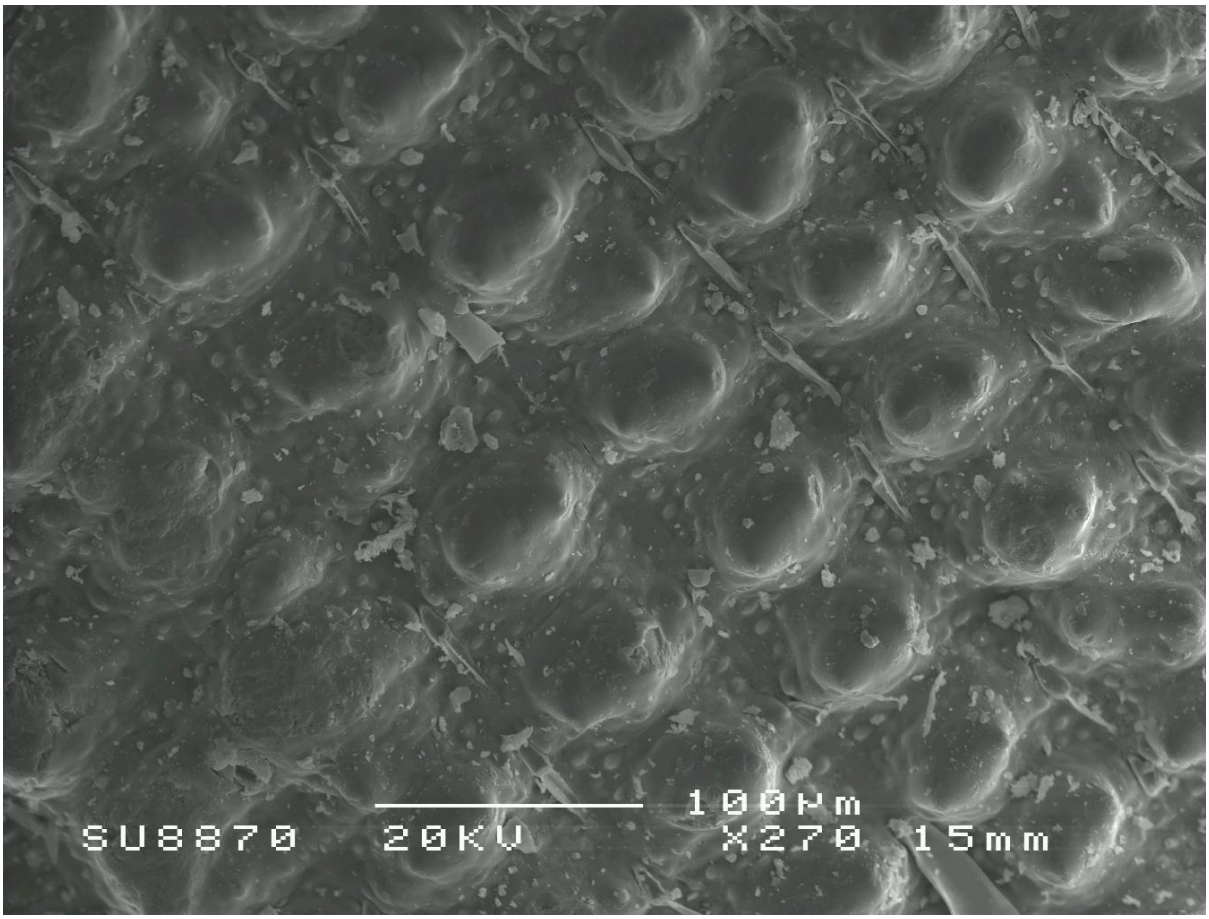

Figure 48 SEM of grain husk at a scale of 100µm

The SEM images show the organic, non-symmetrical nature of the grain, and go some way to explaining how properties vary from grain to grain.

4.1.1 SEM of Brown and Polished grains

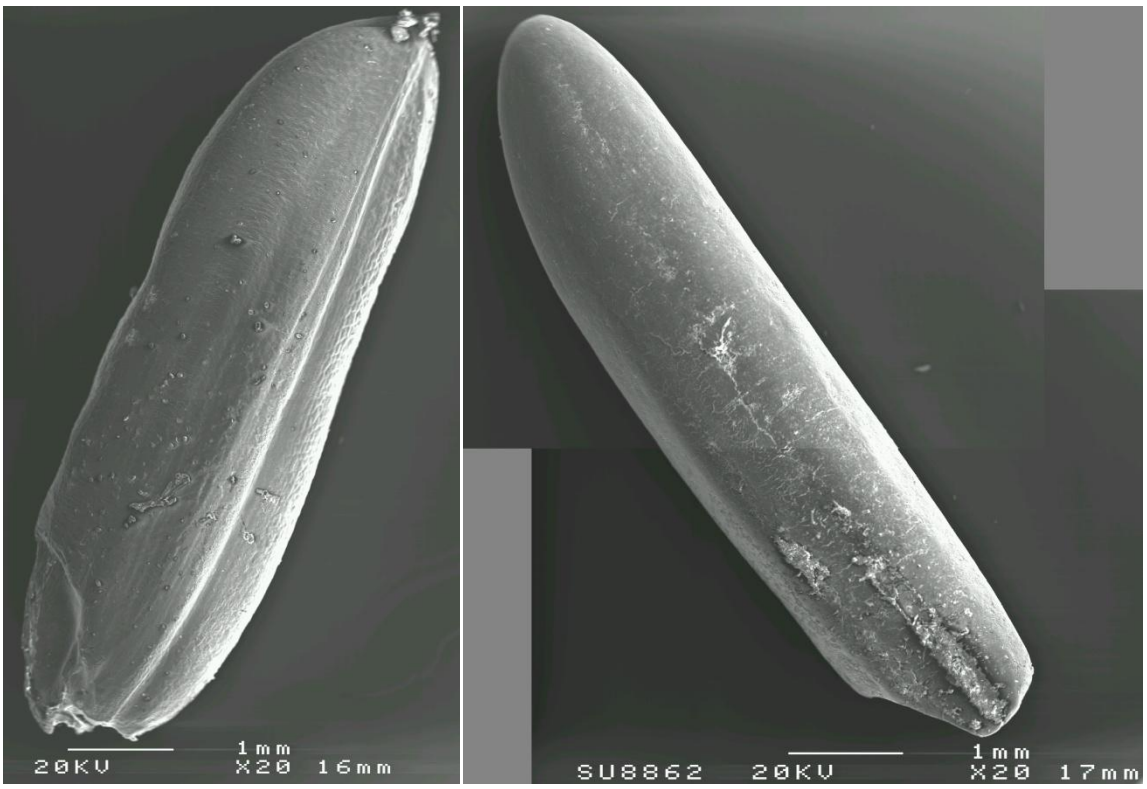

Figure 49 SEM images at a scale of 1mm of (a) brown rice and (b) white rice

There are some notable differences between brown and polished grains on the micro level (Figure 49). It can be seen that the embryo has been stripped away from the brown grain, and the apex at the other end of the grain rounded. The bran has been removed, a process which evidences itself as the ridges of the grain have been smoothed. Looking deeper (see Figure 50) the smoothing process is more obvious.

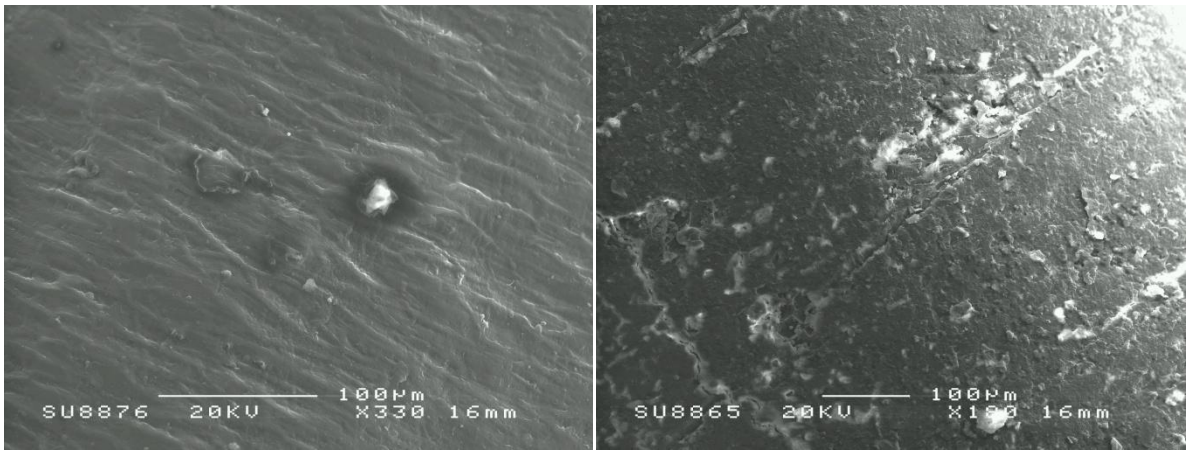

Figure 50 SEM images at a scale of 100µm of (a)brown rice and (b) polished rice

Some damage has occurred to the grain during the polishing process which is evidenced in the scratches, however this does not affect the macro appearance of the grain.

Looking even deeper into the polished grain, (Figure 51) the surface reveals spalling giving indication to the mechanisms involved in bran removal.

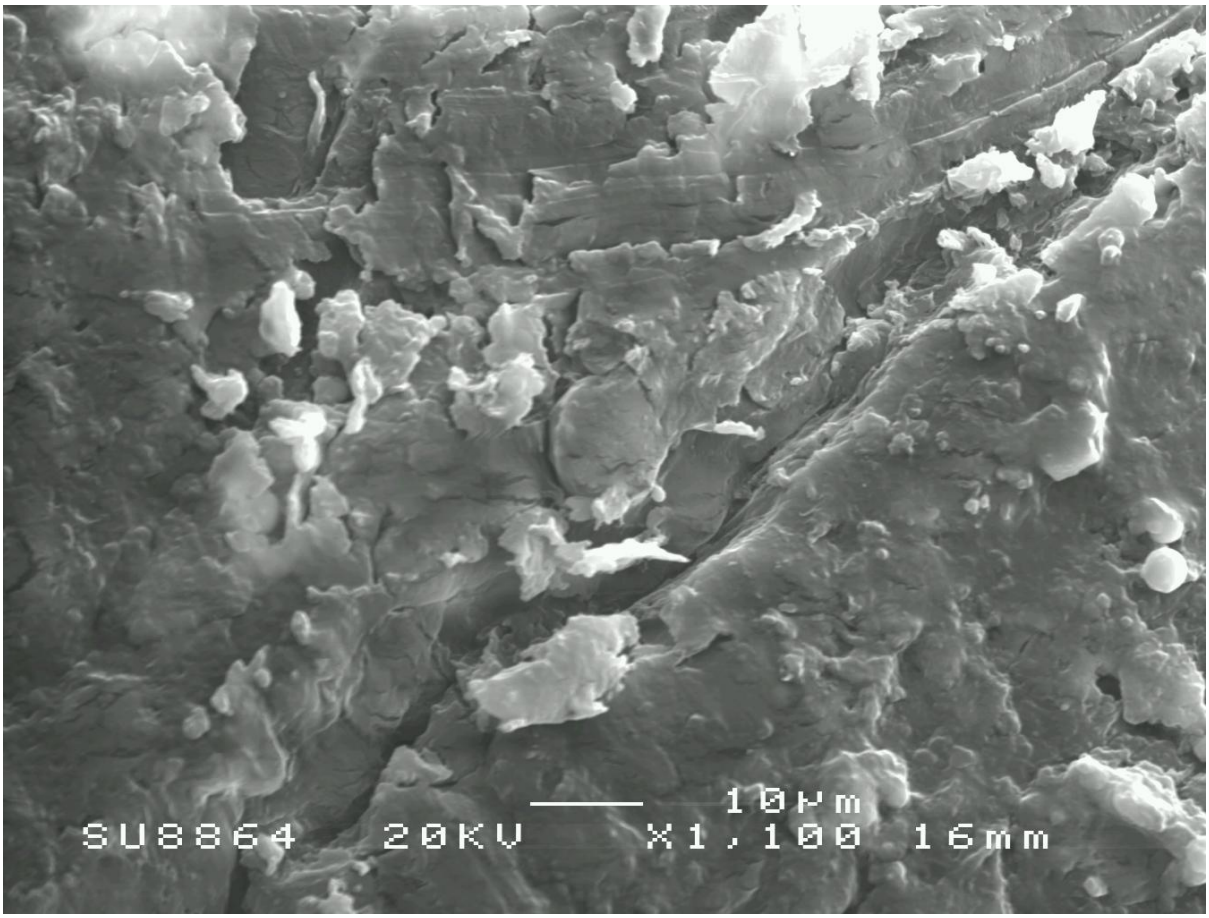

Figure 51 SEM image of polished grain at a scale of 10 µm

4.1.2 SEM of grain cross sections

Following the examination of brown and polished grains using scanning electron microscopy, grains have been carefully cross sectioned to be examined. The grains have been cold set into epoxy resin, ground and then finely polished. As above, the grains have then been gold coated before being placed into the SEM in order to increase their electrical conductivity.

The image below (Figure 52) shows an overview of the grain cross section. Clearly visible are the epoxy medium used to set the grains (left and right edges) along with the husk (with visible rippled texture). The grain itself appears uniform aside from a single internal fissure, and the various bran layers are visible surrounding the grain.

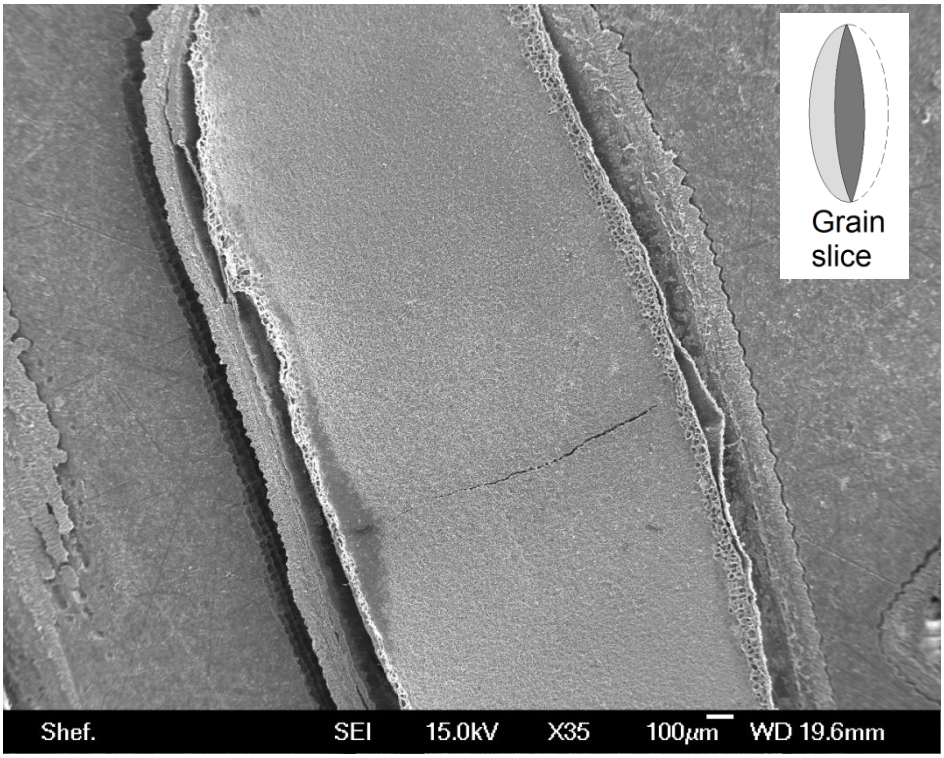

Figure 52 Grain cross section SEM

The inner most bran layer (aleurone) exhibits a different structural network to the pericarp layers.

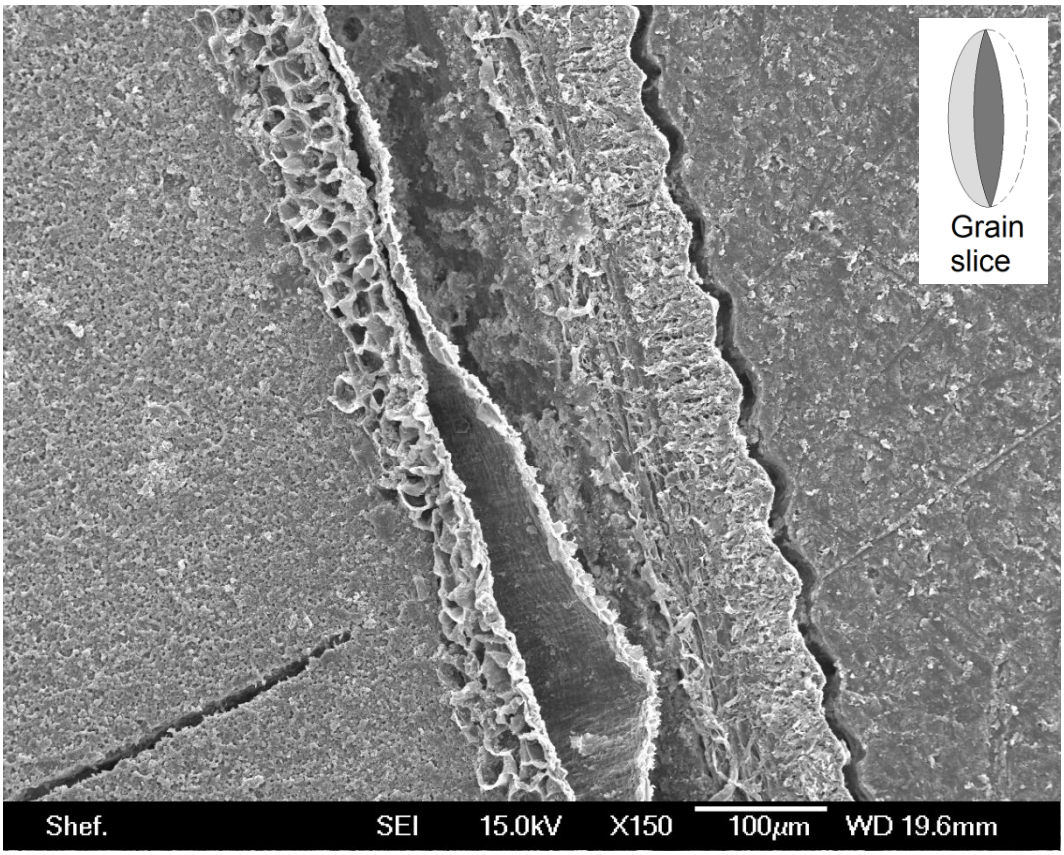

Figure 53 Grain cross section SEM showing (left to right) kernel with bran layers (aleurone and pericarp) and husk

The above image (Figure 53) shows the delamination of the pericarp bran layer from the aleurone layer. The pericarp layer is often removed during husking operations.

The slice shown below (Figure 54) intersects the bran layer. It is cut so that the bran layer is effectively visible at various depths (decreasing from left to right until the grain itself is visible). This has been achieved by the angling of grains in the epoxy stub and the cutting and grinding until the radius of the grain allows such a visible bran gradient (akin to looking down onto the grain from above having skimmed the top).

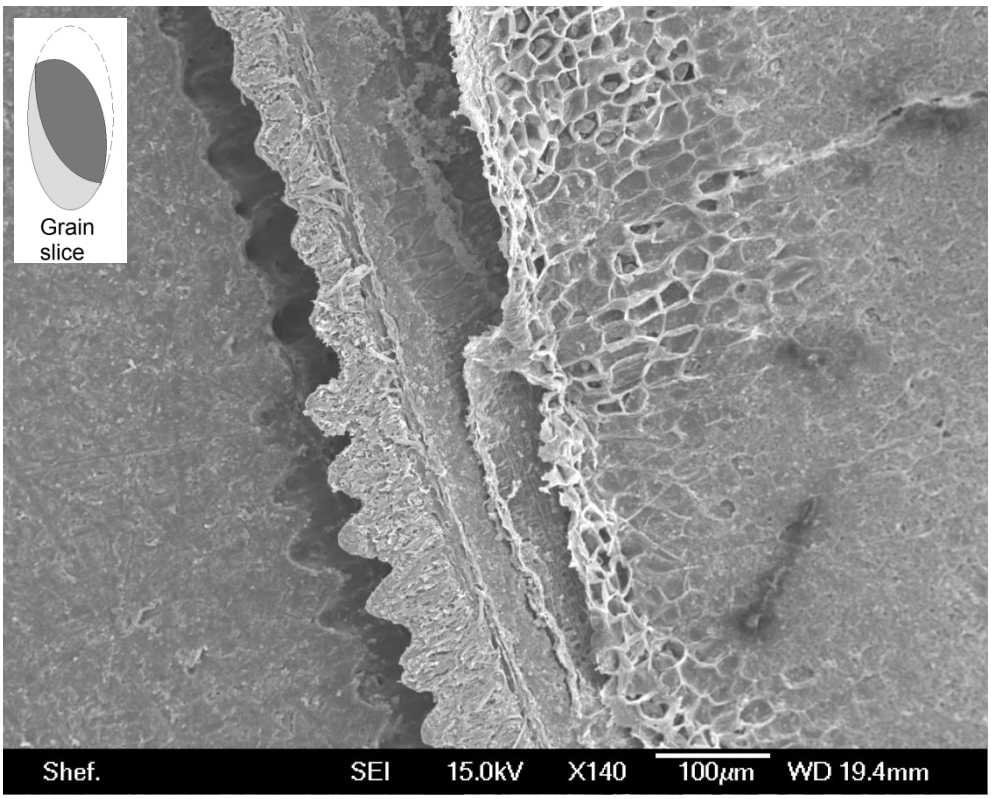

Figure 54 SEM showing husk and bran layer

It is clear that the aleurone layer has a foam like structure which junctions directly with the starchy endosperm. The closed-cell-foam-like structure increases in cell volume relative to the proximity to the endosperm and cells are irregular in shape and size.

This structure could indicate the cause of improved polishing performance with only minimal water addition. If water is absorbed and has a softening effect on the outer bran cells, they may be more easily "burst" revealing a more angular and abrasive surface texture. This would then continue the aggressive polishing action resulting in a higher efficiency of cell destruction. Similarly, further increase in water misting volume would have limited effect and could simply result in making the bran more difficult to disperse as it becomes "tackier".

The aleurone layer has been measured from the images and varies in depth between 50µm and 90µm, averaging 65µm.

Figure 55 and Figure 56 show that the grain husks are highly fibrous providing protection for the developing grain.

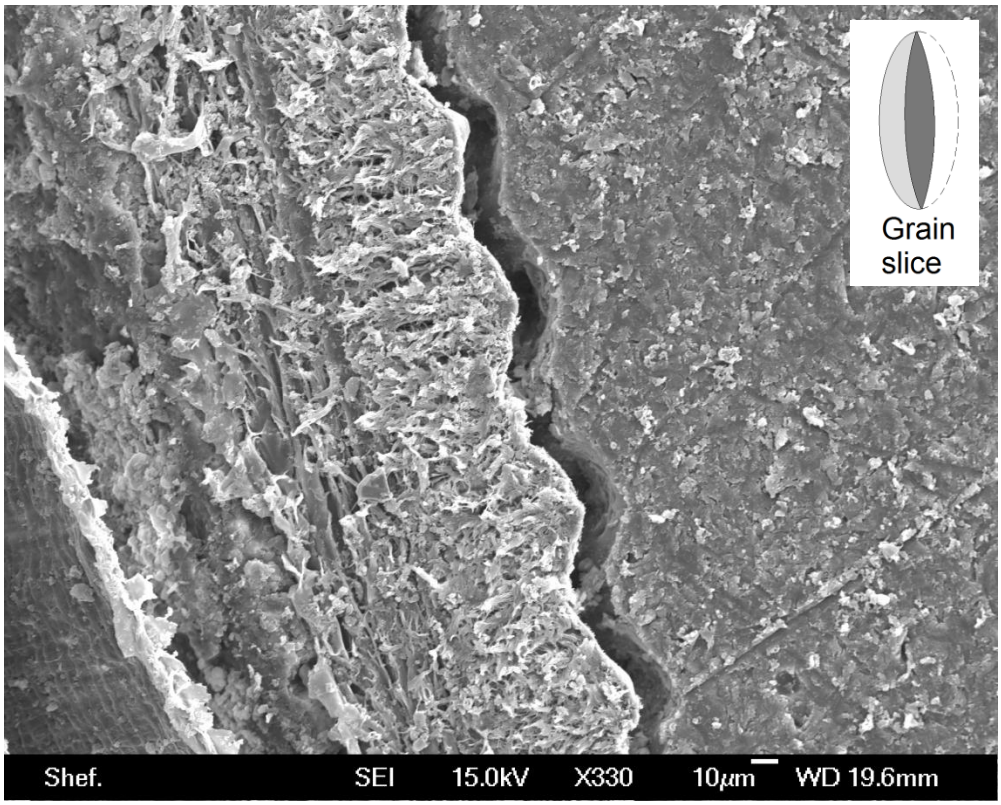

Figure 55 SEM cross section of fibrous bran layer

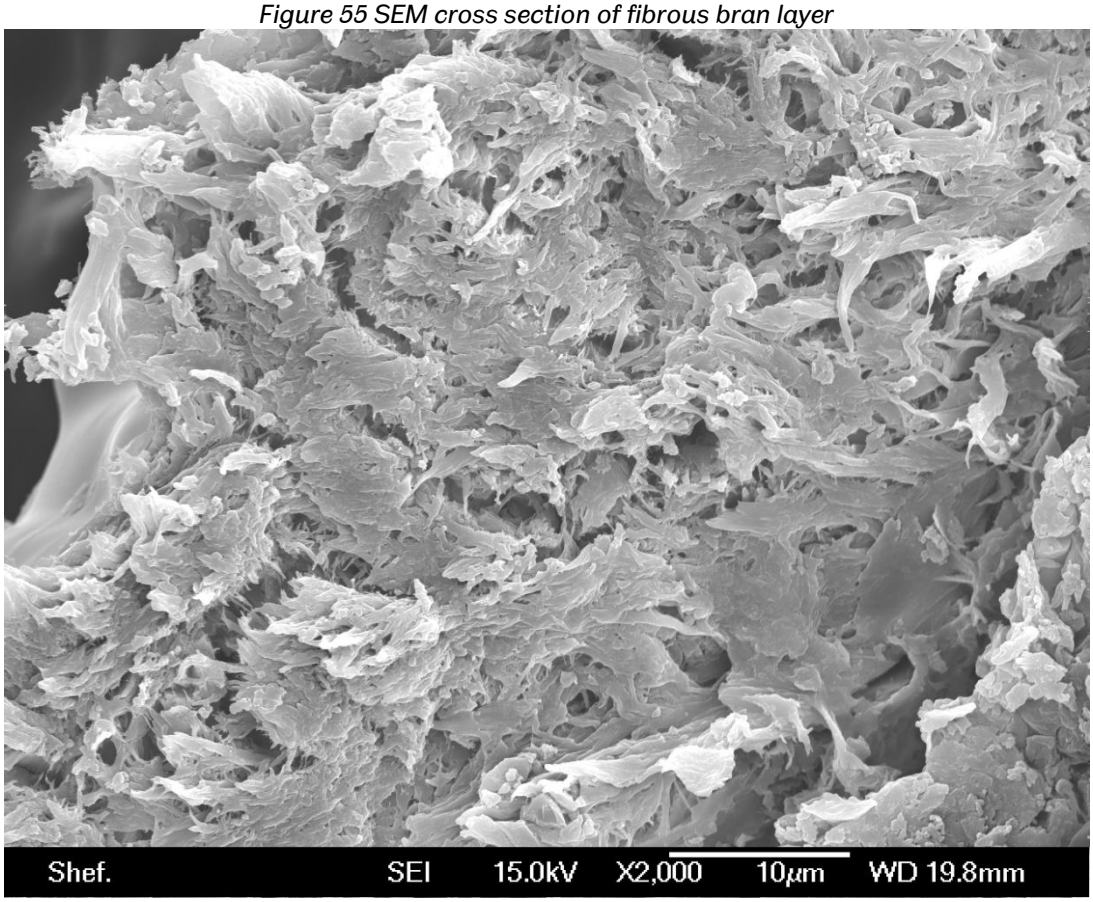

Figure 56 SEM cross section of bran layer at higher magnification

The fibrous mesh of the grain husk gives a three dimensional structural rigidity and a level of elasticity whilst protecting the developing grain from external contaminants and biological threats.

Further, grain ends are seen to have voids which give the developing grain space to grow (Figure 57).

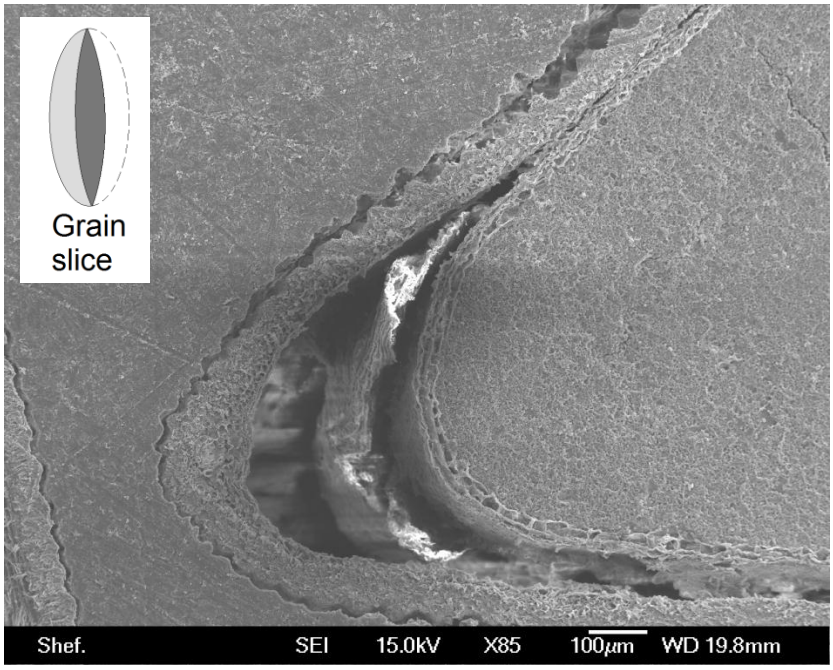

Figure 57 SEM end of grain cross section

By observing the cross section of the grains using powerful microscopy two things are apparent. Grain profiles are again seen to be organic and varied with structures which assist the developing grain (bran layers and husk). Secondly, the nature of the bran layers has been observed clearly, with the often delaminated pericarp and aleurone layers showing different properties. The aleurone layer (which is removed during polishing) has a closed cell foam like structure and it is hypothesised that it is this structure which gives rise to the increase in polishing efficiency with only minimal water misting.

4.2 Analysis of Brown and Polished Grains

The analysis of grains before and after the polishing chamber is significant since a means of determining how successful a polishing operation is has never formally been proposed. Whilst attempts can be made at quantifying a "degree of polishing", millers often disagree over what constitutes a good polished grain. The primary method of determining degree of polish is generally by human touch, therefore relying on the miller's tactile perception rather than a repeatable and reliable representation. Whilst it is known that grains undergo both a textural (tactile)

change and an appearance change during polishing, it is unknown precisely how these relate to the perceived degree of polishing.
The second stage of determining a quantifiable degree of polish, having already observed SEM images of the grains surfaces, is to look at the physical changes occurring to the grain's surface before and after polishing. This involves characteristics such as mass change, surface profile and coefficient of friction of grains.

4.2.1 Mass change during polishing

The mass change during polishing gives insight into the nature of the polishing mechanism. 1000 grains sampled before and after the polishing chamber have been simply weighed using digital scales accurate to 10^{-5}g.

1000 unpolished (brown) grains were found to weigh 13.9809g whilst 1000 polished grains weighed 13.8101g. This represents, on average, a 1.2% reduction in grain weight through the polishing chamber. The material lost, which also evidences itself as a rounding and smoothing of the grain gives rise to the change in appearance and texture.

4.2.2 Grain profiles

A grains surface profile can give a good indication of the textural change occurring during the polishing process. A profilometer has been used to accurately study the rounding effect of polishing. A fine detector needle is drawn across the surface of the grain and as its height changes it logs a position. The experimental set up is shown below in Figure 58.

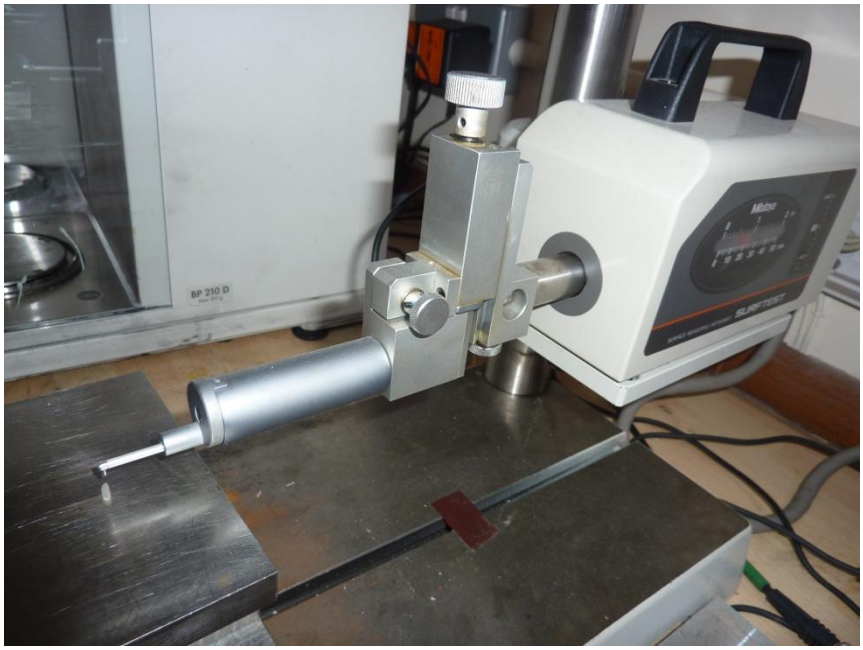

Figure 58 Profilometer set up

The profiles of a single unpolished grain and a single polished grain are shown below (figure 58). The results show a general smoothing of the grain in two different scales.

The ridges seen in the SEM image of a brown grain have been smoothed, but also the surface roughness has been much reduced by the polishing process.

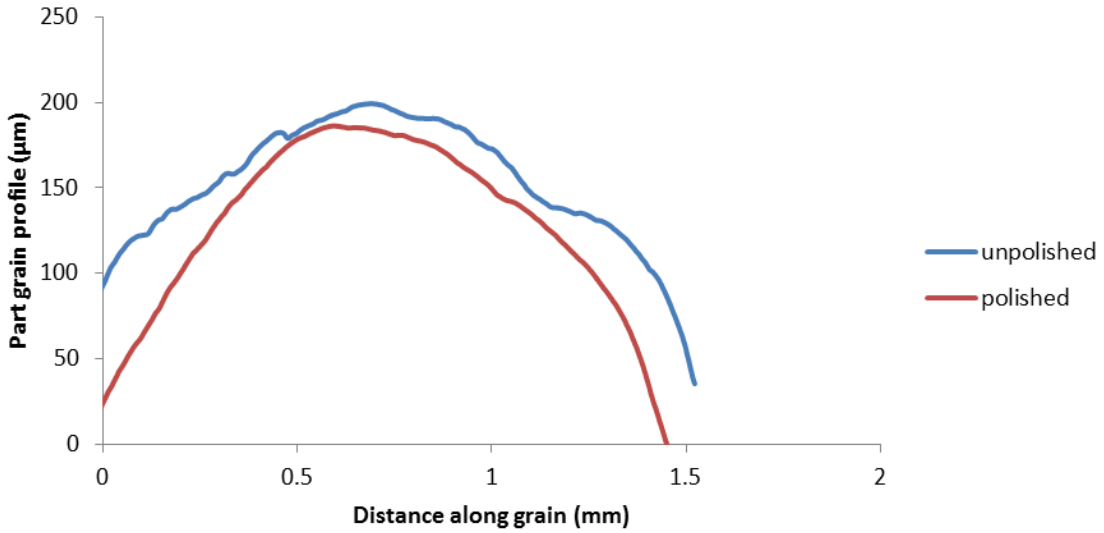

Figure 59 Polished and unpolished grain radial profiles

A large wavelength filter has been applied to the profiles from Figure 59 in order to observe the reduction in roughness by the polishing process (Figure 60).

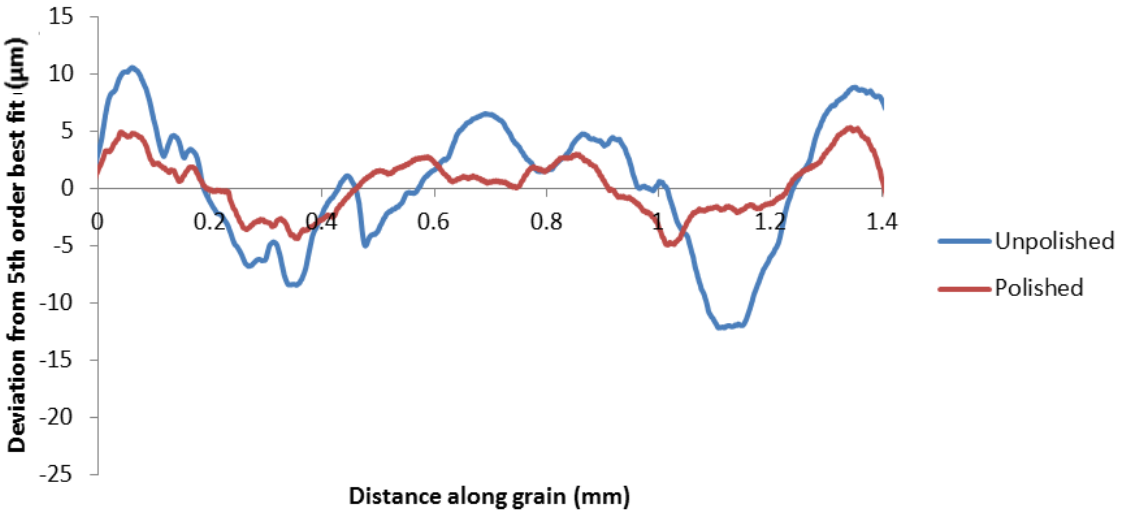

Figure 60 Polished and unpolished grain radial profiles with large wavelength filter

The results help to give an indication of the change in the nature of the grain before and after polishing. The smoothing of the grains will be observed both visually and texturally.

4.3 Coefficient of Friction

The static coefficient of friction of a granular material is approximately equal to the arctan of the angle of repose of a conical pile of the material[58]. This means that if grains are piled up in a conical heap, the static coefficient of friction is found by dividing the pile height by radius of the base of the pile (see Figure 61).

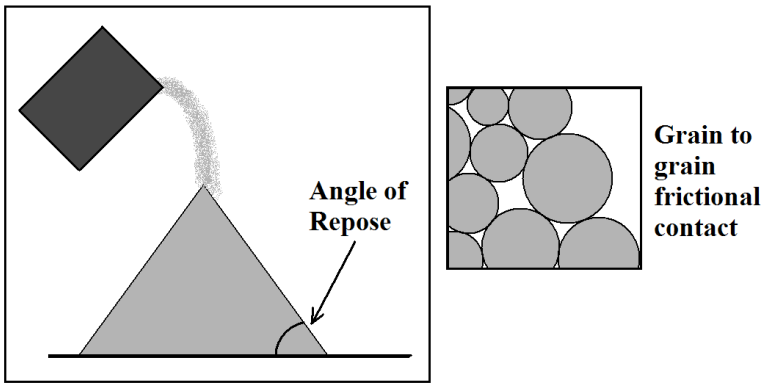

Figure 61 Angle of repose from a conical pile of granular material

Brown grains taken from directly before the polisher were found to have a static coefficient of friction of 0.74 which after polishing was reduced to 0.66. The pile size used is shown below in Figure 62.

Figure 62 Brown rice for angle of repose measurement

4.4 Grain Dimensions

The mean (sample size 100) dimensions of the long grain paddy rice used in this study have been determined to the nearest 0.01mm using digital callipers and are shown in Table 4.

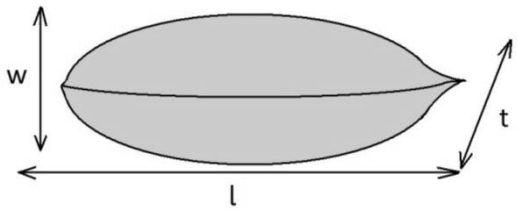

Grain length	*Longitudinal dimension*	*l*	9.45	mm
Grain width	*Dorsoventral dimension*	*w*	2.30	mm
Grain thickness	*Lateral dimension*	*t*	1.89	mm

Table 4 Mean dimensions of a rice grain (long grain paddy)

Figure 63 shows a histogram of the samples lengths to illustrate the spread of the data (Standard deviation of 0.70)

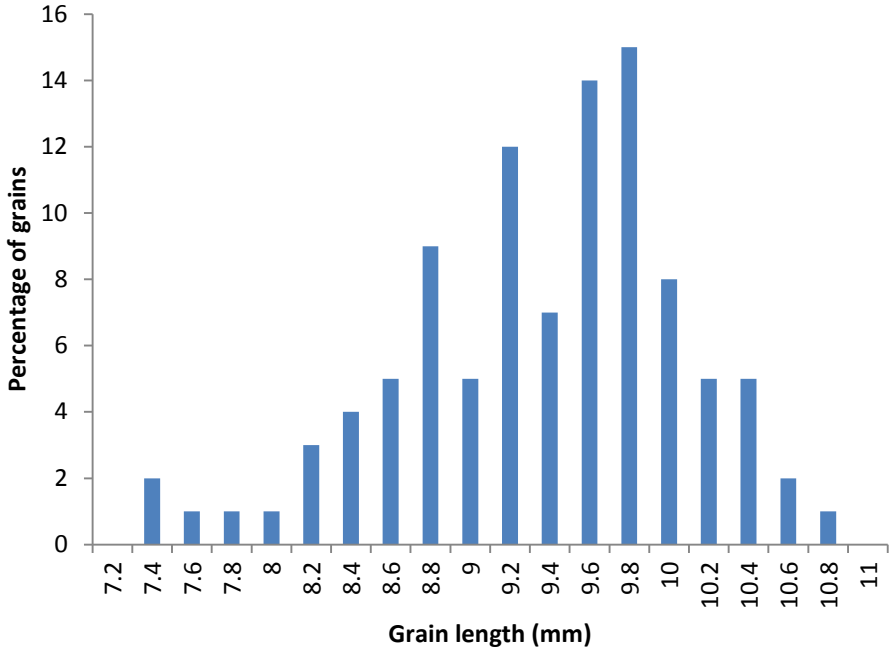

Figure 63 Histogram of paddy lengths from sample of 100 grains

The dimensions of husked brown kernels are shown below in Table 5

Grain length	*Longitudinal dimension*	*l*	7.39	mm
Grain width	*Dorsoventral dimension*	*w*	2.07	mm
Grain thickness	*Lateral dimension*	*t*	1.70	mm

Table 5 Mean dimensions of a husked rice grain used in these studies

Figure 64, below, is a histogram showing the spread of the brown grain lengths.

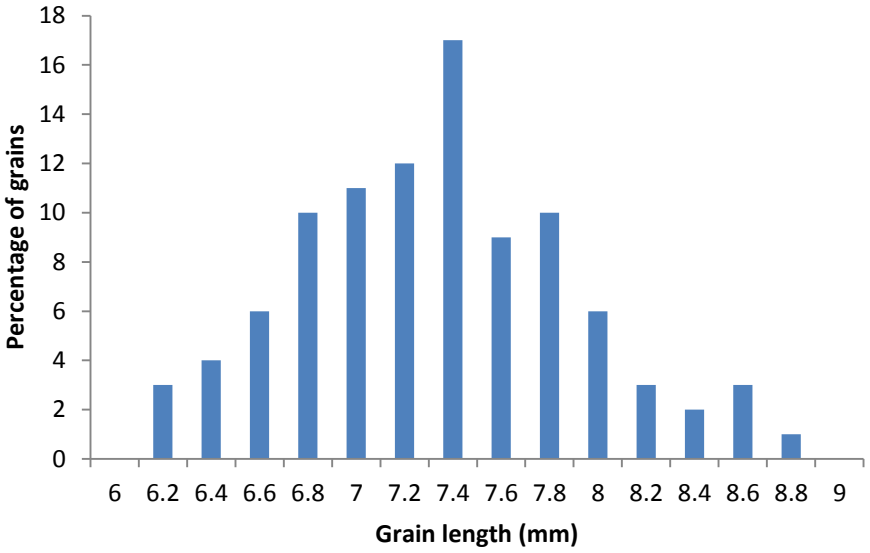

Figure 64 Histogram of brown grain lengths

4.5 Hardness

The hardness of grains is of interest since the hardness of a granular material is often proportional to the wear rate of the surface with which it is in contact[30]. A micro-hardness indent test has been conducted in order to determine the hardness of both brown and polished grains.

The equipment used is shown below (Figure 65), and uses a square diamond tip to imprint the surface at a specified load. The hardness of the surface is determined by measuring the size of the imprint. The softer the surface, the deeper the penetration and hence the larger the imprint.

Figure 65 Micro hardness indent test set up

Averaging 5 readings of grain external hardness indicates that brown grains have lower micro-hardness than polished grains (6.23HV and 7.84HV respectively)

Grains have also been set into a polymer (Figure 66) and ground in order that the micro hardness across the grain can be measured. A metal tie is used so that the grains remain perpendicular to the grinding surface during the hot setting process.

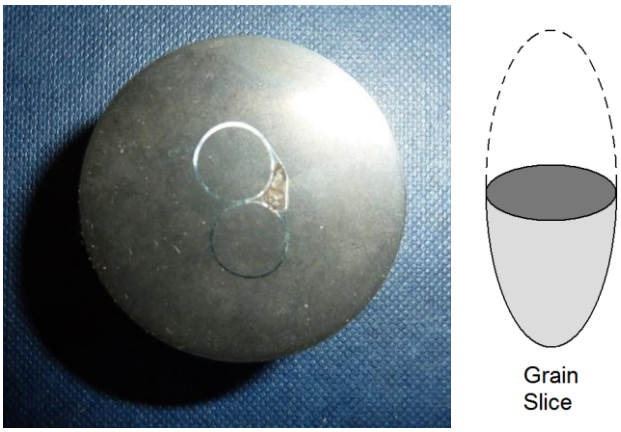

Figure 66 Grains set into polymer and ground to reveal cross section

Some microscope images of the cross section of polished and paddy samples are shown below (Figure 67 and Figure 68). The cells which make up the kernel are visible and the husk can be clearly seen surrounding the grain in the image of the paddy sample.

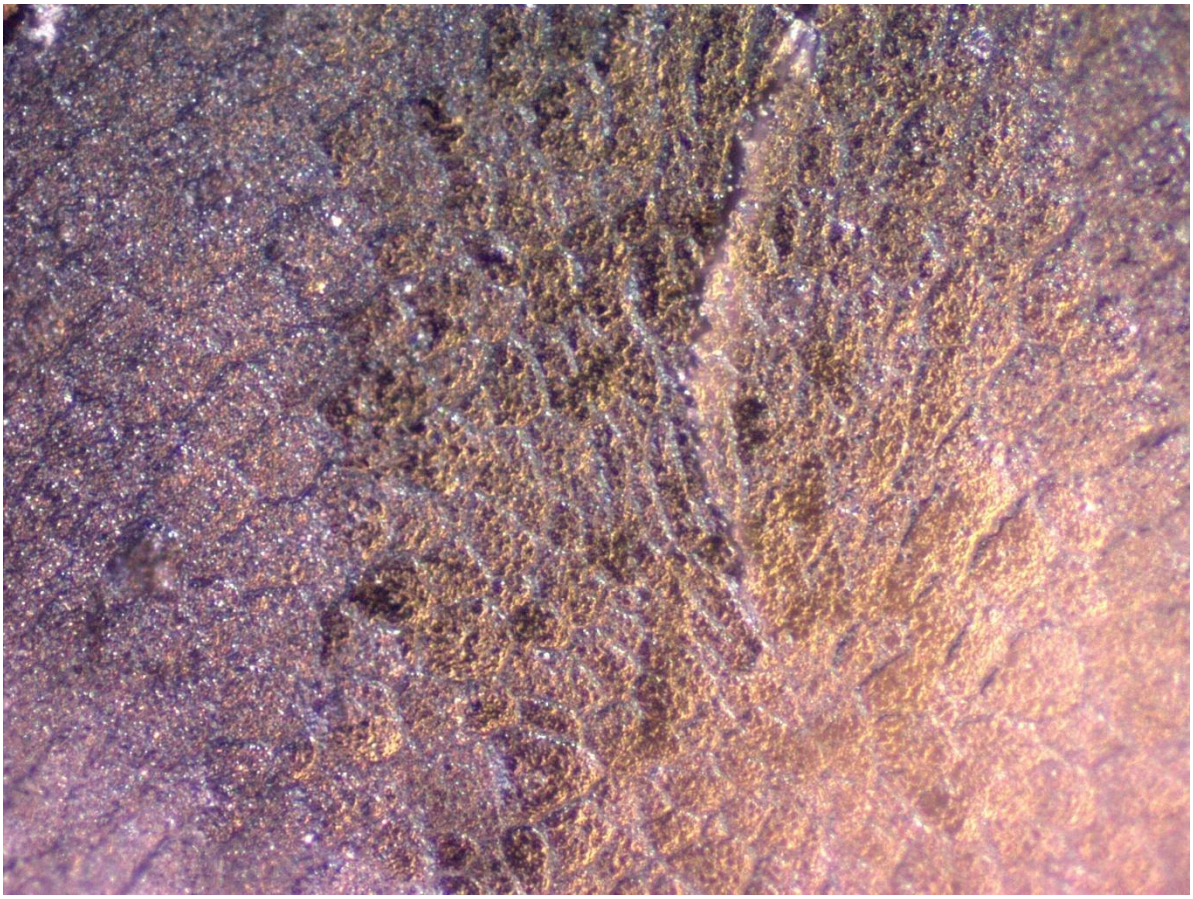

Figure 67 Microscope image of cross section of polished grain

Figure 68 Microscope image of paddy cross section

Some cracking can be seen in the paddy sample cross section. This is most likely an effect of the grinding process used to reveal the cross section. It is not thought that this will significantly affect the properties of the grain.

The micro-hardness of the paddy sample has been measured across the grain width (see Figure 69). Error bars are derived from the difference in the diamond indent's width and height.

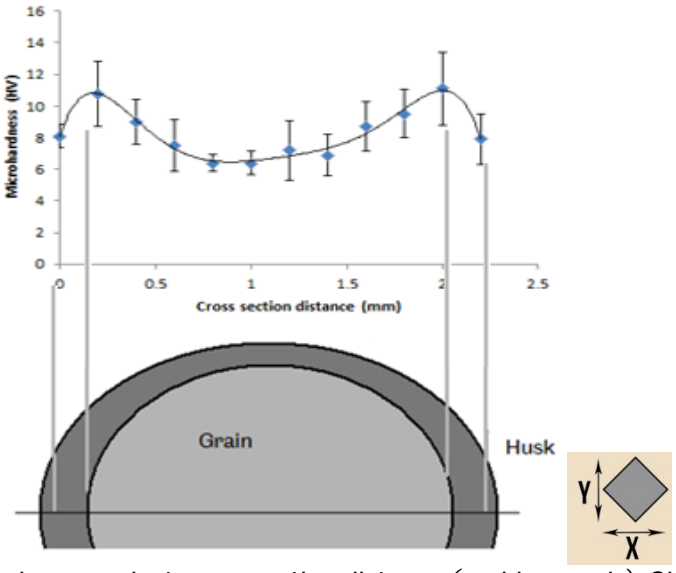

Figure 69 Graph of hardness against cross section distance (paddy sample): Shown underneath is a grain cross section to demonstrate where measurements were made relative to the grain and to the right, the ratio of X and Y gives the error bars.

At either side of the grain, the husk hardness is observed to be around 8HV. The edges of the grain are much harder than the centre of the grain (12HV and 6-8HV respectively). The hardness of the bran cannot be measured in this way since the

layer is too thin to be tested directly. Table 6 shows some hardness data from these experiments. Husk and grain centre are given approximate values due to the errors in measurement from grain curvature.

Grain/component	Microhardness (Hv)
Brown external	6.23
Polished external	7.84
Husk	8
Grain centre	7

Table 6 Hardness data

4.6 Compressive Strength

Since grain breakage is a known problem during processing, it is important to have a basic measure of grain strength to be certain that any machine design does not create an excessive broken percentage. Since it is difficult to directly measure the tensile properties of such particulates, and since the grains are thought to mostly undergo compression during processing (squashing during husking and impact during polishing) the compressive strength properties have been measured.
Compressive properties of grains have been measured using a CETR tribometer (Figure 70).

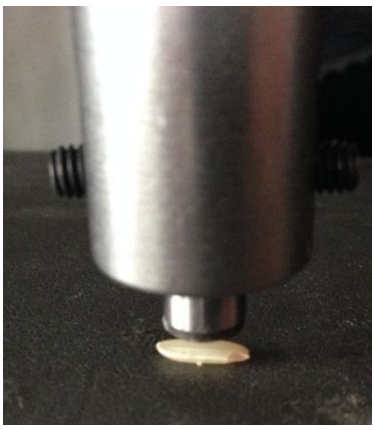

Figure 70 Compression test set up

A script has been written such that a constant displacement is made until the grains reach brittle failure.

The average compressive properties shown above have been made by testing 10 grains. Figure 71 below shows the compressive response of five of the tested grains together for comparison.

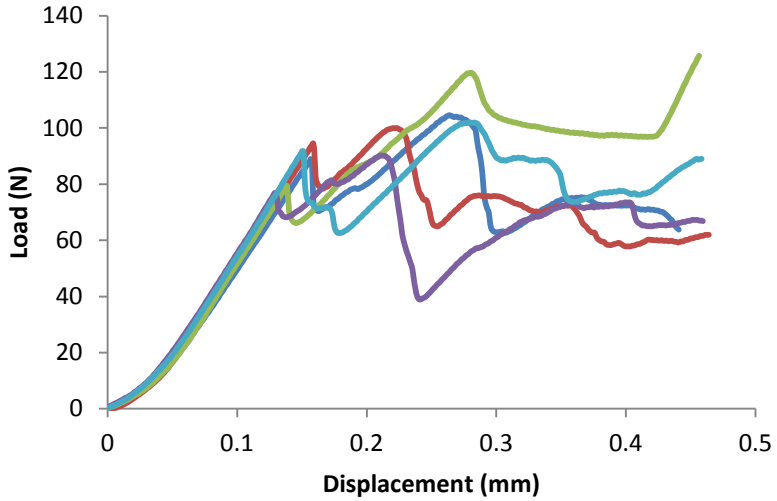

Figure 71 Load against displacement for brown grain compression for five different grains

The results indicate an elastic deformation of grains up to a relatively consistent fracture load (average of 87N with standard deviation 6.5N)

Following initial fracture loading has continued. The loads recorded after initial fracture are often higher but contact pressure is not determinable as the surface of the grain has already been deformed to an unknown degree.
This compressive test has been used to determine grain stress (load divided by area) and strain (change in grain thickness divided by original thickness) and hence elastic modulus (stress divided by strain). The average modulus recorded was 0.46GPa.

4.7 Bulk Density

The bulk density of rice grains is a measure of their ability to fit together. It is an important property, having relevance in the flow dynamics of the grains since it helps to dictate the particle packing observed.
Bulk density is defined as the mass of many particles of material divided by the total volume they occupy. It is not a specific material property since it varies depending on how the particles are handled and is normally reported as “freely settled” and “tapped” density.
The freely settled bulk density of the brown long grain and polished grains have been measured using a measuring cylinder and scales. The freely settled bulk density of the long grain brown rice was found to be 757kg/m³ whilst that of the polished grains was 774kg/m³. Whilst only a small difference it indicates a change in one or more other properties including coefficient of friction, grain mass or particle size. Since individual grains are not found to increase in density, an increase in bulk density during polishing means that grains pack more closely due to a change in either friction coefficient or particle size.

4.8 Poisson's Ratio

In a 2010 paper published in the Spanish Journal of Agricultural Research [59] , Kibar et al. determined the poisons ratio of an Oryza Sativa variety of rice grain for various moisture contents by analytical methods, based on equations developed by Qu et al[60] based on angle of internal friction φ.

Eq 1.

$$\upsilon = \frac{1 - \sin\varphi}{2 - \sin\varphi}$$

Their results show a marginal linear decrease from 0.335 to 0.315 from increasing moisture contents of 10% up to 14%. As such, a value of 0.33 is used for grain poisons ratio throughout this thesis.

4.9 Conclusion

The various physical properties give a good insight into the mechanical changes occurring to the grain by polishing operations. Grain mass decreases on average by 1.2% during the polishing process due to the rounding of grains and removal of bran. The coefficient of friction is reduced by 11% whilst the micro-hardness of the grains surface is increased from 6.23HV to 7.84HV by polishing. It is likely that the increase in micro-hardness is an effect of the work hardening of grains caused by the impact of the grains against one another. The compressive force required to fracture a grain was found to be 87N with average modulus of 0.46GPa.
The bulk density of the grains also increases with the polishing process from 757kg/m³ to 774kg/m³. This is most likely due to the reduction in coefficient of friction and the smoothing of grains allowing them to pack together more tightly.
It is very difficult to suggest one method by which polishing efficiency is determined since it is the combination of these various properties that give an indication of the degree of milling of a rice grain.

The various properties have been studied for one particular variety, which is thought to reflect rice in general though there may be exceptions within the vast number of varieties that exist.

5 TRIBOLOGICAL ANALYSIS OF RICE MILL COMPONENTS

Since rice is an abrasive material, the wear life of components which come directly into contact with it presents a serious operational issue. The flow rate of the grain changes depending on variety but is usually between 3 and 8 tonnes per hour[18] and the expected roller life would be somewhere between 40 and 100 tonnes[8]. There are a number of variables which will affect roller wear which are explained in this chapter along with known mechanisms involved in the husking of rice grains. Wear mechanisms of various components are analysed and compared with known wear mechanisms to develop a more complete understanding of the nature of rice as an abrasive.

5.1 Rubber Roll Husker Wear

5.1.1 Wear Observations

Rubber rollers begin to show signs of wear typically from 10 tonnes to 30 tonnes processed depending on how the machine is operated and the variety of grain. Figure 72 shows worn rubber rollers.

Figure 72 Worn rubber roller[61]

The wear is typical of erosive wear with pitting leading to material removal, although within this case the sliding aspect is enhanced by the pressure of the other roller and the speed differential. It is generally uneven and the roller is eventually left with areas which will husk more effectively than others. Roller parallelism is in fact the limiting factor in roller width as with increasing wear the roller becomes less efficient at husking[3].

5.1.2 Husking Mechanisms

Little is documented specifically referring to the mechanisms involved in husking rice. Without this in depth knowledge, a full understanding of husker optimisation cannot occur. However, there are certain factors which are known to influence the wear of rubber rollers:

- Roller clearance – which affects the load on each grain.
- Roller parallelism has been noted to be of importance to roller efficiency and this in turn limits the width, and hence capacity, of the rollers. If the rollers are not parallel then the load applied to the rice grains changes along the length of the roller, hence the roller wears unevenly.
- Contact distance
    - Shitanda et al. [62] performed experiments with rubber roll huskers and derived an equation for contact distance based on the radius of curvature of the grain. They used a high speed camera to monitor grain

motion and an empirical relationship was found to give a better indication of contact distance than previous equations.

- Roller dimensions [6]
- Angular speed of the rollers [6]
- Ambient conditions
- Other factors
    - Rubber hardness
    - Rubber thickness

Initial hypotheses suggest that perhaps an increase in rubber conformity would yield an increase in husked ratio, requiring a lower energy input to obtain a given husked ratio.

5.2 Rice Polisher Wear

The components of the rice polisher (Buhler DRPF[20]) have been analysed and any wear observations noted. Some components are more prone to wear than others and these have been given more attention. Generally, the components which wear most quickly are designed to be replaced easily, most notably the polisher screens. The current life span of a screen is around 2-10 weeks of continuous usage, dependant on amount and variety of rice passing through and the usage of water (which can as much as quarter the screen wear life). Also, the 4 screen half shells are often rotated to even out the wear across the whole machine.

5.2.1 Wear Observations

Wear of the polisher screens can ultimately lead to catastrophic failure once the material becomes too weakened to support the pressure of the grains inside (see Figure 73).

Figure 73 Screen catastrophic failure

Some observations of worn screens (pre-failure) can help to indicate the nature of the wear. Various methods can be adopted to this end, such as microscopy and profiling.

5.2.1.1 Microscopy

The image below (Figure 74) shows the wear patterns occurring over the majority of the screens.

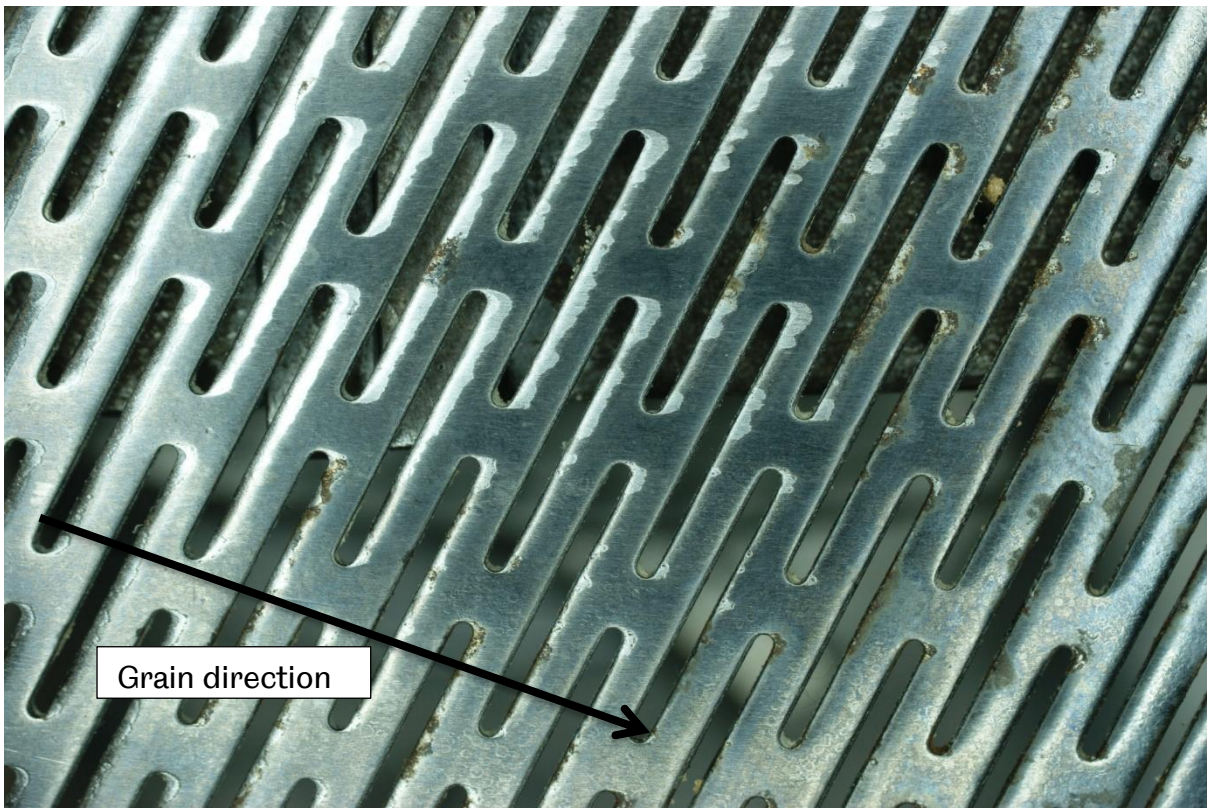

Figure 74 Polisher screen with worn slot edges

Part of the surface treatment has worn away, and this represents the beginning of the failure of the screen. Rice movement is from the left of the image to the right, so it is the trailing edges of the slots which show the highest levels of wear and rounding of edges. It can be seen that on the trailing edges of the slots, the surface treatment has been entirely removed. The leading edges tend to remain much sharper, showing little sign of wear. This wear pattern is consistent with the flank wear seen in cutting tools[63] (see Figure 75) although the cratering wear is generally not seen until the treated surface has been fully removed.

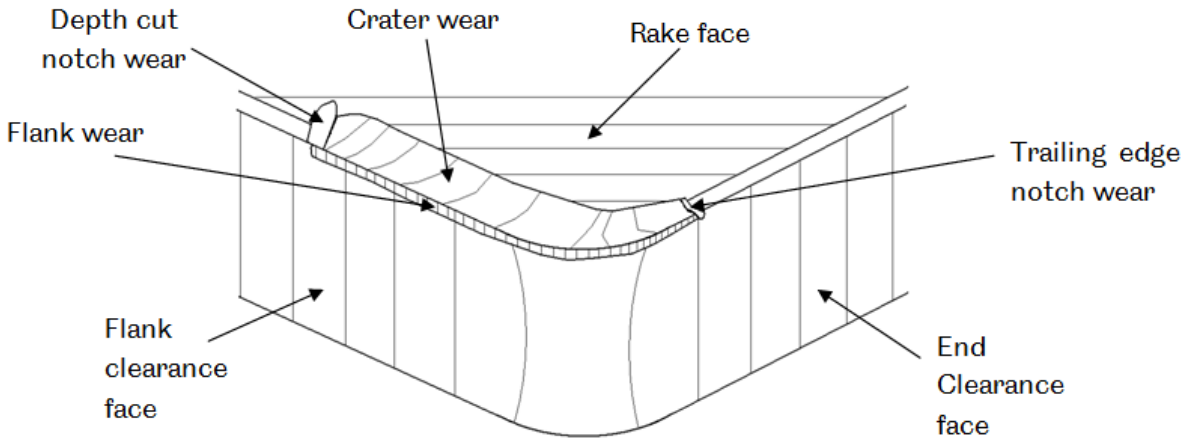

Figure 75 Principal wear zones on a cutting tool

A microscope has been used to observe the screen wear in detail. The three images below (Figure 76-Figure 78) show in order an unworn slot, a partly worn slot in which some surface treatment is still present and worn slots in which the treated surface has been entirely worn away. In each case, the direction of rice motion relative to the slots is from bottom to top of the image.

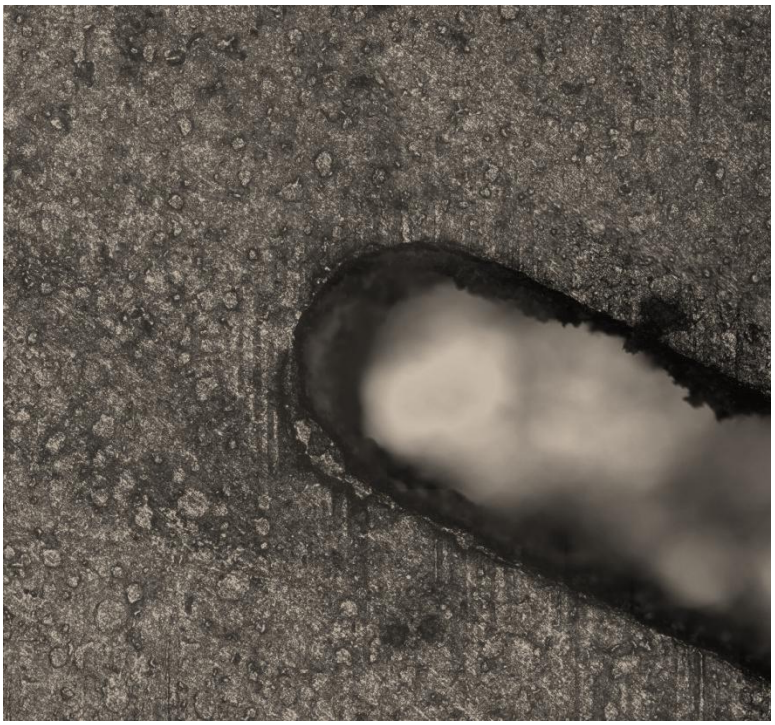

Figure 76 Microscope image of unworn screen slot

Figure 77 Microscope image of part worn slot

Figure 78 Microscope image of worn slot

The rounding of the trailing slot edges can be seen clearly. The surface treatment failure is also clear and shows signs of erosion by the grains. There are a number of long scratches which indicate abrasion by individual particles on the micro scale. These scratches indicate the direction that the rice was moving whilst in contact with the screen. When the mean angle of these scratches is taken, it can be used to analyse the motion of the rice throughout the machine.

5.2.1.2 Scratch direction

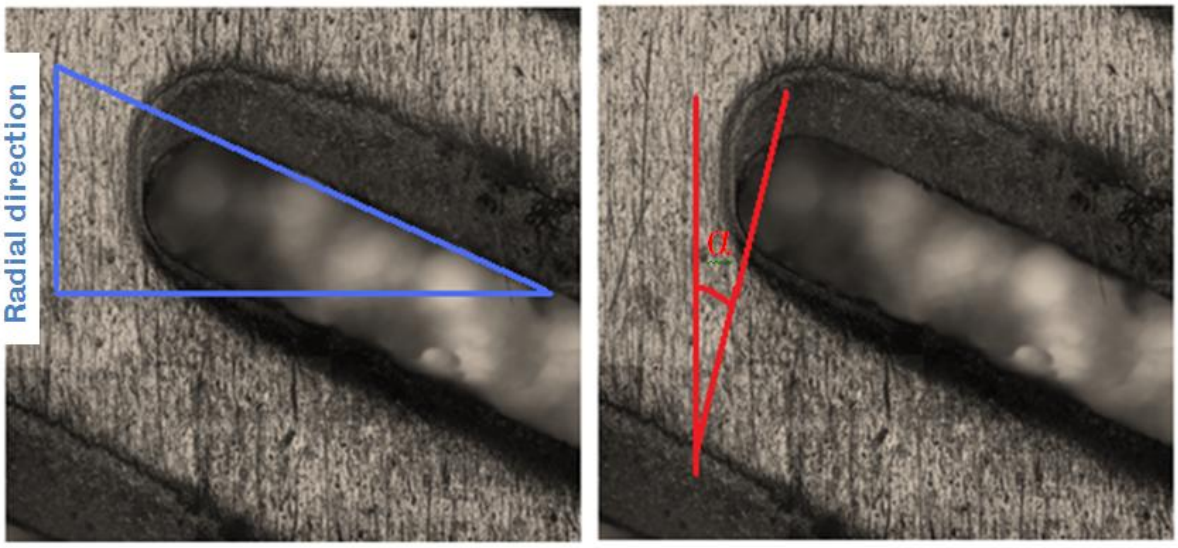

Figure 79 Scratch angle measurement showing slot alignment to screen radial direction (left) and scratch angle (right)

The scratches are measured relative to the screen slots and then corrected to align the measurements with the radial direction as shown in Figure 79. A positive angle indicates that the scratches tend towards the outlet whilst a negative angle indicates the opposite.

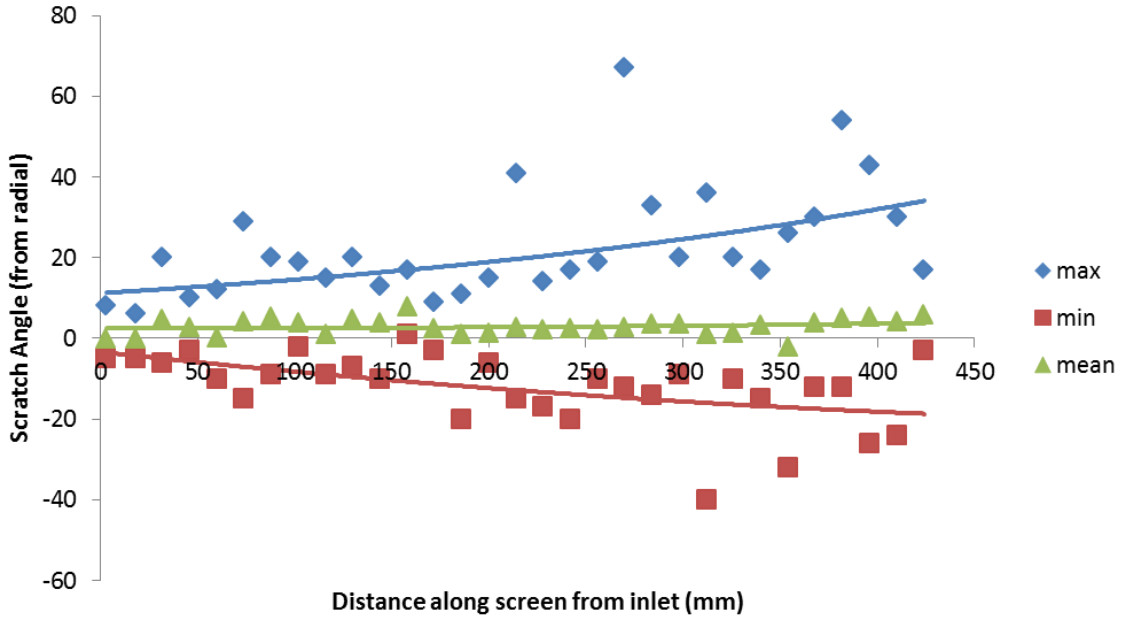

Figure 80 Scratch direction from radial along length of polisher

These measurements (Figure 80) indicate that the motion of the rice becomes more turbulent the further down the polishing chamber. The effect is most likely due to the effective pressure difference along the length of the polisher. At the outlet, the effective pressure of the granular medium drops and the rice is scattered non-uniformly.

Below are some further microscope images showing the nature of the worn surface treatment.

5.2.1.3 Surface treatment wear

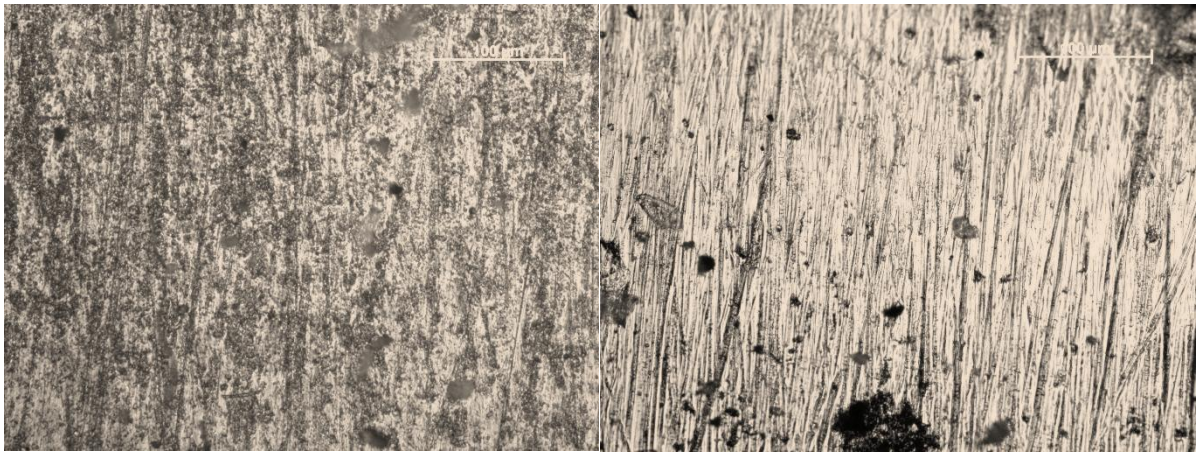

Figure 81 Surface treatment wear: surface remaining (left) and completely removed surface (right)

The treatment under a microscope (Figure 81) shows signs of scratches and pitting though these are much more pronounced once the surface has worn away. The deeper scratches of the untreated surface are the result of the difference in hardness between the surface treatment and the base metal.
In areas where the surface treatment transitions, there are strong signs of erosive wear as seen below (Figure 82):

Figure 82 Surface treatment failure (surface remaining on bottom left side of image)

5.2.1.4 Wear Pattern Profiling

A profilometer has been used to observe the screen deformation caused by the abrasion of the rice grains. Several portions of the screen have been observed, notably the areas where some of the surface treatment remains intact (see

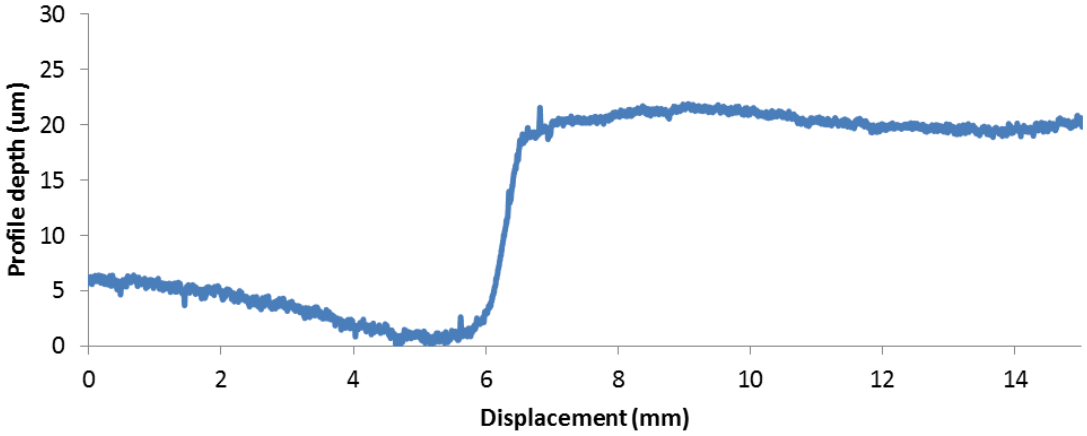

Figure 83).

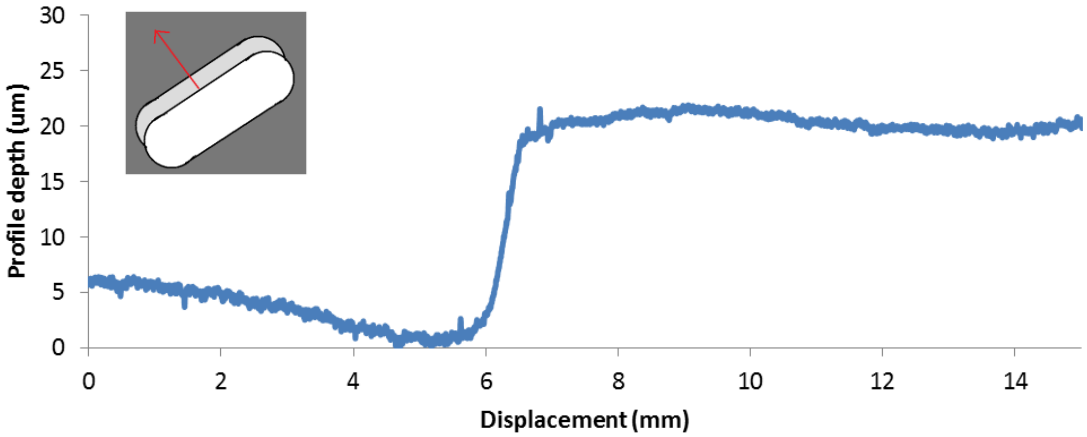

Figure 83 Profile of part worn screen showing the location of the measurement relative to a slot

The above images strongly indicate erosive wear of the screen. Once the treated surface has worn away, the base material wears much more quickly leaving protrusions of surface treatment. This process is similar to the mechanisms involved in waterfall formation whereby erosion of the softer layers of rock underneath harder top layers forces the retreat of the falls upstream[64].

5.2.1.5 Profile of Screen Slots

The same equipment has been used in order that the profile between slots can be observed and compared along the length of the machine. Figure 84 shows a comparison of slot profiles along the machine length (separated for clarity).

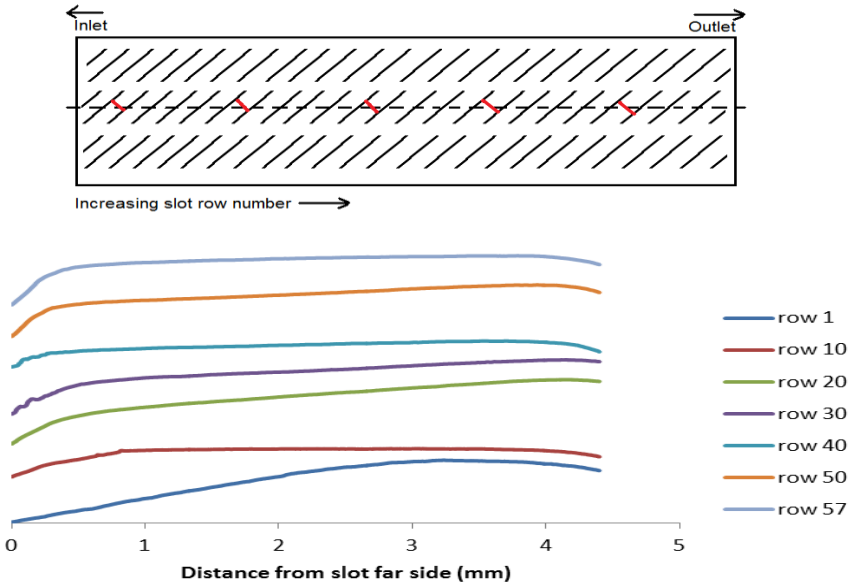

Figure 84 Comparison of slot to slot shape along length of machine (rice flow left to right) showing how locations have been selected above

The above profiles indicate that there is a larger rounding effect towards the inlet of the machine. All profiles indicate some degree of flank/crater wear but it is more prominent between slots towards the inlet. The mechanism of wear is unlikely to change down the length of the machine so it must be assumed that the above profiles represent a timeline of wear until catastrophic failure.

5.3 Conclusions

The factors affecting the husking performance of a rubber roll husker cannot be fully understood until the underlying mechanisms involved in husking are known. The wear observed in the rollers is characteristic of erosion with pitting leading to material loss. Unevenness of the wear leads to the loss of efficiency of the rollers. This means that the rollers must be replaced every 40-100 tonnes of grain processed depending on operating conditions and grain variety.

The most significant wear observed in the rice polisher is that of the screens, most notably at the inlet and secondarily, a rounding action of the slots. The areas seen to wear the most initially also fail first, since once the surface treatment has been worn away, the substrate material provides a much lower resistance to the erosive power of the rice grains.
Whilst material properties may improve and help to increase the wear life of these components, a fundamental understanding of the wear processes involved, along with an understanding of how the grains are polished is essential in order to develop the technology in a meaningful manner.

6 TRIBOLOGY OF RICE HUSKING

Understanding the mechanics of husking and how rubber properties affect performance is very important when considering the wear life and efficiency of the husker. There are still a great many things unknown about the fundamental mechanisms of husking and this chapter attempts to fill some of those gaps. The two main approaches adopted provide a means of small scale testing using both cuts of rubber materials and a lab scale husker. The objective of this chapter is to define the loading conditions that dehusk rice grains.

6.1 Small Scale Test

Producing full scale rubber rollers is a costly inefficient way in which to conduct testing. Thus, test procedures have been developed which require only a small quantity of rubber material yet demonstrate the principals involved in husking clearly. A coupon test scheme allows small quantities novel rubber materials to be acquired and tested much more rapidly than otherwise possible.

Husking using coupons of rubber material simulates the shearing action of the rollers and allows a much greater control over the linear speed ratio of the rubbers and the pressure applied in order to husk the grains.

This method has been used to determine both the nature of the mechanism of grain husking and to identify the major properties required to ensure efficient grain husking as seen below.

6.1.1 Fast Capture Imaging

A fast capture camera has been used to observe the husking of grains. Individual grains have been placed between two small rubber samples and a constant load applied as seen in Figure 85. The lower sample was then moved by worm-driven base plate to which it was mounted in order to create a shearing action and the grain husked.

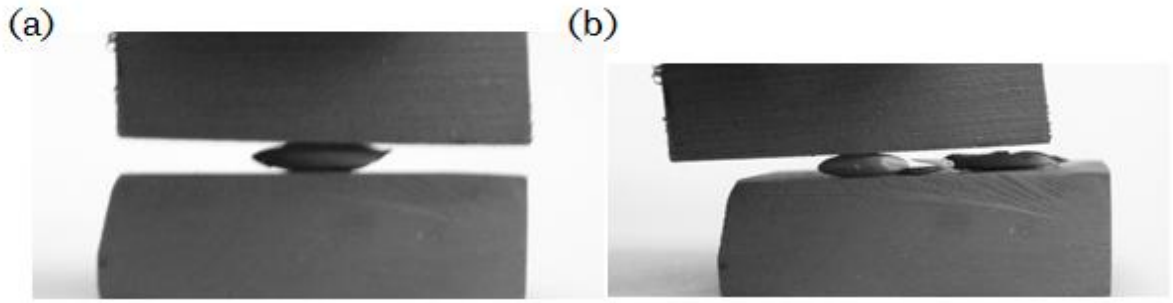

Figure 85 Stills extracted from high speed video footage of rubber samples with grain between, before (a) and after (b) husking

Grains were found to rotate between the samples before husking occurred as shown schematically below in Figure 86.

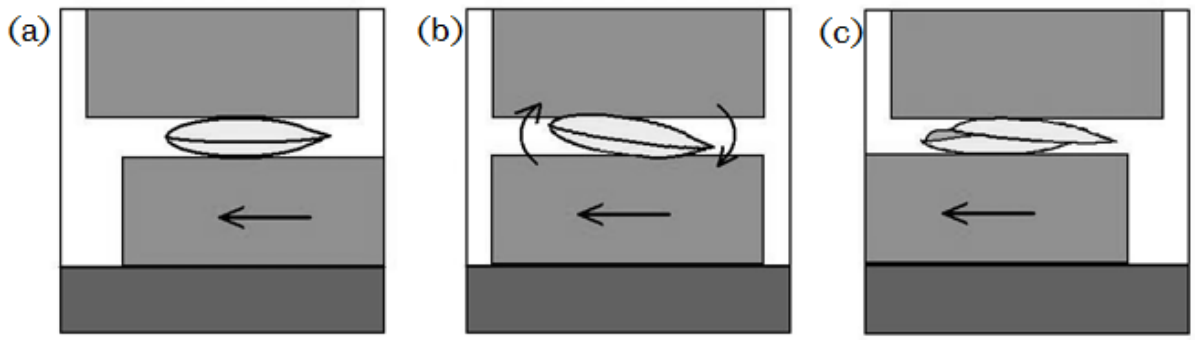

Figure 86 Schematic diagram of the husking mechanism, before (a), during (b) and after husking (c)

This test successfully indicates how grains are husked using this method, leading to the conclusion that grains husk more efficiently when they are allowed to rotate into a position which requires a lower energy to husk.

6.1.2 Rubber Properties

An understanding of various properties of the rubber rollers allows for an attempt at an analytical method of determining the husking efficiency of the material. This has significance, since accurate prediction of efficiency could eliminate the need for a trial and improvement method of rubber selection. The rubbers used in this study came from various sources. Three were selected from those currently in use as commercial roller materials (GRPL T-4, GRPL T-2 and YNOX90), four were Polyurethane (PU) blends which provide a good spread of hardness values (and are labelled by their hardness values), and one was a sample of Food Quality Nitrile (NI65), a material often used in other food applications due to its high wear resistance and thermal stability up to 100°C[65]. The Poisson's ratio for all rubber samples has been estimated at 0.45[68].

6.1.2.1 Elasticity

It is important to demonstrate that the rubbers are behaving elastically (rather than viscoelastically for example) since following models are based on this assumption.
A CETR tribometer has been used to compress rubber samples by 1mm at various rates (0.5mm/s, 1mm/s, 2mm/s, 3mm/s and 4mm/s). A 10mm diameter ball has been used as an indenter and the position and load data captured. Figure 87 shows the load against time for YNOX rubber samples.

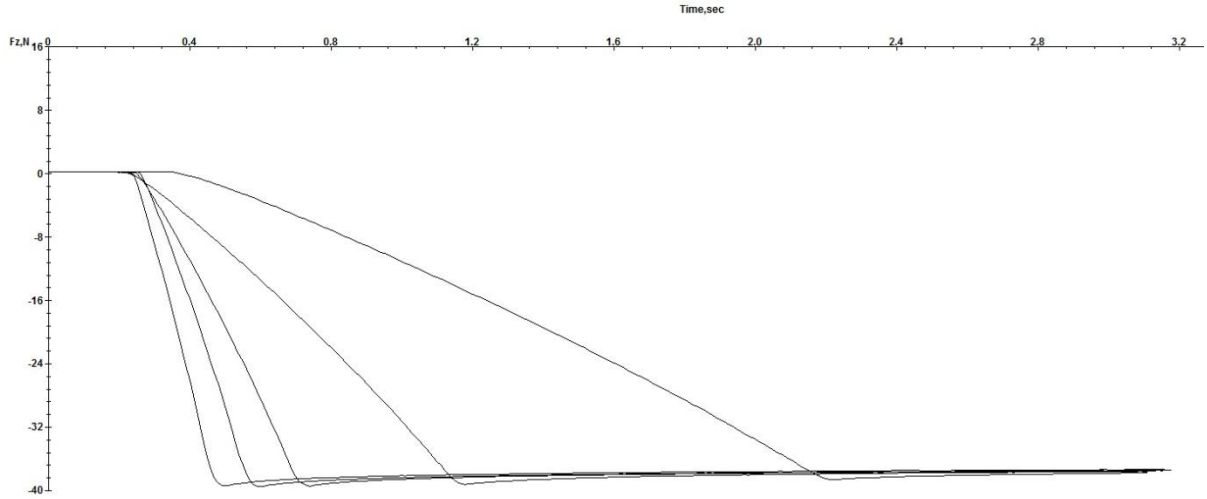

Figure 87 Load against time for YNOX indentation

The various rates of strain can be seen clearly. When the load data is plot against the position, the effect of strain rate on the elasticity of the sample can be seen. This is shown in Figure 88

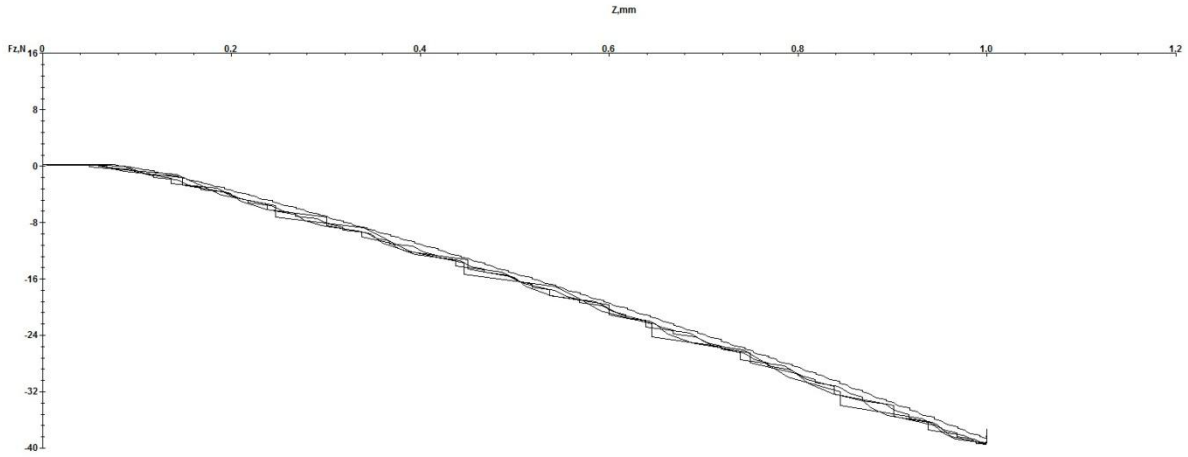

Figure 88 Load against deformation for various strain rates for YNOX rubber

Since the load under increasing deformation is the same for different strain rates, the rubber sample can be said to be behaving elastically. This is true of all of the rubbers tested.

The strain rate can be determined from the rate of change in angle of deflection (d/R) for comparison of these results with the grains in a full scale husker (see Figure 89).

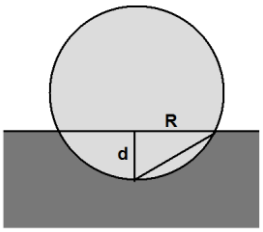

Figure 89 Strain rate at contact region

For the test samples, this is equal to 0.2/s. In full scale huskers, the grains pass through the rollers deforming it much more rapidly (resulting in strain rates approximately 100 times higher). It is uncertain whether the trend in strain rate independence continues into higher rates, however for the purposes of this thesis it is assumed that it does.

6.1.2.2 Modulus

The deformational properties of rubber are generally well understood[65]. Some work had been undertaken to determine basic physical properties of rice[1], [66], [67]. Since rice is an organic material, and the grain size small, it is usually difficult to determine precise mechanical properties though properties have determined for the variety used in this study (see Chapter 4).

Some simple testing was carried out on the rubber samples to determine their elastic modulus. A circular point contact experiment was constructed. A smooth spherical ball was pressed onto the surface of each of the rubber samples under

increasing normal load. The rubber surfaces had been inked so that the contact dimensions could be readily measured. Figure 90 shows the measured diameter of the area of contact plotted against the applied normal load.

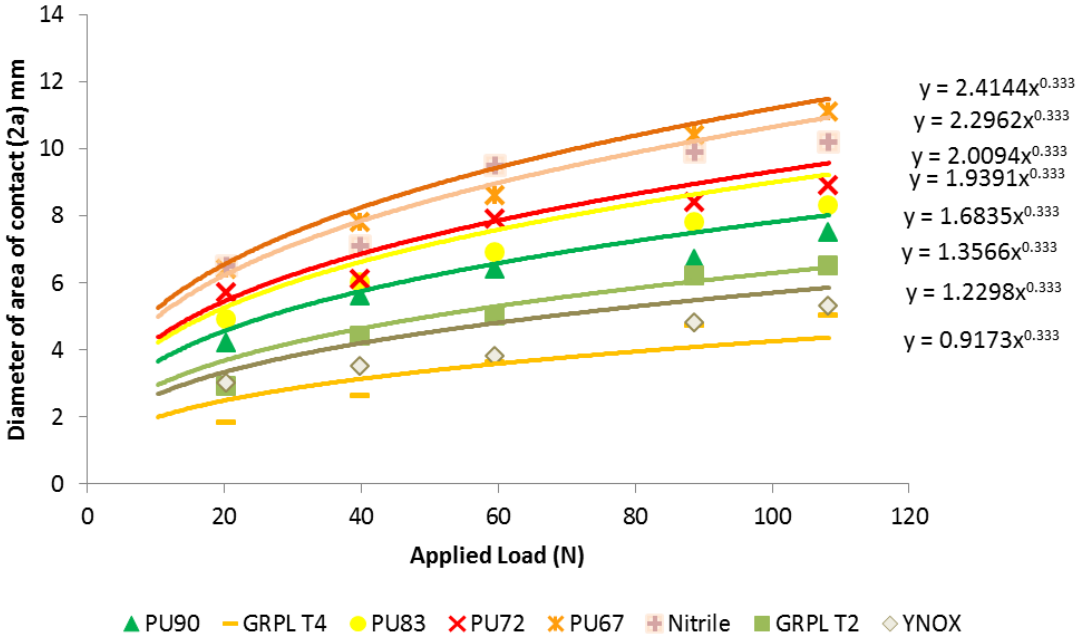

Figure 90 The diameter of the area of contact for a steel sphere pressed against the rubber samples. A power law curve fit is used to estimate the Young's modulus.

The Hertz analysis of elastic contact for a circular point contact [69] gives that the radius of the contact area, a, is proportional to the load P to the power of one third according to:

$$a = \left(\frac{0.75PR'}{E^*}\right)^{\frac{1}{3}} \qquad \text{Eq. 2}$$

$$\frac{1}{R'} = \frac{1}{R_1} + \frac{1}{R_2} \qquad \text{Eq. 3}$$

$$\frac{1}{E^*} = \frac{1-\upsilon_1^2}{E_1} + \frac{1-\upsilon_2^2}{E_2} \qquad \text{Eq. 4}$$

R' and E^* are known as the reduced radius and reduced modulus respectively and subscripts 1 and 2 refer to the rubber material and steel respectively. For the case of a steel sphere pressed against a rubber flat the reduced radius is simply the radius of the sphere.

A cube root power curve ($y=Cx^{1/3}$) has been least squares fitted to the data points of Figure 90. The use of the curve fit constant allows the reduced modulus to be found in equation 4. If the modulus and Poissons ratio of the steel is known then the Young's modulus of the rubber samples can readily be determined.

In addition, the Shore A hardness of each sample was found using a HT-6510A digital hardness tester. For each material, 10 readings were recorded and a mean determined. Table 7 summarises the rubber materials tested.

Sample	Composition	Shore A	Modulus (GPa)
GRPL T-4	Commercial Roller	89	54
GRPL T-2	Commercial Roller	91	17
YNOX90	Commercial Roller	90	22
PU90	Polyurethane	90	8.8
PU83	Polyurethane	83.1	5.7
PU72	Polyurethane	71.5	5.2
PU67	Polyurethane	66.6	3.0
NI65	Food Quality Nitrile	65	3.5

Table 7 Calculated elastic modulus and measured hardness of rubber samples
Calculated elastic modulus and measured hardness of rubber samples

6.1.2.3 Friction Coefficient

The friction coefficient between grains and rubber is significant as it defines the "grip" that the rollers have on a grain in order to husk them. Friction coefficient has been measured using the following apparatus (Figure 91).

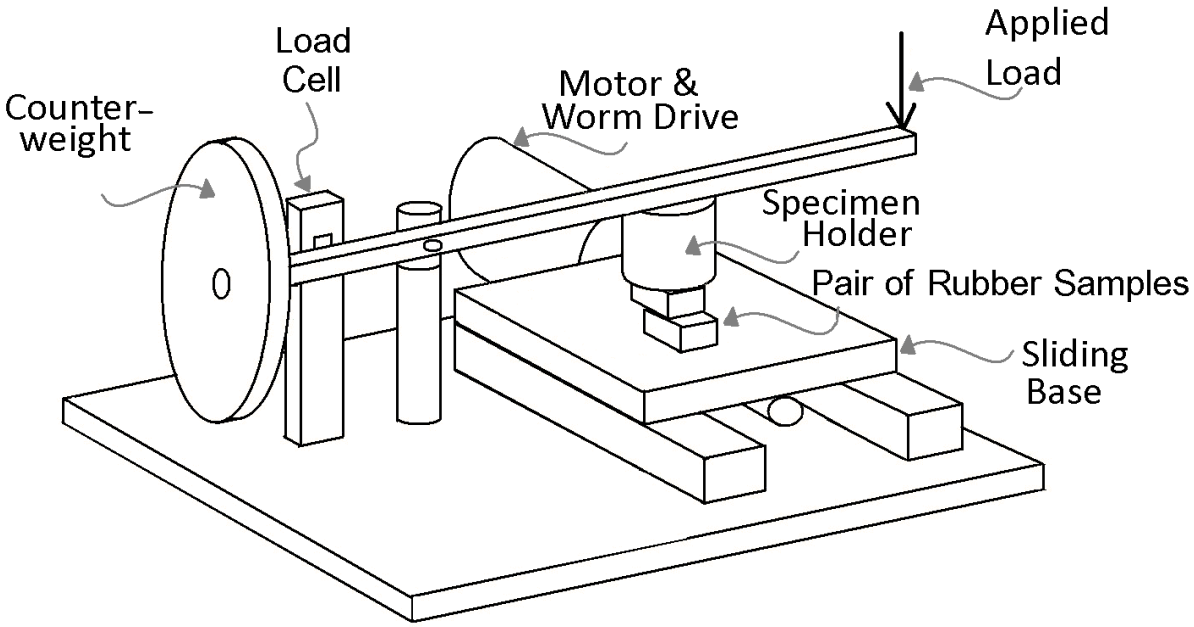

Figure 91 Experimental apparatus for husking and friction testing

A lever arm is mounted on an axis with two degrees of rotational freedom. A load is applied to the end to create the desired load onto the samples, one of which is attached to the lever arm and the other to a sliding base. As the base slides (driven by a motor and worm drive) the samples rub together and the lever arm presses against a load cell. In this way, both the normal force applied, and the resulting tangential force at the contact are known allowing the calculation of the coefficient of friction (by simply dividing the tangential force at contact by the applied normal

force at contact). The calculation is automated by Labview to output friction coefficient data.

To establish the coefficient of friction between the rice grains and the various rubber samples, an array of grains has been glued to a solid block as below (Figure 92):

Figure 92 Grain mounting for friction test

Five measurements were made for each rubber sample. Figure 93 shows some example raw results from the friction tests described above for the rubber samples against un-husked grains, sampled at 20Hz.

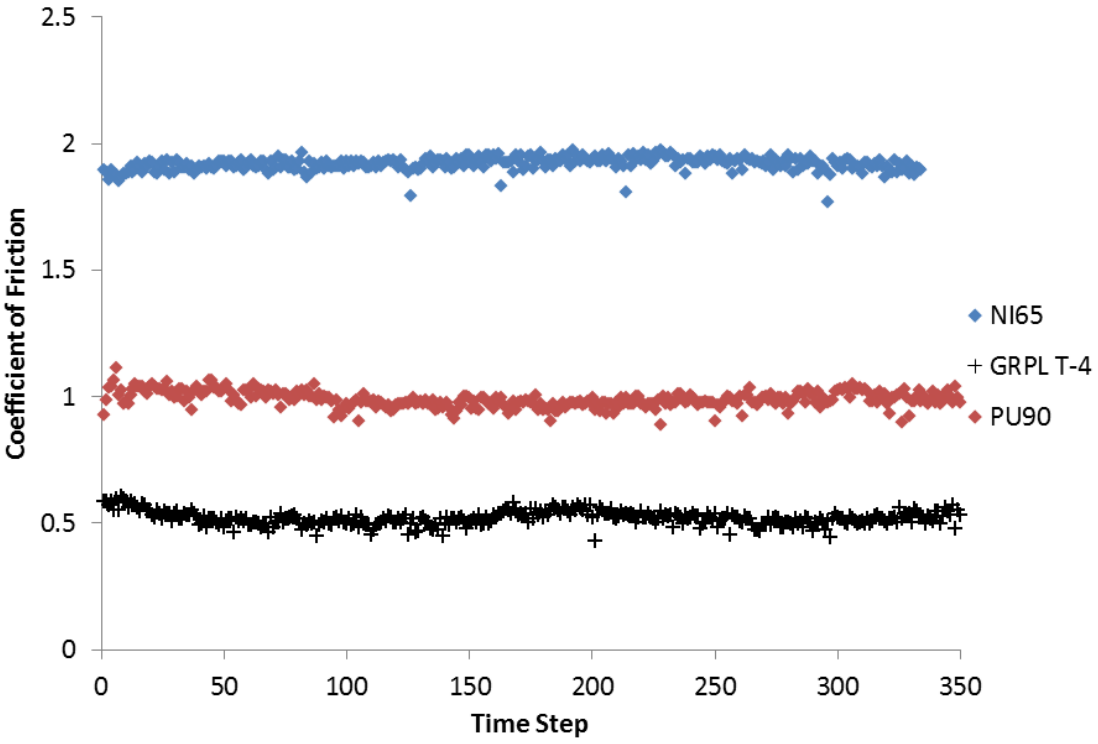

Figure 93 Coefficient of friction recorded as un-husked rice grains slide against for polyurethane samples.

The oscillation in the data is due to the pattern of the rice glued to the block. Table 9 presents this data as an average friction coefficient and a standard deviation. Clearly the selection of rubber has a large effect on the friction between rubber surface and rice grain. The different values indicate varying abilities for the rubber samples to grip the grains and it is thought that a higher coefficient of friction between rubber and grain would provide a more efficient husking process. However, the data shows that the softer rubbers in this study generally have higher friction coefficients. It was observed (Figure 94) that this same group of materials was less efficient at husking grains. It has therefore been concluded that efficient husking is dependent on more factors than simply coefficient of friction.

Sample	Dynamic Coefficient of Friction	Standard deviation
GRPL T-4	0.5	0.10
GRPL T-2	0.5	0.11
YNOX90	0.5	0.10
PU90	1.0	0.05
PU83	0.5	0.08
PU72	1.3	0.29
PU67	1.3	0.09
NI65	1.8	0.10

Table 8 Coefficients of friction for un-husked rice against a range of rubber samples

6.1.3 Load to Husk a Grain of Rice

Individual grains have been husked using the experimental set-up shown in figure 87. The proportion of husked rice grains for each applied normal load is shown in Figure 94 for each of the rubber materials tested. Each data point was the husked ratio determine from 40 grains of rice being tested. The data correlated reasonably well indicating that 40 runs per data point was sufficient to allow a prediction to be made of the load required to husk a certain percentage of grains. It was clear that the higher the load, the more likely a grain was to be husked. The higher the load the more normal and shear loading on the grain and therefore the more likely the husk is to separate from the grain.

There were clear differences between the different rubber materials (as seen in figure 90). Rather surprisingly the softer rubbers tended to be less effective at husking at the same loads than the harder rubbers. The husking process does not appear to require the surrounding material to conform around the rice grain. Indeed for the softest rubbers (PU67 and NI65) the husked ratio did not reach 100%. This is because at the higher loads the rubber samples deform sufficiently such that they conform around the rice grain and contact with each other. The increase in load therefore does not increase further the contact between rubber and rice, but rather

the load is supported by a growth in the rubber-rubber contact area. An ideal situation is one in which the maximum husking ratio is achieved at the minimum load. This means that frictional forces will be low, thus reducing the loss of energy and likelihood of wear.

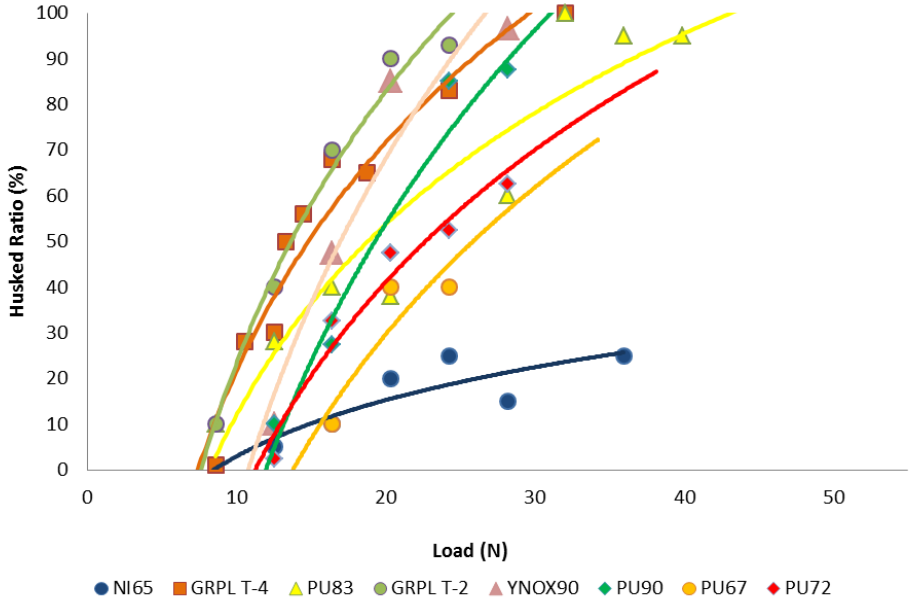

Figure 94 Graph showing husked ratio for various loads and different rubber samples

The data shows that there is clearly a trade-off between modulus and coefficient of friction as seen in Table 9 Rubber properties and husked ratio at a load of 20N to achieve the higher husked ratios.

Material	Modulus (GPa)	Coefficient of friction	Husked ratio at a load of 20N (%)
GRPL T-4	54	0.5	78
GRPL T-2	17	0.5	92
YNOX90	22	0.5	80
PU90	8.8	1.0	60
PU83	5.7	0.5	55
PU72	5.2	1.3	42
PU67	3.0	1.3	28
NI65	3.5	1.8	10

Table 9 Rubber properties and husked ratio at a load of 20N

Figure 95 shows the proportion of rice grains broken or cracked during the husking process. Breakage rates were low at the loads tested here. The softer polyurethane rubbers did not cause any breakages. There is a broad correlation, as expected between breakage rate and applied load. However, the data is subjected to considerable scatter, largely because the sample size is low and also because of the variability amongst the grains themselves.

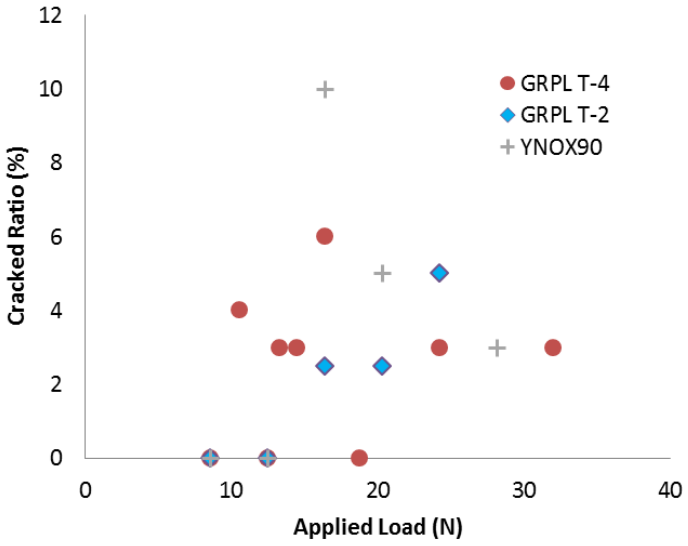

Figure 95 Graph showing proportion of broken grains for various loads and different rubber samples

Shitanda et al.[70] define a specific husking energy as a parameter to define how much energy is being imparted to the rice;

$$Q = 2\mu p \phi_n l_d \qquad \text{Eq. 5}$$

Where μ is the coefficient of friction between rubber and rice (obtained from the data reported in section 6.1.2.3), p is the specific normal force (i.e. the equivalent normal force applied to 1 kg of rice: force per grain multiplied by the number of grains in 1 kg), ϕ_n is the peripheral velocity difference (for the coupon test 50 mm/min) and l_d is the contact distance which was assumed to be the average grain length (9.94 mm).

The husking data for GRPL T-4 from the present tests is presented in Figure 96 with experimental data collected by Shitanda et al.[70] on the husked ratio for rubber roll huskers for long grain rice.

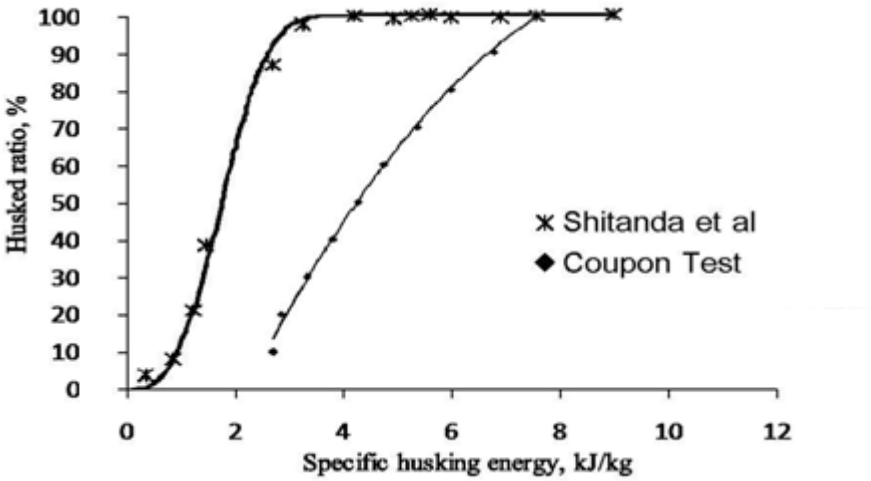

Figure 96 Plot of the rice husked ratio against specific husking energy

Clearly, for both tests increasing the specific husking energy increases the proportion of grains husked. However, the plot shows some significant difference between the coupon husking and the full size husker. The full size machine would appear to be more efficient than the simple coupon test. This could be due to differences in the rubber samples used but also demonstrates perhaps that optimisation of load and speed in a husking machine can save significant husking energy. It should however be noted that the equation used by Shitanda et al is very loosely defined and doesn't include information on rubber type, roller diameter, or rice type which could also explain the differences in husking energies found.

6.1.4 Contact Pressure and Shear Stress

The load applied to the contact between a rice grain and the rubber surface will cause deformation of the rubber and the formation of a region of contact between the surfaces. The extent of this contact region will control the magnitude of the contact pressure and shear stress along the interface. In order to determine these parameters a simple elastic contact model is assumed.

For simplicity, a grain of rice is modelled as a cylinder of length, *l* and radius of curvature, R_{ay} (as shown schematically in Figure 97). This is then pressed against the rubber material to form a rectangular area of contact which then has a length, *l* and a half width, *b*. The Hertz elastic solution for this contact case (1), gives:

$$b = \left(\frac{4\left(\frac{P}{l}\right)(R_{ay})}{E^{*}\pi} \right)^{\frac{1}{2}} \qquad \text{Eq. 6}$$

And the mean contact pressure is given by:

$$p_m = \frac{2bP}{l} \qquad \text{Eq. 7}$$

It is possible to calculate the contact dimensions by assuming the rice grain is an ellipsoid (rather than a cylinder). If this is performed the length of the area of contact is found to extend beyond the length of the grain. This violates Hertz assumptions of small regions of contact relative to the geometry of the body. The contact is therefore closer to a line contact.

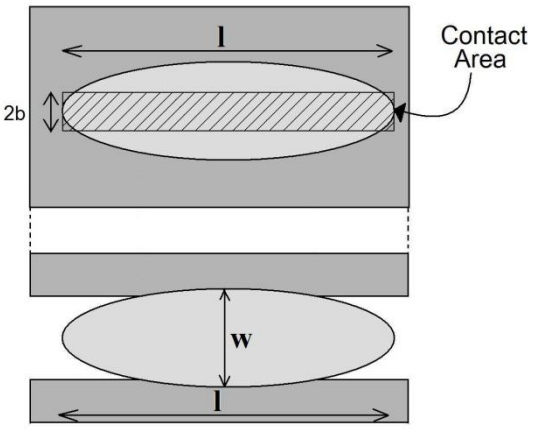

Figure 97 Hertz Line Contact Model

The load to cause both 20% and 80% husking for each rubber material is shown in Table 10. This was used along with the rubber modulii determined from section 6.1.2.1 and the dimensions of the rice grain, to calculate the mean contact pressure for 20 and 80% husking.

	load at 20% (N)	load at 80% (N)	p_m at 20% (MPa)	p_m at 80% (MPa)	τ_m at 20% (MPa)	τ_m at 80% (MPa)
GRPL T-4	9	22	2.92	4.57	1.46	2.29
GRPL T-2	9	20	1.68	2.51	0.84	1.26
YNOX90	13	22	2.33	3.03	1.17	1.52
PU90	14.5	26	1.56	2.09	1.61	2.15
PU83	11.5	31	1.13	1.85	0.54	0.89
PU72	15	34	1.22	1.84	1.59	2.39
PU67	17.6	38	1.01	1.48	1.31	1.92
NI65	26	42	1.32	1.68	2.38	3.02

Table 10 Load, mean contact pressure, and mean shear stress, to achieve a 20% and 80% husked ratio.

The mean contact pressure determined for each rubber sample is shown graphically with respect to the rubber modulus in Figure 98. The average contact pressure increases with increasing modulus despite the decreasing load required to husk 20% or 80% of grains. This is because the contact area is much smaller for higher modulus rubbers.

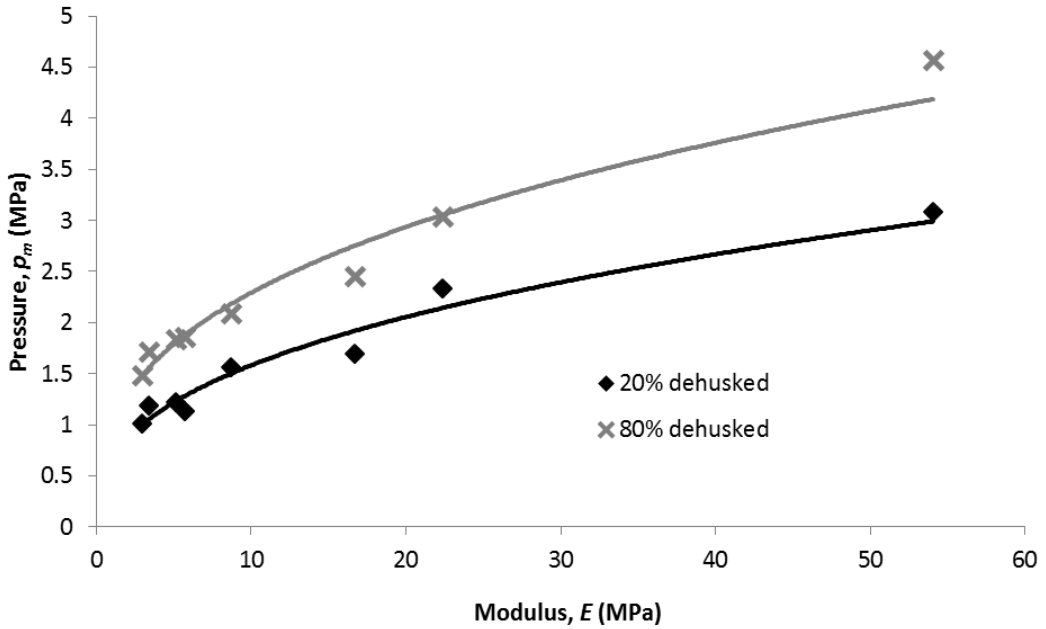

Figure 98 Mean contact pressure to achieve a 20% and 80% husked ratio plotted against the modulus of the rubber sample.

It is more relevant to consider the shear stress at the interface. The husk will separate from the rice kernel when shear yield has been achieved. The shear stress

was calculated by multiplying the mean contact pressure by the coefficient of friction obtained from the experiments of section 6.1.2.3 (equation 8).

$$\tau_m = \mu p_m \qquad \text{Eq. 8}$$

The calculated shear stress for each rubber material at husked ratios of 20% and 80% is shown in Table 10 and again graphically against rubber modulus in Figure 99. Also shown in this figure is a linear least squares fit to the data.

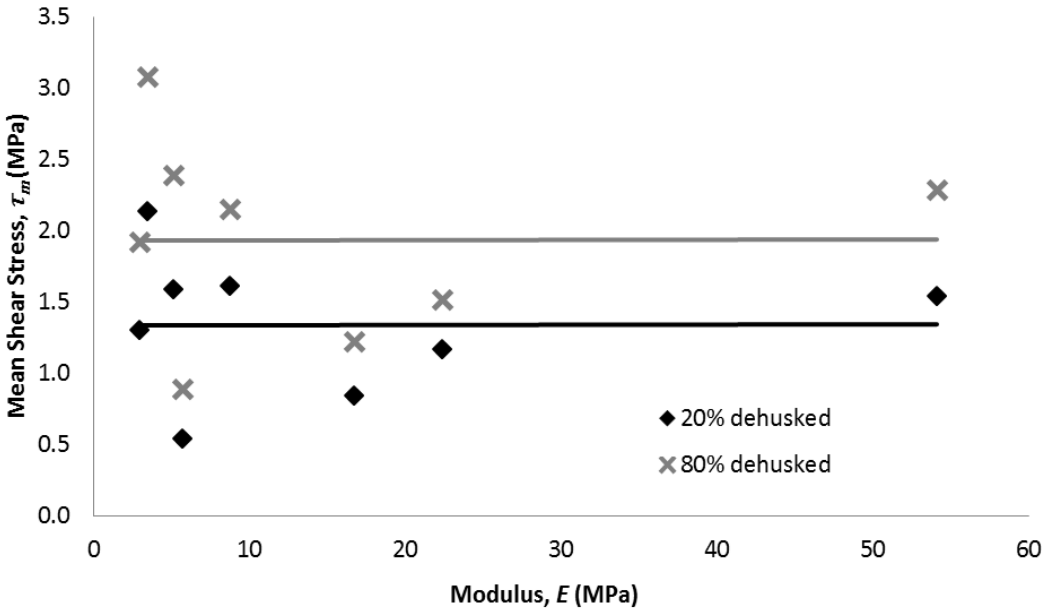

Figure 99 Mean shear stress to achieve a 20% and 80% husked ratio plotted against the modulus of the rubber sample with linear least squares fit

Although there was a lot of scatter (standard deviations around 0.5MPa), due to the statistical nature of the grain husking, there is an apparent constant limiting shear stress required to cause the husking of a rice grain regardless of what rubber material is used. It would appear that the applied shear stress was the main controlling factor over the husked ratio.

The limiting shear stress was determined in this way for each of the applied load and husking ratio data pairs. Figure 100 shows the shear stress required to achieve the given husking ratio. It can be seen that to achieve higher husked ratios it was necessary to increase the applied shear stress to the grain. It should be noted that since figure 96 is derived from a mean of data points (from figure 95), the magnitude of the scatter is significantly reduced.

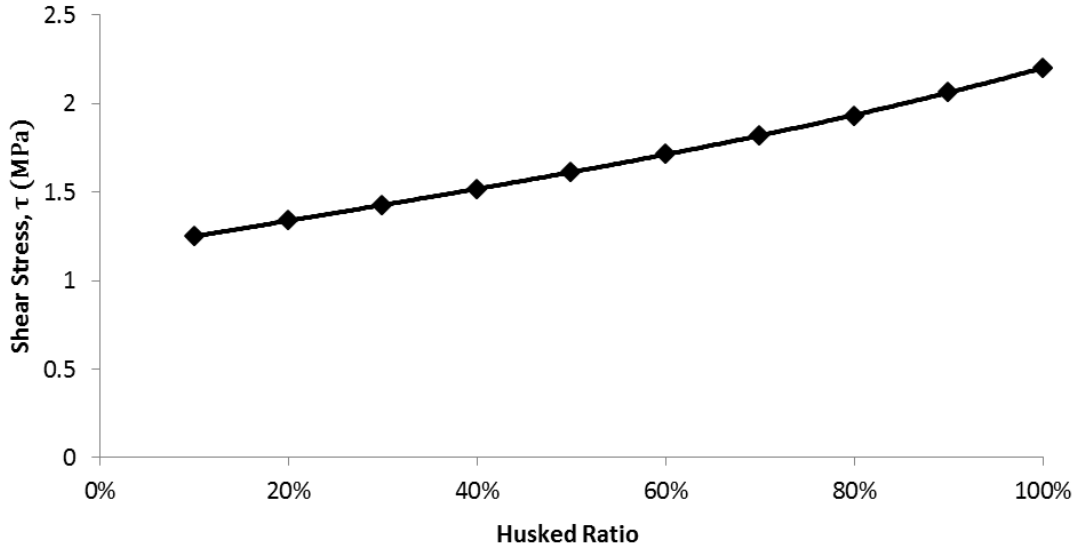

Figure 100 The mean limiting shear stress (assumed to be constant for each rubber sample) required to husk rice plotted against the ratio husked.

6.1.5 Conclusions

Husking using the coupon test has revealed that as husking efficiency is linked to shear stress imparted by the rubber rollers. This in turn is developed by the combination or rubber modulus and coefficient of friction. It is both the increase in pressure on the grain with harder rubbers and the increase in coefficient of friction which lead to the increased shear stress imparted on the grain.

The shear stress to achieve a given husked ratio increases linearly with desired husked ratio. Whilst this may appear to be a logical result, it implies that an increase in husking efficiency is gained when the contact area is small with high force rather than the same force spread over a larger contact area.

When using this coupon test, a maximum point is reached whereby the grains are either engulfed by the rubber or are crushed as the compressive yield is reached.

One drawback to using this method is that in husking a single grain at a time, husking sufficient grains to reduce the error caused by grain property variation is very time consuming.

6.2 Conclusions

The mechanisms involved in husking rice grains using rubber roll type huskers, has been investigated using some simple experiments on individual grains pressed between sliding rubber surfaces. Fast capture camera footage showed that grains rotate between rubber counterfaces before husking effectively creating a high pressure region at either end of the grain (though on opposing sides).

Experiments have shown that the harder rubber samples require a lower normal force to achieve a given husked ratio. For a given load a harder rubber will have a

smaller area of contact between rice and rubber rand therefore a higher contact pressure.

The friction coefficient between rice and rubber was measured for the various rubbers tested; values ranged from 0.5 to 1.8. A higher coefficient of friction means that the shear stress along the husk – grain interface will be higher for a given load.

Some simple calculations showed that whilst the load required to husk a rice grain varied with the rubber type, the shear stress required was, within the scatter in the data, constant at 1 to 2 MPa. This implies that to effectively husk rice this value of shear stress needs to be applied. The modulus of the rubber and the degree with which it conforms around the rice grain appears not to be a controlling parameter. The target shear stress can be achieved by either a high normal force with a low friction coefficient, or conversely a low normal force with a high friction coefficient. It is suggested that the latter case is more appropriate because it is likely to lead to reduced wear to the surfaces.

7 ANALYSIS OF LAB HUSKER

Small scale testing is important since the large flow rates required for full scale machines make it impractical in lab based settings. In order to reduce the cost of testing, and to increase the practicality, a lab husker has been used to determine various aspects of the husking process. This chapter details those findings and outlines where possible, how they compare to full scale operation.

7.1 Introduction

An issue with analysing huskers in practise is that with the requirement of large rice flow rates and the removal of a husker from service for testing would make testing costly. A small scale husking machine (shown in Figure 101) has therefore been used to conduct investigations requiring the full rolling contact. The rollers here are 100mm in diameter (compared to the full scale rollers which are 25.4cm).

Figure 101 Lab husker set up

As for a full scale husker, the two rubber rollers rotate with a speed differential in order to impart a shear to the grain, removing the husk. The husker has feed control (by changing the area of the feed flow) and three collection points for husks, immature/broken grains and acceptable product separated out by air aspiration. The principles involving this husker are the same as full scale, the ratio of the roller speeds and their matching diameters are thought to provide a reasonable comparison with any full scale operation. The most notable difference between this lab husker and the full scale husker, aside from the smaller roller dimensions, is the means by which a load is applied to the grains. With the lab husker, the applied load is controlled by altering the roller separation. In full scale huskers the load is controlled automatically, using a hydraulic ram to apply a constant pressure to one of the rollers. This highlights the necessity to understand the relationship between roller separation and actual applied load when using the lab husker.

Other notable differences include the lack of automatic feed control and positioning (available in full scale huskers) and the inclusion of a set of drawers to collect the husks and grains that have fed through the lab husker.

The lab scale husker gives the opportunity to study various aspects of husking from the relationship between roller separation and husking efficiency to the analysis of the mechanism by which rice grains are husked.

7.2 Grain Dynamics

It is important to understand the precise manner in which rice grains move through the husking rollers in order to advance the process and determine the most efficient method of husking grains.

One method of monitoring grain dynamics involves using fast capture imaging techniques which alleviate the issues of directly observing the high speed husking process. Another process developed involves the indirect observation of the contact region between grain and roller which also assists understanding of the wear mechanisms involved.

7.2.1 Fast Capture Imaging

Fast capture imaging is a relatively simple yet powerful technique in which a camera capable of recording at a very high frame rate is used to observe high speed processes. The main difficulty associated with this technique is achieving adequate lighting since the shorter the length of each frame of footage, the fewer photons collected on each pixel in the sensor and hence the weaker the signal. The experimental set up is shown below in Figure 102.

Figure 102 High speed capture set up

The frames are recorded digitally and can then be analysed to determine the precise manner in which a grain has been husked (see Figure 103).

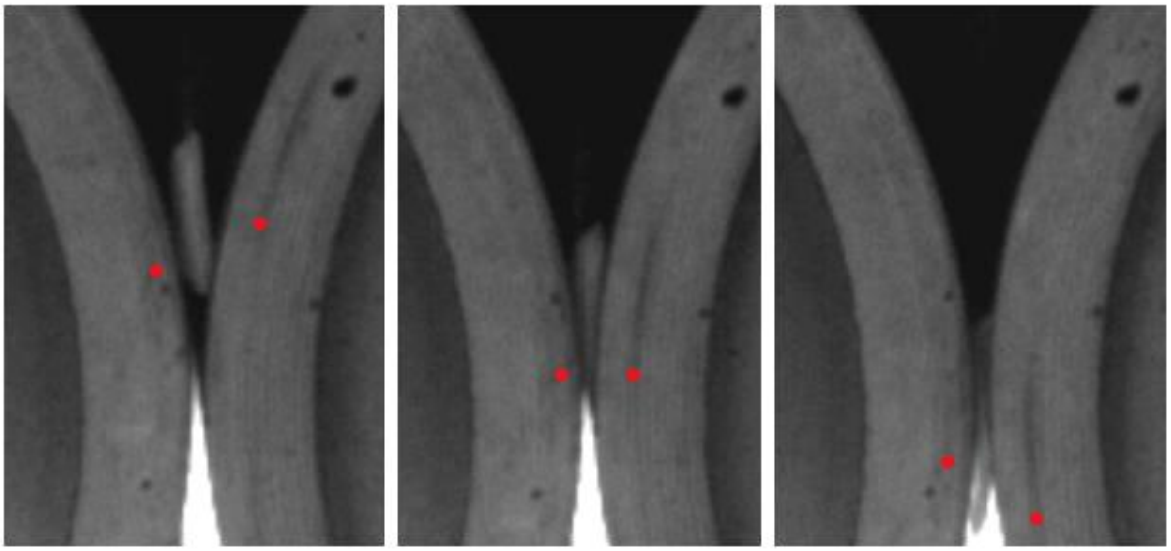

Figure 103 Stills from fast capture showing slow roller (left) and fast roller (right)

Individual grains are dropped between the two rollers directly so that both rollers contact at the same time (as is the case for the full scale machines). The grains pass downwards through the rollers and the contact noted. The grains appear to reliably remain in contact with the slow roller for the entirety of the pass and the husk segment in contact does not slide. Some initial sliding occurs against the fast roller after which point husking occurs. The process can be described as follows (in Figure 104):

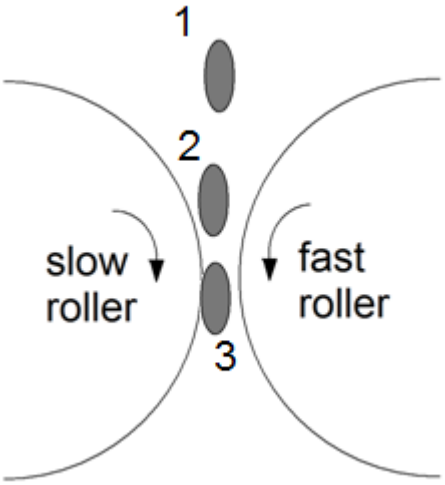

Figure 104 Grain motion through rollers

1. Grain slower than slow roller (S)
2. Grain accelerates to slow roller speed
3. Static friction on slow roller, dynamic friction on fast roller (F)
4. $\mu_S > \mu_d$ means that grains slide on fast roller and stick to slow roller

It is difficult to define the exact moment at which the grain is husked however it reliably occurs before the narrowest portion of the roller when operating under sufficient load to husk the majority (around 70%) of grains. Since the grains husk before the narrowest section, further sliding against the fast roller occurs as the husked segment sticking to the slow roller passes through. As the rollers open out again beyond the mid-point, the grains are free to fall and so further sliding does not occur against either roller.
Grains were often found to move slightly before being drawn in between the rollers indicating that some alignment occurs. This also suggests that grains rotate to husk in the same manner as the coupon test demonstrated. This is a useful result as it suggests that the use of a coupon test is a valid means of identifying rubbers that will husk efficiently.

7.2.2 Stick/Slip of Grains

Since the grains are thought to slip against the fast roller and stick to the slow roller a test has been devised to demonstrate this point. Grain husks have been inked and then fed singly through the rollers. The contact region is evidenced by the imprint of the ink on the roller.

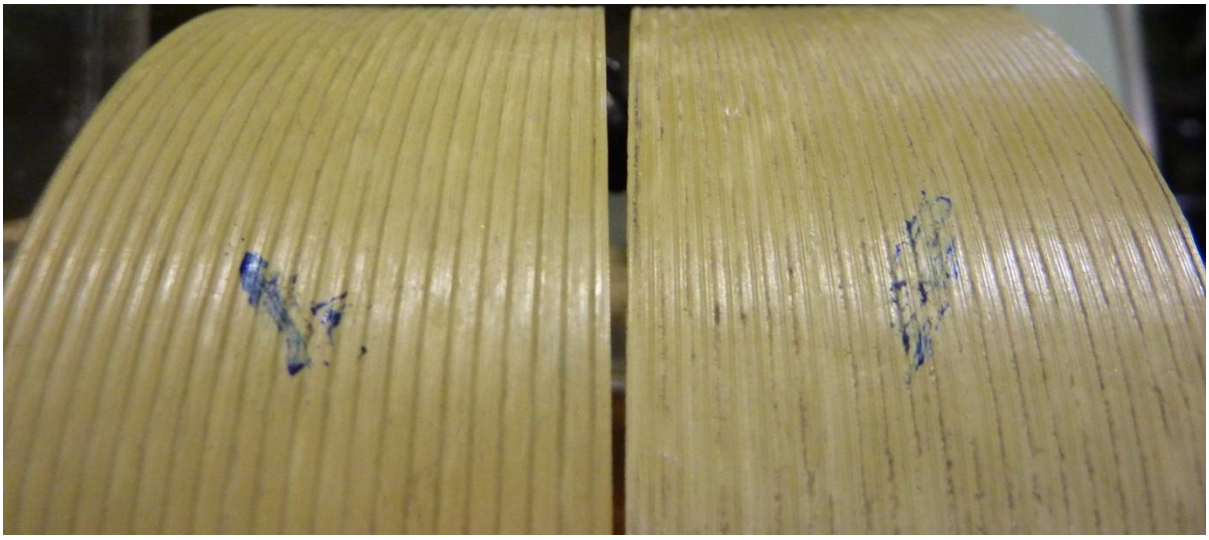

Figure 105 Sample result from ink test

Figure 105 shows the ink imprints which are then measured to determine the length of the contact that each roller experienced against the grain. The results are shown below.

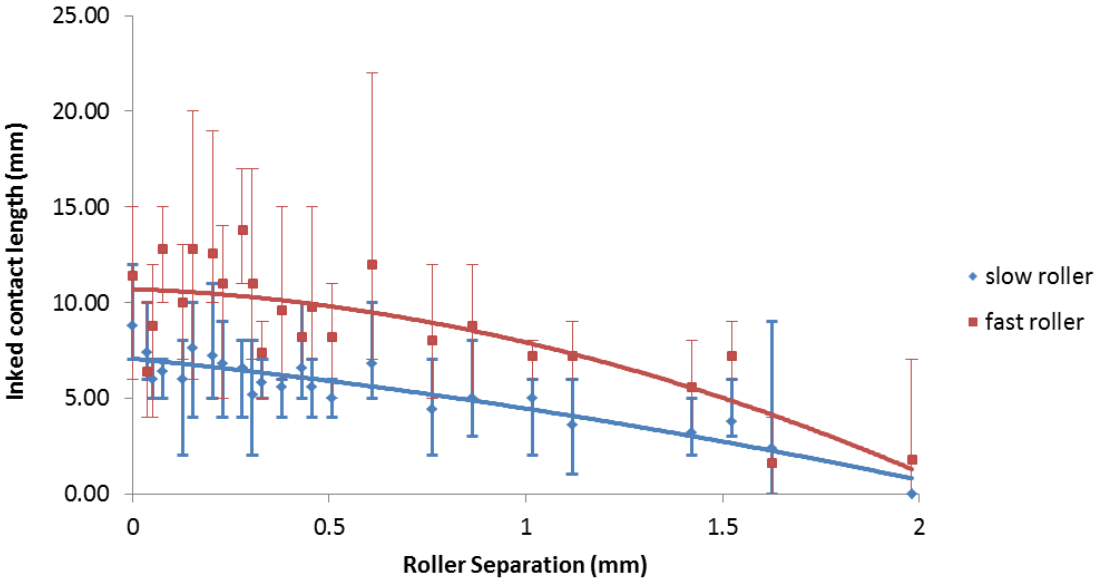

Figure 106 Inked contact length vs Roller Separation

Each point in Figure 106 represents the average of 5 grains tested at each roller separation and error bars show the maximum and minimum contacts for each separation.

The results show that the fast roller is in contact with the grain for longer than the slow roller which validates the theory that grains stick to the slow roller whilst sliding over the fast roller. It can also be seen that as the roller separation becomes smaller, the grains are in contact for longer with the slow roller. At zero roller separation, it would be expected that the contact, engulfing the grain, would be equal to the length of the grain. This result is within the error of the data.

From this test, it is therefore possible to calculate through Hertzian analysis (Equations 2 to 7) the contact pressure on the grains for different roller separations (assuming the contact area is that measured by ink plot on the slow roller). This is shown in Figure 107.

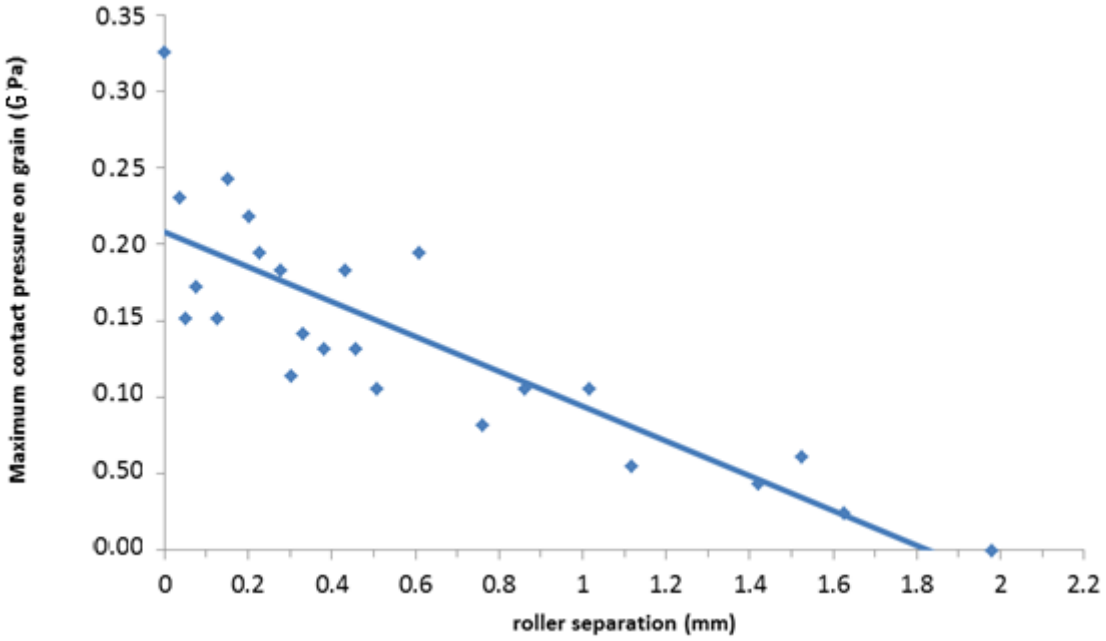

Figure 107 Maximum contact pressure based on roller separation

7.3 Performance Based on Roller Separation

The most important observation to make regarding husking is the understanding of the relationship between load and husked ratio. The small scale lab husker does not have direct load measurement capabilities, however, it relies on the adjustment of the roller separation to change the loading on the grain.

Therefore, a simple experiment has been carried out in order to directly measure the relationship between roller separation and husked ratio for this lab husker. 100 grains are passed through the husker at each roller separation (see Figure 108).

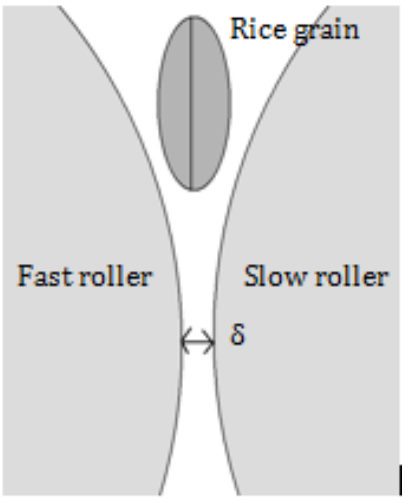

Figure 108 Test for performance based on roller separation

Results are shown below in Figure 109 and are the husked ratio for 100 grains passed through for each separation.

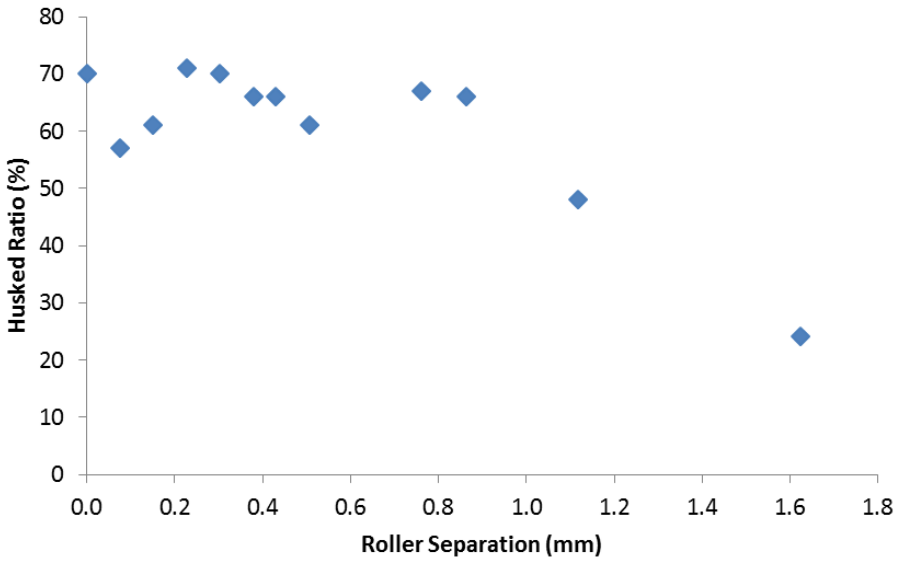

Figure 109 Husked ratio at various roller separations

It can be seen that as the roller separation decreases, the husked ratio increases. A maximum husked ratio of 70% appears to be reached at separations below 0.8mm. This is likely to be caused by a combination of the rubber properties and the machine sizing. The data is plotted again below (Figure 110) with reference to the ratio of roller separation and grain width.

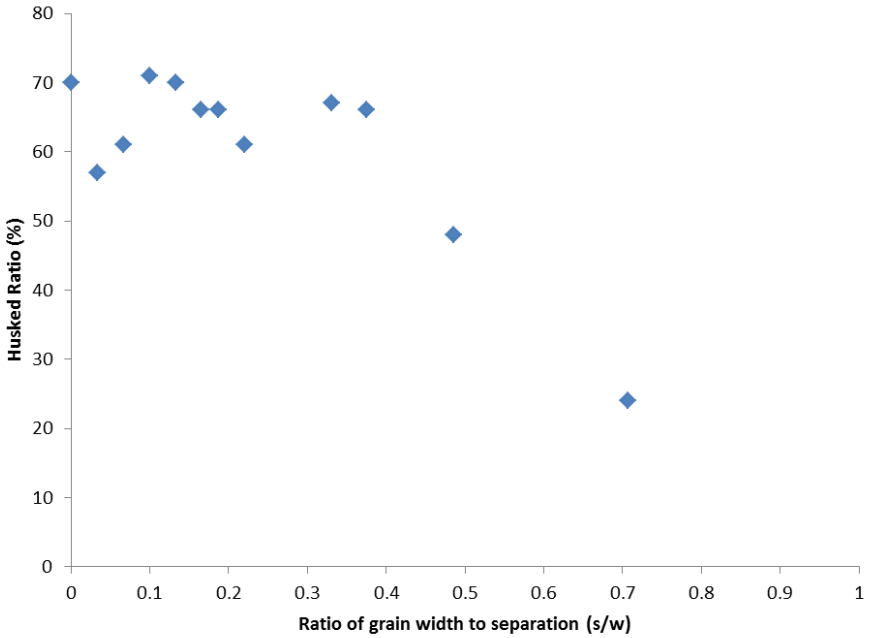

Figure 110 Husked ratio against grain width to separation ratio

In this case, where the ratio of grain width to separation is zero, the grains are fully engulfed as they pass through. When the ratio is 1, grains fall freely through the rollers.

7.4 Contact Loading

The contact load is changed by altering the roller separation as seen above. This allows a useful method of comparison with the coupon tests already conducted, since a Hertzian contact can be assumed and then a husked ratio predicted by the coupon test can be calculated. Further to this, knowing the maximum load that can be applied by a full size husker allows comparison with industrial practise.

In Figure 107, a comparison is made between predicted husked ratios for YNOX material, Lab husker and the maximum load that can be applied by a Buhler-Sortex DRHC husker.
The YNOX predictions have been made based upon the assumption that the rubber deforms around the grain (see Figure 111). From this assumption, a contact area can be calculated for various roller separations and Hertzian contact equations (Equations 2 – 7) used to calculate the load required to achieve this condition. The load has then been compared with the coupon test husked ratio at that load.

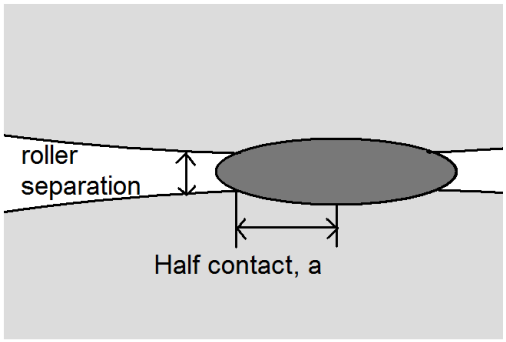

Figure 111 Measurement conditions for YNOX predicted husked ratio

The maximum load that can be applied by full sized huskers has been calculated based on the control mechanism of the machine. Rather than setting a separation between the rollers, a pressure is applied and maintained automatically by hydraulic control. The maximum load that can be applied by the hydraulic system has been analysed mechanically by the lever mechanism. For a cylinder pressure of 600kPa and diameter of 80mm, the theoretical force that can be applied is around 3kN. This leads to a load between the rollers of around 4kN. Assuming that there is a constant stream of grains passing through the rollers evenly, and at a flow rate of 6tonnes/hr, and that each grain takes an equal share of the load, the maximum load that can be applied to the grain is 82N. Assuming Hertzian contact conditions (Equations 2 – 7), a mean contact pressure of 0.67MPa can be calculated. From the load applied, and again assuming a Hertzian contact, a theoretical rubber deflection can be determined, allowing a calculation of the effective roller separation (0.73mm).

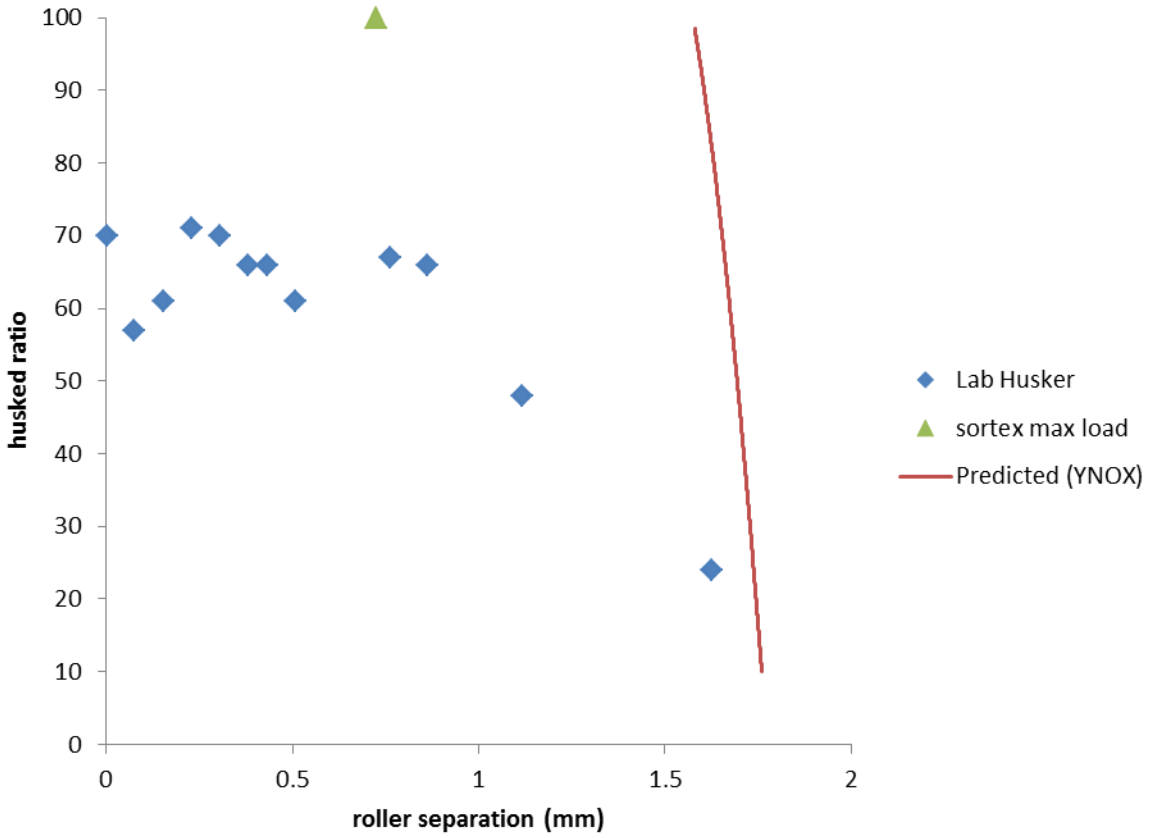

Figure 112 Graph comparing predicted husked ratios for YNOX material, Lab husker and Buhler-Sortex DRHC husker maximum appliable load

The predicted YNOX husked ratio based on roller separation from the coupon test agrees well with lab husker results for larger separations. For lower separations, the results are less comparable suggesting that there is an additional factor should be considered when comparing cylindrical rollers against flat coupons. This result indicates the limitations of the lab husker and suggests that there is a lower load at the contact than expected. This results in the model above over predicting the husked ratio for lower roller separations. It is likely that these differences arise due to the roller radius but it is possible that a larger roller with greater stability is more resistant to contact variation as grains pass through.

7.5 Axial Vibration Experiments

It is known that vibration can be an issue in full scale huskers and is generally an undesirable characteristic. However, since it has also been hypothesised that the dynamic/static coefficients of friction between rollers and grain are the dominant cause of uneven roller wear between the fast and slow rollers, an experiment has been conducted in an attempt to analyse the effect of creating a region of dynamic coefficient of friction on both rollers. The experiment aims to observe the effect of vibration in a controlled way which could also be useful in husking.

Axial vibrations have been applied to the slow roller by means of a series of opposing magnets. One magnet has been secured to the machine body, whilst an array of four

(in alternating attract, repel pattern) have been attached to the slow roller (see Figure 113).

Figure 113 Magnet layout on roller (left) and casing (right)

The roller was allowed some free degree of axial movement by modifying the shaft fixings.

A laser vibrometer was used to measure the movement of the roller. A noise signal was also measured against the fast roller (no magnets) for comparison (Figure 114).

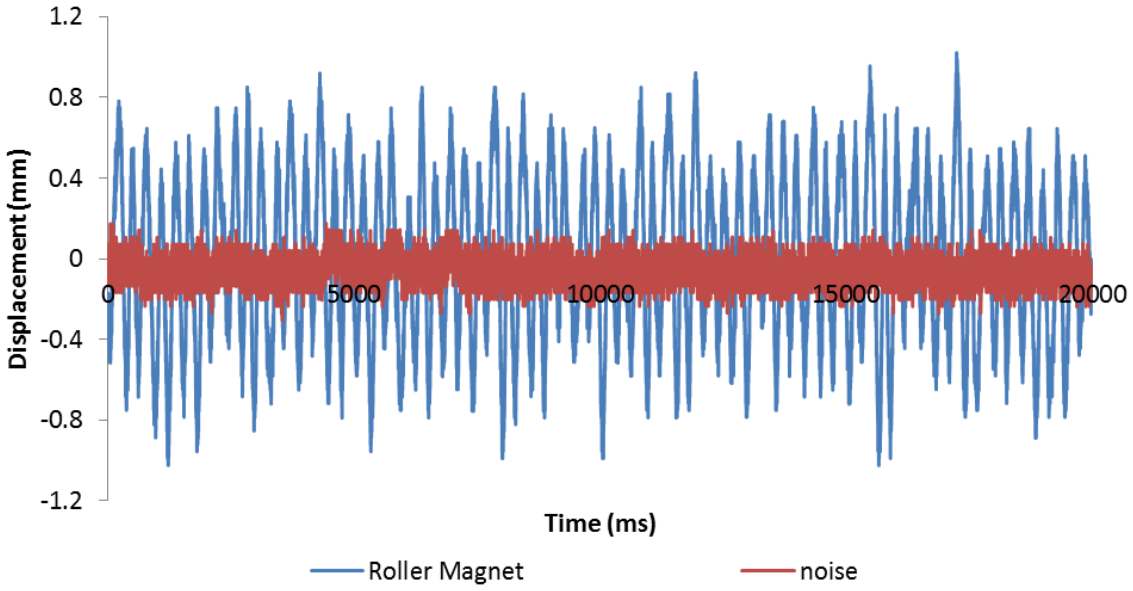

Figure 114 Vibration data for slow roller and noise signal

The average displacement of the roller is 1.1mm which was thought to be sufficient for the trial purposes.
A Fourier transform of the data has been calculated (Figure 115) to demonstrate the natural frequencies of the system and confirm that the magnetic layout gives a consistent pulse.

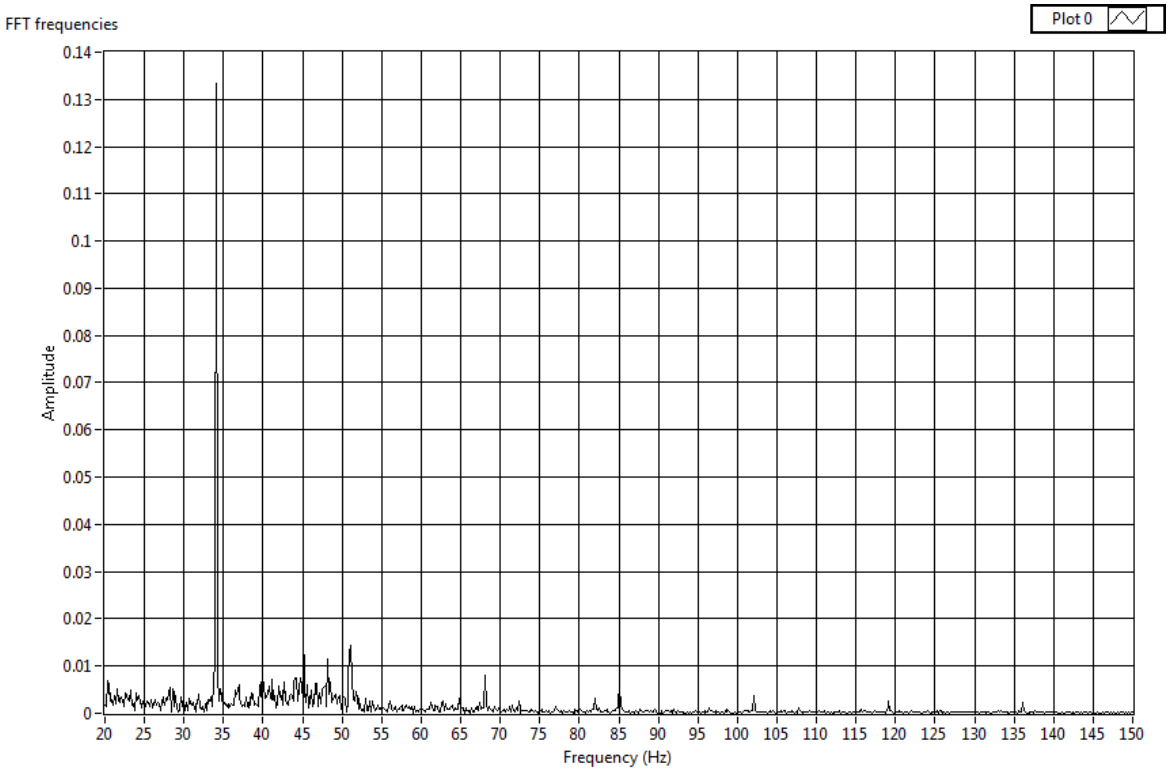

Figure 115 Fourier transform of vibration data for slow roller

The single frequency peak around 34Hz indicates that there is a consistent pulse of the slow roller meaning that there is a consistent vibration of the roller.

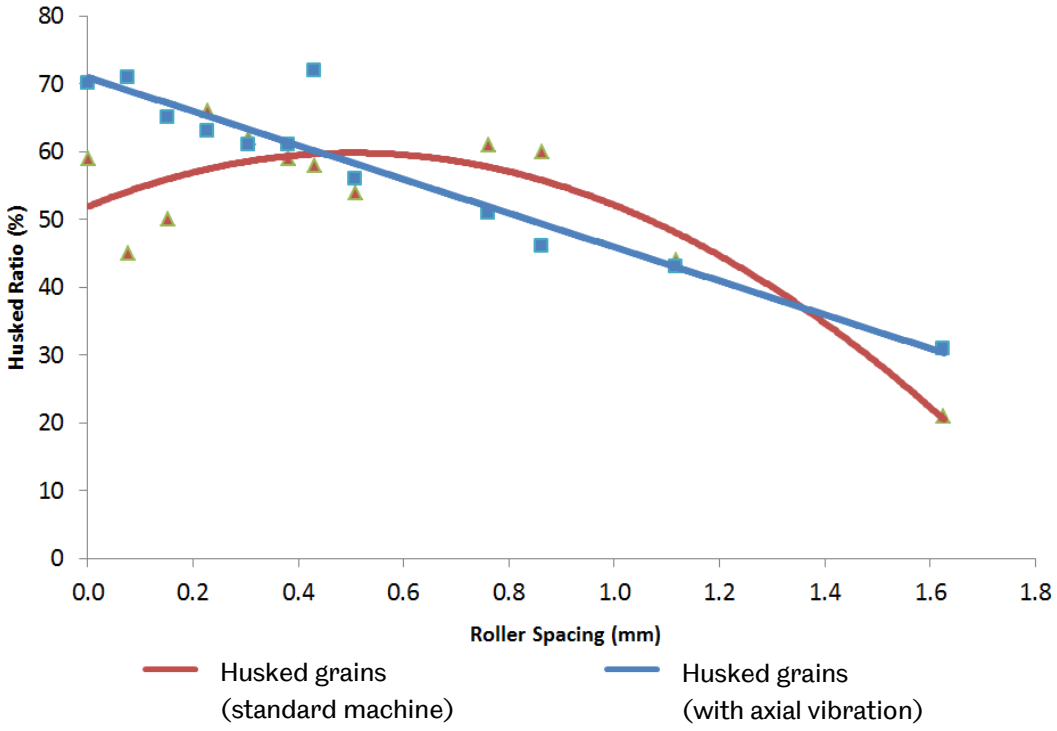

Figure 116 Husked ratio for various roller spacing with and without axial vibrations

The results in Figure 116 show that for small roller spacing, axial vibrations result in a larger percentage of grains being husked. This is a significant result as it shows the

potential to improve efficiency of the rollers when operating under increased pressure.

7.6 Conclusions

Now, two versions of small scale testing have been considered. A low throughput husker has been used to analyse various mechanisms involved in husking rice grains whilst the coupon test described above has been developed in order to quickly determine a rubber samples potential as a husking material.

Husking efficiency of the lab husker has been determined relative to roller separation and shows that as roller separation decreases, efficiency increases up to a maximum of around 70%. This has been compared to the coupon test using Hertzian contact theory. The results are comparable for larger equivalent separations, however smaller separations show the coupon test to have a higher effective efficiency. This is most likely due to the difference between the two materials and the relative efficiency of a cylindrical roller against a flat coupon.

Grain dynamics have been observed for the lab huller using fast capture imaging, which has revealed that grains maintain their initial contact with the slower roller throughout whilst sliding against the fast roller once husked. Inked grains fed through the rollers have confirmed this, showing that the contact region of the fast roller is larger than that of the slow roller regardless of separation.

A theory has been developed in which husking efficiency can be increased by the addition of an axial movement of the slow roller. It is thought that the difference in contact region between slow and fast rollers is due to the grains needing to accelerate from low falling speeds, initially up to the speed of the slow roller, at which point the contact experiences a static coefficient of friction. Since the static coefficient of friction is higher than the dynamic coefficient between grain and fast roller, the grain sticks to the slow roller and continues to slip against the fast roller. By introducing an axial movement, it is thought that the contacts will all experience a dynamic coefficient of friction, creating an equal movement across each roller. A secondary, but not insignificant effect is thought to be that due to the structure of the husk (being in two halves) there is likely to be an orientation of the grain which requires lower energy to break the bond of the husk. By introducing axial movement, grains are allowed to rotate and will husk more freely when oriented to a lower energy fracture. Experiments were carried out and it was found that the introduction of axial vibrations increased husking efficiency for small roller spacings.

8 TRIBOLOGY OF RICE POLISHING

There are two different aspects to polishing tribology; namely grain-grain contact and grain-machine contact. The desired outcome from each are polar opposites. The abrasion of the grain surface (the polishing action) is desirable, whilst the abrasion of the machine is not. It is intended that in determining the underlying mechanisms involved in polishing and also those that create the wear of the surface will lead to both improved polishing performance and increased wear life. Two machines are used to observe the tribology of rice polishing, a lab scale polisher with low capacity requirements and a full scale polisher with normal grain flow. These two approaches give the scope to analyse polisher performance without the need to take a polisher out of grain production for small scale testing.

8.1 Understanding Polishing Mechanisms

The underlying mechanisms which result in the removal of bran from the grains are generally rarely and poorly discussed in literature. Whilst the work of Satake[3] gives details which relate to the nature of bran during different regimes of polishing he fails to give substantiated evidence for the findings. Since machine design relies on the improvement of the polishing efficiency it is impossible to reduce wear rates by redesign without first considering the underlying polishing mechanisms.

Satake suggests that the action of friction evidences itself as a tearing effect under high load and a heating effect under lower load. He suggests that friction action is the primary action in low speed milling but that it is extremely inefficient.

Cutting, is a further low speed milling action which usually occurs in conjunction with friction action. Satake suggest that a "low-speed system (peripheral speed of 600m/min) with a pressure of 100g/cm² or more cuts the rice grain deeply and long, resulting in large pieces of bran"[3]. As the speed increases, the bran becomes finer. When blades are attached to the inside surface of the milling cylinder, or to portions of the milling roll, the cutting action becomes a grinding action when the speed exceeds 600m/min. It is also suggested by Satake that broken rice grains are created by low-speed action creating a bending moment that breaks the rice coarsely whilst high speed actions produce fine breaking by impact. Further, grinding is described as a shearing action combining impact and friction. It is suggested that grinding is more efficient than low speed actions even for milling starch layers with a hardness of more than Hv7.

Finally, impact action is discussed briefly by Satake. He states that "it is difficult to experiment on the actual action of impact milling. The secondary action of impact often becomes the effective action in the case of grinding at high speed."[3]

8.1.1 Determination of Polishing mechanism

Although Satake gives figures for the actions above and the limits of their effectiveness, the details are not substantiated with evidence. Whilst 600m/min is given as the peripheral speed at which there is a distinct change in polishing action, no mention is given to the machine used or results from a study other than observation. Therefore, rather than the above actions, the following is proposed as a simplified means of observing the polishing mechanism for any polishing technology. The grain interactions fall into two categories; grain-grain contacts and grain-machine contacts. Observations of polishing mechanisms therefore consider these two cases.

In the case of grain-machine contacts, there are two conditions to consider. A grain can either impact with a surface or can slide over the surface. In impacting the surface, the nature of the bran removal is most likely by fracture and delamination of the bran layer.

Milling efficiency can be defined as the extent of bran destruction or removal in the process relative to the energy required for the combined action.

8.2 Low Throughput Wear

When the wear life of a component is several weeks of continuous operation, it is impractical to make design adjustments and then put the component into full use to see how the wear is affected. Such is the case of the polisher screens, so it is of great interest that a test method be developed which accelerates the observable wear, but in a way that simulates the mode of wear. Simply increasing the loading or the speed of impact with the screen is not sufficient since the wear regime may change dramatically. In the case of the polisher, it is also necessary to develop a test with low requirements since access to full polishers in operation is limited in terms of accessibility and cost.

8.2.1 Lab Polisher

A lab scale polisher has been produced in order that operating conditions be analysed at scale with a limited hopper of rice (see Figure 117).

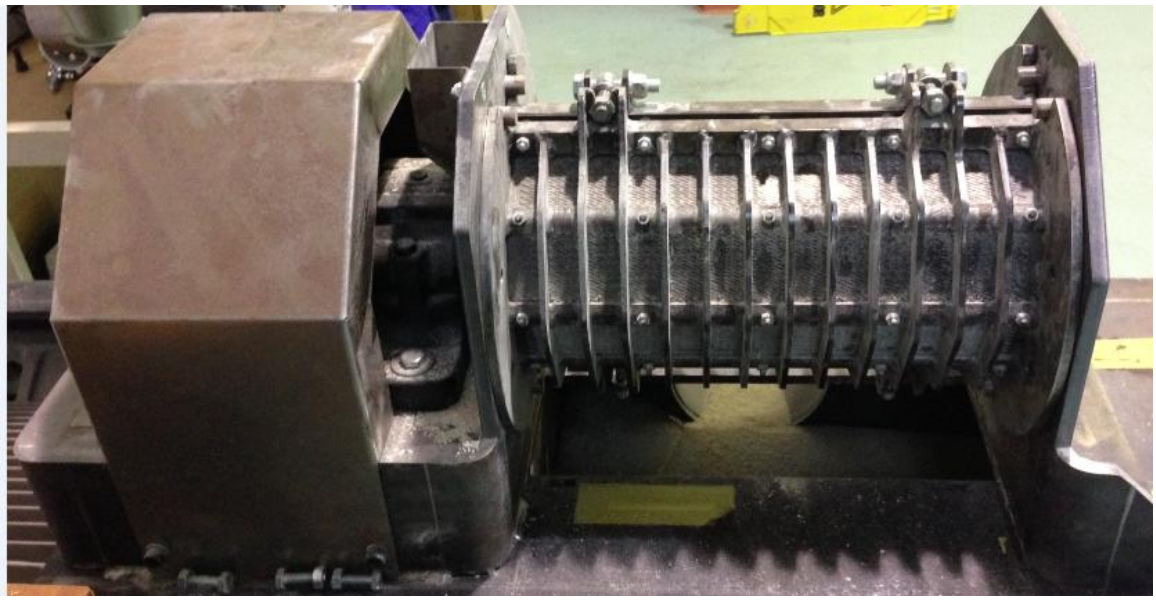

Figure 117 Lab Scale Rice Polisher

The chamber has the same diameter as a full scale machine (200mm) but is only half the length (523mm). Rice is placed into the chamber via the feed hopper and remains within the chamber until replaced. The dimensions of the lab polisher are such that its length is half of that of a full polisher, and its diameter is the same. Similarly, the cam roll section used is the same as the second stage (horizontal blade) of a full polisher. In this way the lab polisher, as far as possible, matches the operating conditions of the full polisher.

8.2.2 Paint test

Screen samples have been painted with a metal suitable paint evenly and thinly. Since the paint layer is much softer than the screen materials, it wears much more readily allowing an observation of the wear pattern after only 20 seconds of full capacity operation (shown in Figure 118).

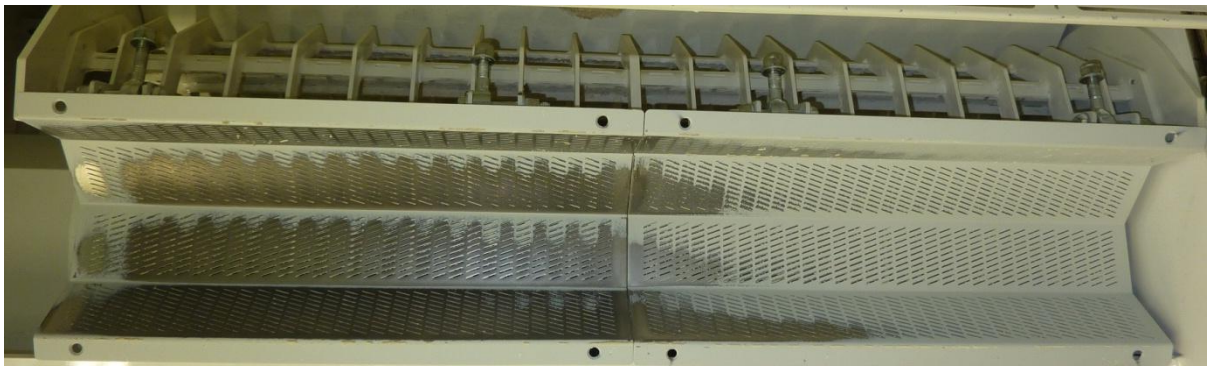

Figure 118 Paint wear test results (rice flow left to right, rotation from bottom to top)

From this simple test, it can be seen that the inlet has worn much more readily than the outlet. Since the chamber geometry is the same down the length of the machine, this suggests a higher pressure of grains at the inlet compared to the outlet.
It can also be seen that there is a pattern in the worn region, roughly corresponding to the cage support positions though with twice the frequency. It is thought that this is either a result of the feed screw entraining the rice in an uneven manner, or that the screen is vibrating at a resonance caused by the cage spacing.

8.2.3 Inlet Wear

The results from the paint test (and a result generally observed during polisher operation) indicate an elevated area of wear at the inlet (Figure 119).

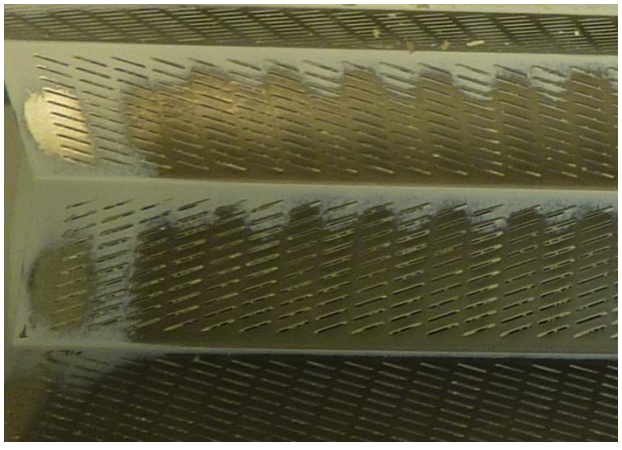

Figure 119 Inlet wear region (rice motion left to right)

Inlet wear is thought to be caused by the rapid scattering of the rice as it enters the polishing chamber. Inlet guide vanes are suggested as a solution to this problem.

8.2.4 Inlet guide vanes

The current cam roll design of a polisher is shown schematically below (Figure 120)

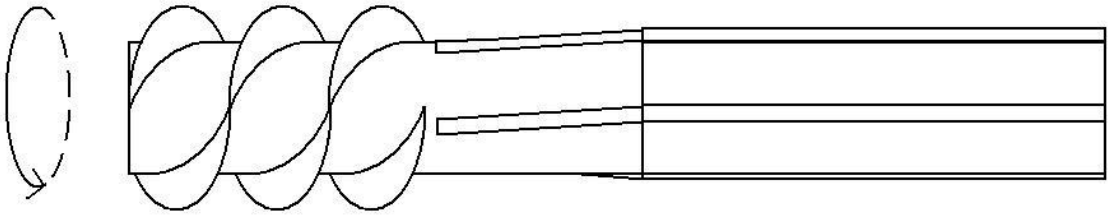

Figure 120 Current cam roll design

This whole cam roll rotates as a single central shaft inside the polishing chamber, however the grain motion does not follow the same path as the cam roll surface. As grains enter the feed screw, they are pushed axially along the machine and as they contact the cam roll blades they are scattered radially. It is thought that the grains accelerate in a non-uniform way which leads to increased noise, vibration and wear in the inlet region. Therefore inlet guide vanes are proposed as a method of changing the grains momentum in a more uniform manner.

In order to maximize guide vane efficiency it is necessary to calculate the correct blade angles. Velocity triangles can be drawn to determine the angles involved in the fluid (rice and air) motion (Figure 121).

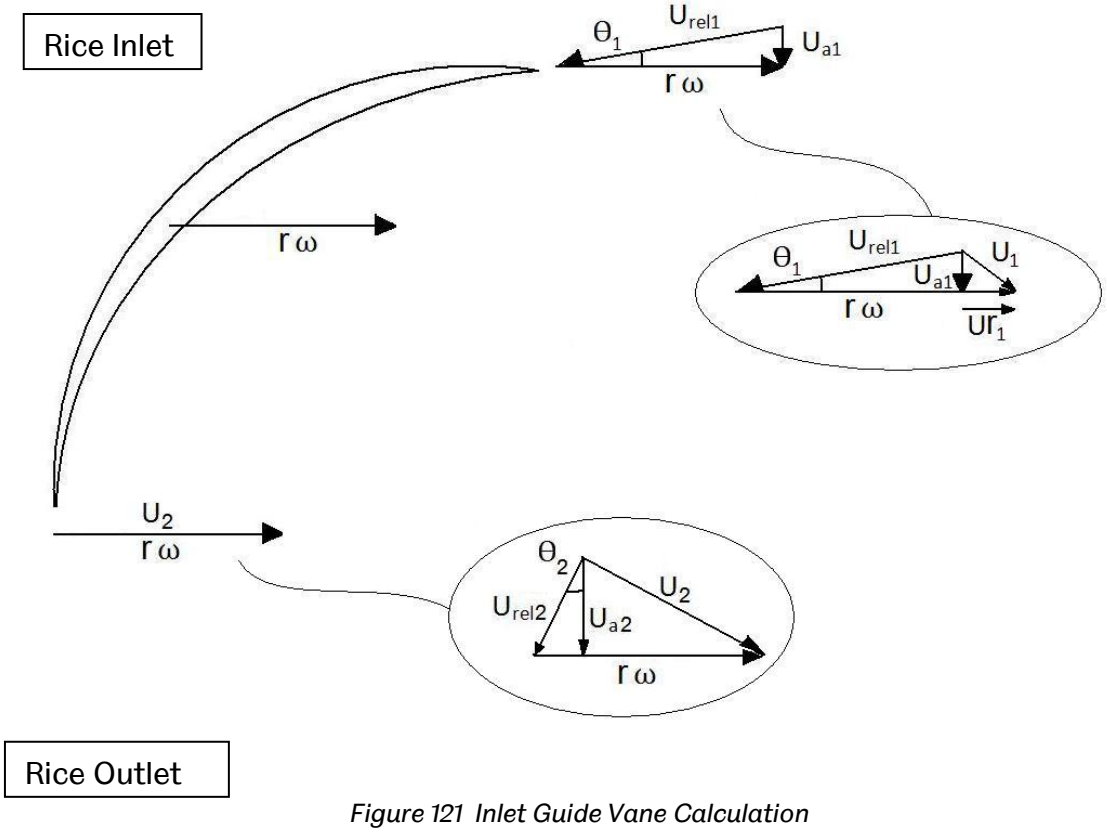

Figure 121 Inlet Guide Vane Calculation

Where; U denotes a velocity, 1 for inlet conditions, 2 for outlet conditions, a is an axial component and r is a radial component. $r\omega$ gives the blade velocity at a given radius.
The circled velocity diagrams are the full picture. In the top instance (inlet conditions), if the radial velocity is zero, then the calculation is simple to determine the appropriate angle of the blade tip θ_1 knowing the feed velocity U_{a1} and the blade velocity $r\omega$.
In the bottom case (outlet) if the rice is moving entirely radially (at the speed of the cam-roll) then θ_2 is 0 degrees. This means that exit angle of the blade should along the axis of the cam-roll.
In a sense, in the current machine, the angled blades are almost acting like inlet guide vanes as used in turbo machinery, albeit at a relatively shallow pitch.

The proposed design for inlet guide vanes is shown below (Figure 122).

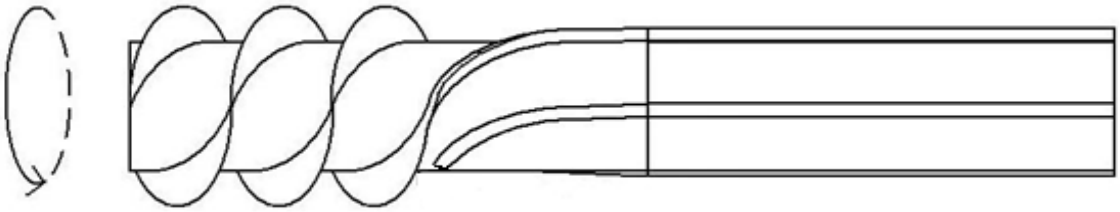

Figure 122 Proposed inlet guide vanes

It is thought that the inlet guide vanes would accelerate the rice more uniformly, potentially resulting in lower vibrations, reduced noise and reduced wear in the inlet region.

8.3 Polisher Operating Pressure

8.3.1 Introduction

Since the screen materials are uniform throughout in terms of hardness and friction coefficient, the operating pressure of the polisher could be used to determine the probable degree of wear in various locations around the screen.
Satake[3] carried out an experiment in an attempt to link milling efficiency with polisher pressure. Pressure was measured using a load cell placed in a hole in the polisher screen. Various locations were measured and the pressure demonstrated to vary across the screen. This method showed that pressure was higher at the minimum roll clearance and lower at the maximum clearance between roll and screen. It also showed that pressure varied along the screen length. In both cases, no numerical relationship was stated between roller clearance and pressure change (assumed linear) meaning that in order to calculate milling efficiency at different pressures, average pressure is used. Average pressure was linked to horsepower and this relationship used to compare pressure and efficiency. This gives an estimate of milling pressure which may not be accurate. Also, this process involves the destruction of a small area of the screen which may interfere with flow, and does not

give a good resolution of pressure (resolution of a 10mm diameter circle). This means that whilst a macro analysis of wear may be estimated using this method, the micro wear would go unnoticed. It should also be noted that this method has only been demonstrated for one machine geometry and one rice variety. Since rice properties vary greatly between varieties and machine geometry differs between manufacturers, it is desirable that a simpler process for determining machine pressure with better resolution be developed.

8.3.2 Feed Screw Fill

The pressure acting on the polisher chamber wall is thought to be a function of several factors, including bulk density of the rice grains and their velocity. Bulk density determines the packing of the particles which in turn allows calculation of the degree of freedom of the rice grains to accelerate and impact with the screen. The flow rate of the grains can be measured through the machine and cross sectional dimensions are known (see Figure 123), so a bulk density can be assumed in order to determine the degree of fill for different flow rates.

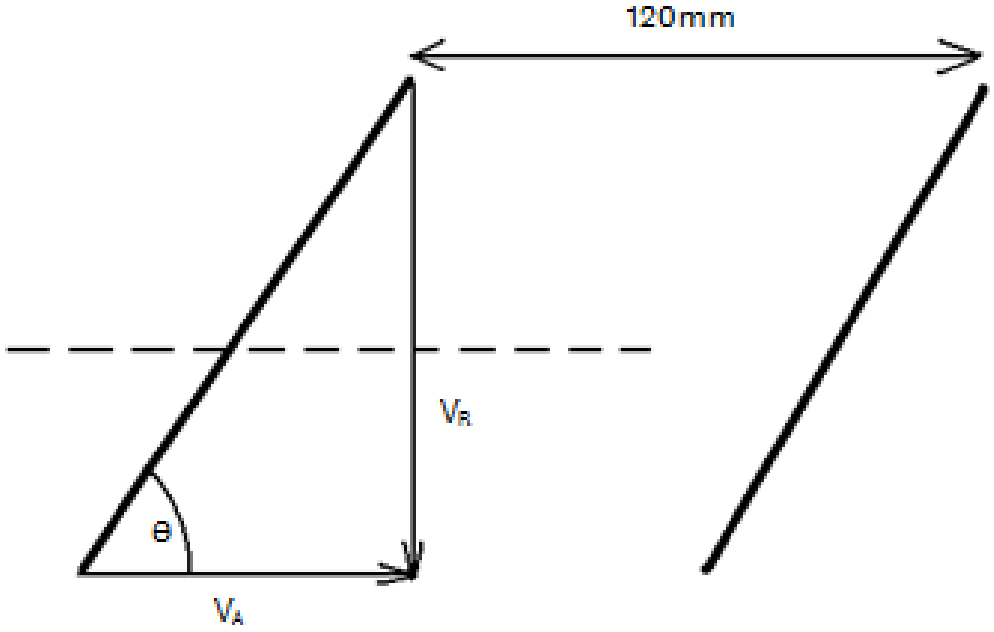

Figure 123 Feed Screw Fill Calculation

The distance between blades is 120mm and the angular velocity known, which allows the calculation of the radial velocity of the blade (V_R).

$$V_R = r\omega \qquad \text{Eq. 9}$$

By trigonometry with the angle of the blade the axial velocity, or blade rate of progression, can be calculated.

$$\tan\theta = \frac{V_R}{V_A} \qquad \text{Eq. 10}$$

This allows the simple calculation of the number of blade passes per hour which, when considering processing rate (tonnes of grain per hour) and bulk density allows the feed fill to be determined (Figure 124).

$$\rho V_b x n = m \qquad \text{Eq. 11}$$

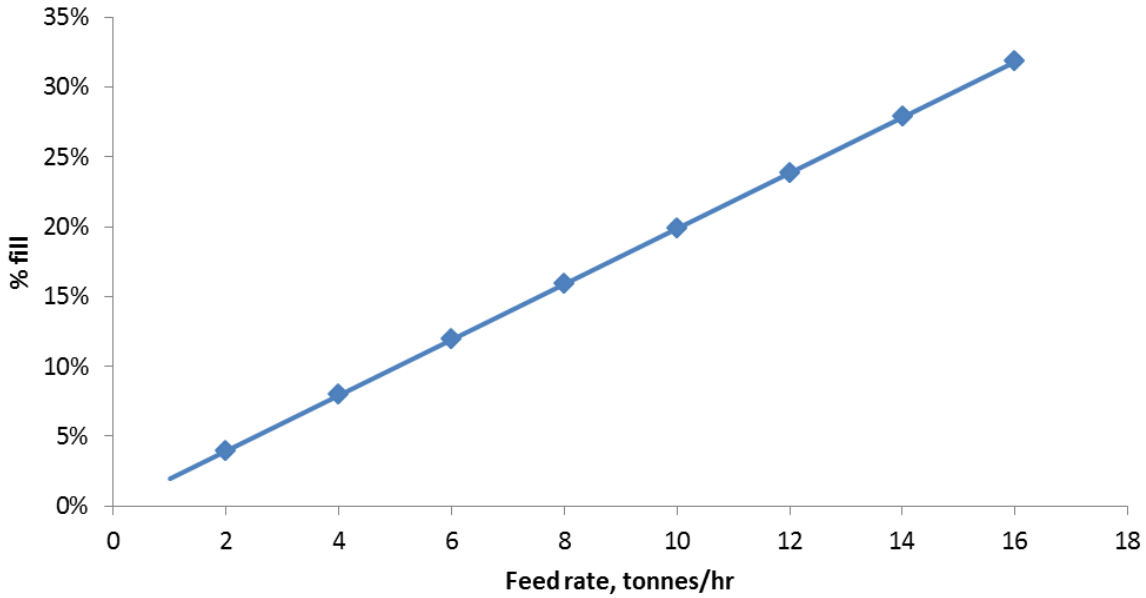

Figure 124 Feed screw fill based on feed rate

The result is interesting as it shows that the inlet is generally operating at around a 15% fill (corresponding to 7 tonnes/hr). The operators believed this to be much higher (by intuition) since the flow appears to be impeded when operating at high feed rates leading to the conclusion that this resistance is not due to the feed chamber being full.

It would also be useful to determine the percentage fill for the main chamber, however, the calculation relies on knowing the axial velocity of the grains. The only portion of the polisher for which the axial velocity of the grains are known is the feed screw. Since the feed screw leads the rice into the chamber, the fill percentage can help to indicate conditions at the main chamber inlet but doesn't provide any means of determining pressure in the polisher chamber.

8.3.3 Using pressure sensitive paper

Pressure sensitive paper is used to determine contact pressure profiles in many applications from gasket interfaces to lamination presses[71]. It was therefore thought that the use of such paper should help to determine very precisely the pressure imparted by the contact of rice with the screen wall.

The pressure sensitive paper works by the use of a colour developing material coated onto a polyester base, with a micro-encapsulated colour forming material layered on top (see Figure 125).

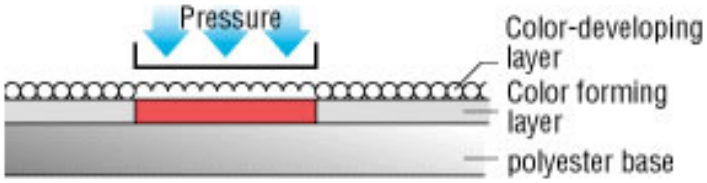

Figure 125 Pressure Sensitive Paper[72]

The film effectively provides a means of measuring the maximum pressure it experienced during loading. The degree to which the colour change occurs indicates the pressure experienced in that area. The colour density then provides a visual representation of the pressure profile which can be converted into a pressure gradient map. For observation of polisher operating pressure, film which operates within the range of 100-500 kg/cm^2 was selected.

8.3.3.1 Pressure paper with closed system polisher

This method was first tested on half length closed system polisher in which the rice is free to move around the cam roll but there is no inlet or outlet. This is a much more efficient way to test such methods as only small quantities of rice are required and the test durations can be precisely controlled.
Samples were simply secured using adhesive tape in a single location (see Figure 126).

Figure 126 Location of pressure sensitive paper in lab polisher

The polisher was run up to speed at a constant acceleration until it reached the normal operating condition (750 rpm). The test was run at full speed for 10 seconds and then decelerated back to rest.

A section of the pressure paper was scanned and converted digitally to black and white for clarity. A worn section of screen from a full scale polisher is shown for comparison in Figure 127.

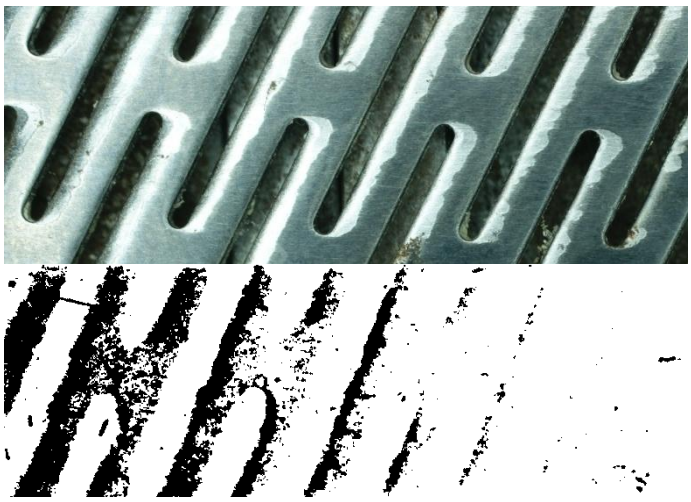

Figure 127 Slot wear (above) and pressure sensitive paper result (for a new screen) (below)

It can be seen that the pressure paper closely corresponds to the wear seen on the slots with sufficient resolution to observe the pressure variation between the slots. This method demonstrated clearly that any macro scale variation in polisher pressure should be observable in the full scale polisher.

8.3.3.2 Full scale polisher pressure using pressure sensitive paper

Half-polisher length strips of pressure sensitive paper were cut and attached to one section of the polisher (see Figure 128). The polisher was then run up to full operating load to ensure that the fill in the chamber was representative of that in continuous use before the flow was halted.

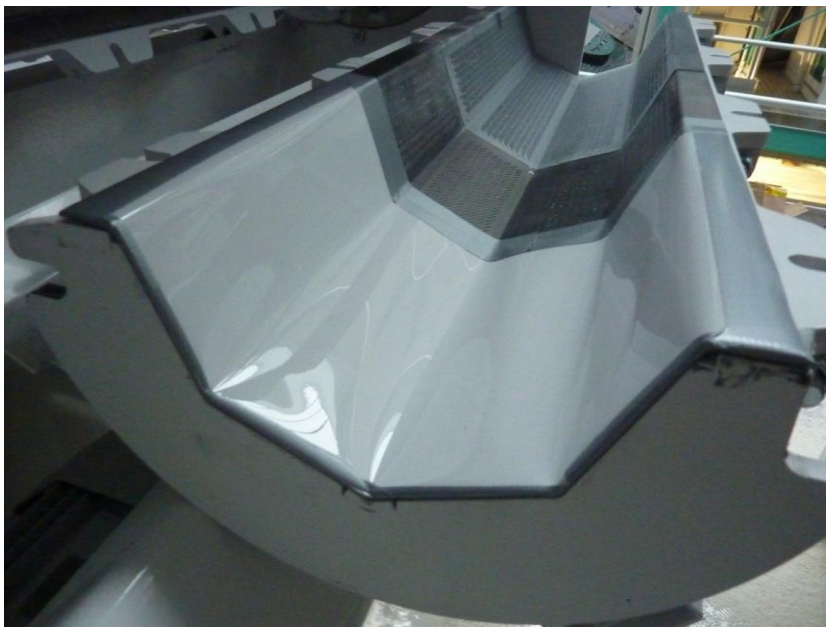

Figure 128 Pressure paper location at inlet, rice direction of travel is from left to right. This section of screen folds up anti-clockwise and is seen here from the inlet.

Since current is the measure of loading for full scale polishers (which is higher as the resistance of the grains increases) it has been used as the basis for loading in these trials. The first trial was located at the inlet with the polisher run up to a load of 75A and run for 10 seconds before rice flow was halted. The loading was controlled by resisting the flow at outlet. It is thought that this simply increases the density of grains inside the polisher. The paper was then removed so that it could be analysed (see Figure 129).

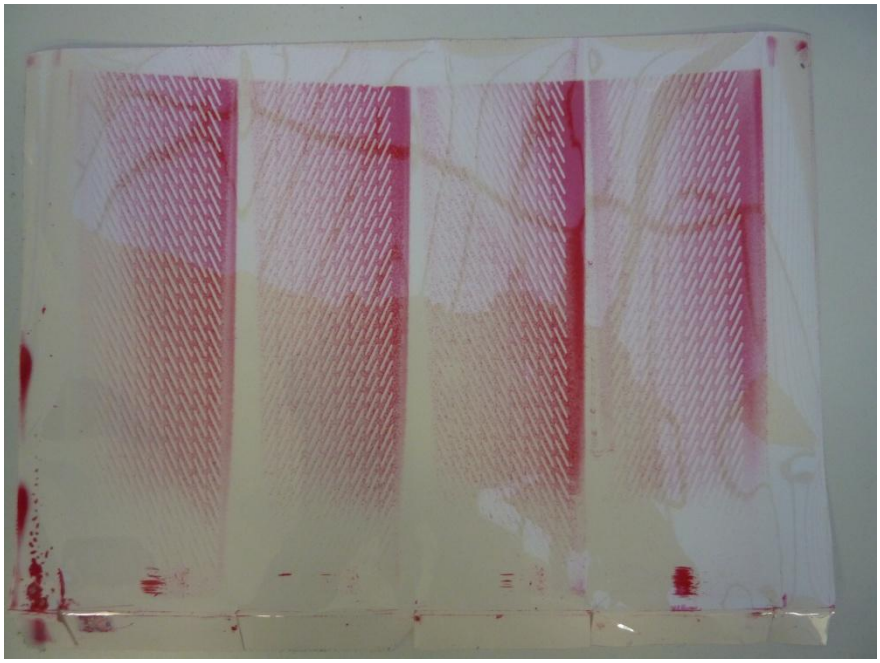

Figure 129 Pressure paper pattern from inlet at 75A loading

The raw result indicates that there is a distinct pressure gradient caused by the contact of the grains. The high pressure regions (seen by the most intense colour) are located on the leading face of each section of the polisher. This result matches closely the highest wear regions found on the screens in practise which is thought to validate the use of pressure sensitive paper to identify high risk regions of wear.

From the pressure paper raw result, the image can be adjusted digitally to identify the pressure density at various resolutions. The papers are scanned and then converted to greyscale. From the greyscale image, a gradient map is computed and the colours set to show the different pressure regions (see Figure 130). Red indicates a high contact pressure whilst blue indicates that the pressure was insufficient to trigger the bleed of colour in the paper.

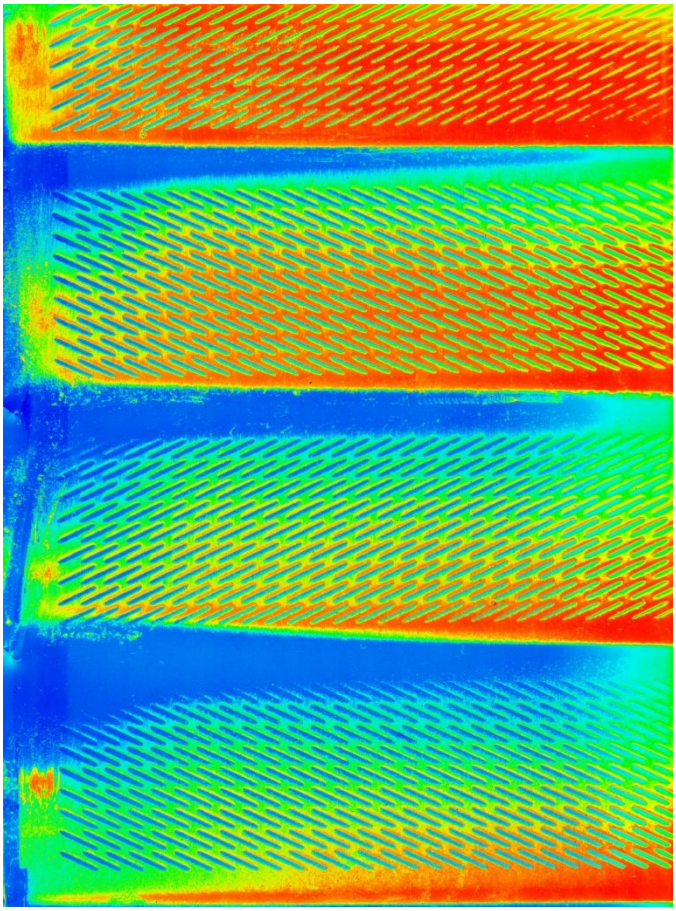

Figure 130 Gradient map for inlet at a load of 75A

Figure 125 above shows much more clearly the areas of high and low pressure as the rice travels around the polisher at inlet. Converting the scale provided from shades of red to match the densities and colours above (Figure 131) allows a much simpler analysis of the pressure regions. It should be noted that the pressures are only indicative since the paper is designed to identify normal pressures and in the case of polishing there is both normal and tangential pressure. The pressure regions are also seen to match closely those seen in the paint wear test.

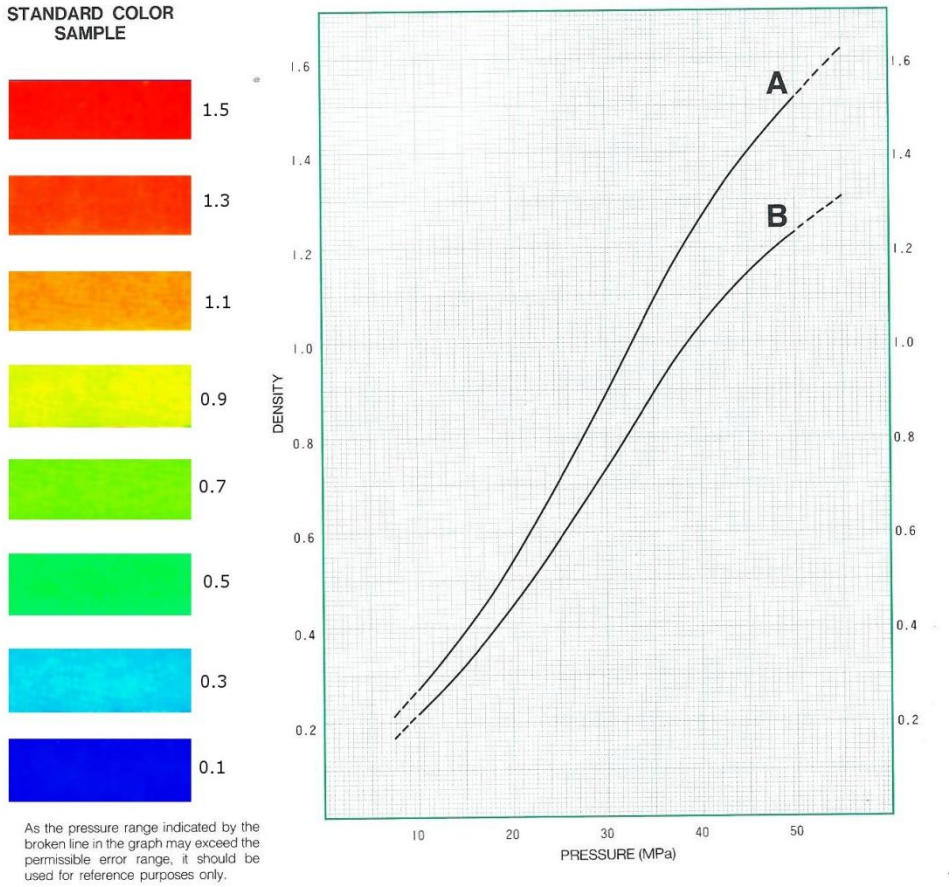

Figure 131 Graph showing how image colour relates to pressure

The resolution of the paper is sufficient to look at the smaller scale of wear affected by the slots themselves (see Figure 132).

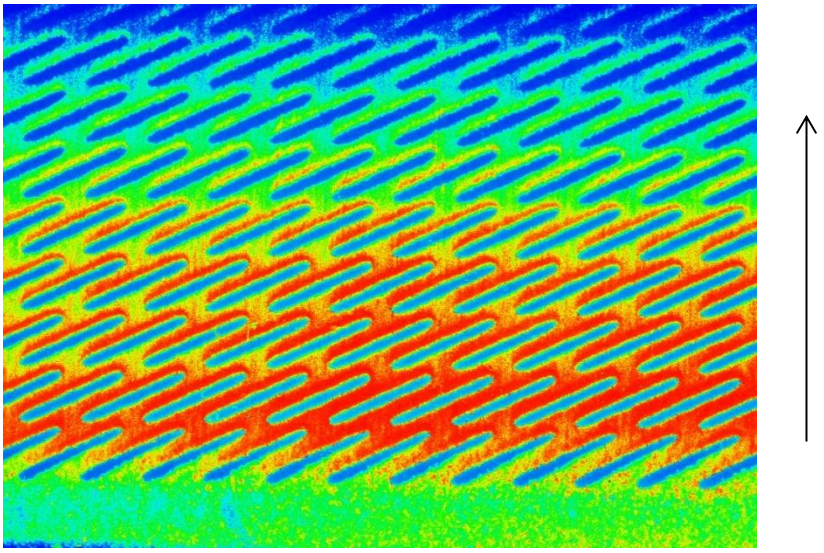

Figure 132 Pressure distribution around slots at inlet at 75A loading. Rice motion is from bottom to top.

The trailing edge of the slots indicate a higher contact pressure with the grains. This is strong evidence that the pressure is responsible for the wear of the polisher as the gradient matches those seen in practise.
Since the method has been shown to be successful, some comparative tests have been run to observe the change in pressure under different scenarios.

Firstly, the pressure at inlet and outlet have been observed by repeating the loading of 75A with paper location at the outlet on the same polisher half-shell (Figure 133).

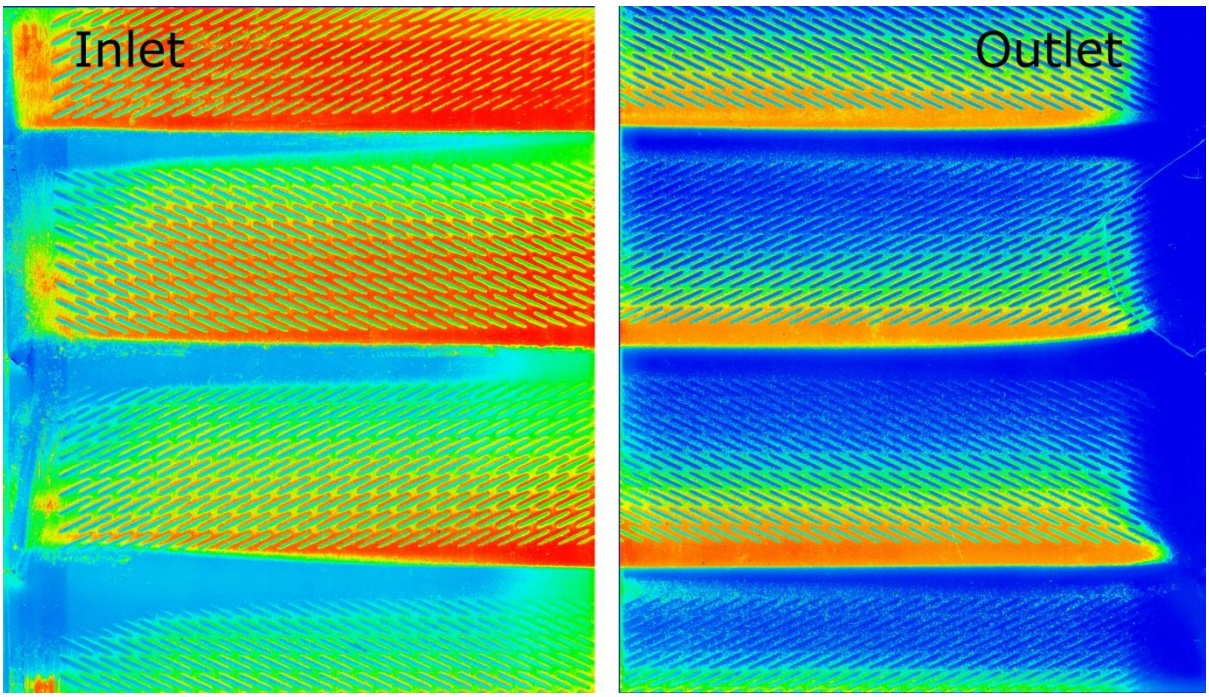

Figure 133 Pressure density map comparing inlet and outlet (rice motion bottom to top)

The pressure at the outlet is clearly much lower than that at inlet generally whilst the pattern of high and low pressure regions remains the same. This is a useful result as it indicates that the rice flows from a higher pressure to a lower pressure, and explains why the outlet shows less wear than the inlet during use. The pressure at outlet has also stabilised generating a similar profile on each screen section. At inlet, a higher pressure is observed on the bottom section (seen at the top of the above image). It is thought that this is due to the rice entering the chamber from the feed screw in an unevenly distributed way. Figure 134 below shows the pressure profile generated by this method at inlet and outlet.

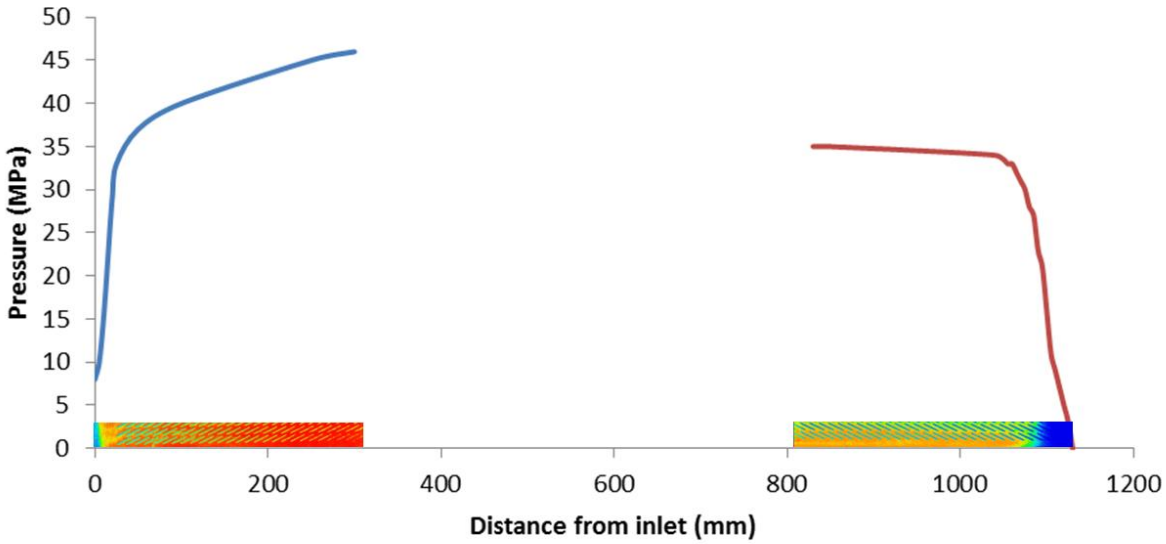

Figure 134 Pressure profile along polisher

The effect of loading has also been briefly studied. The inlet was again observed for consistency and the polisher run to a lower loading of 50A for 10 seconds before the grain flow was stopped (Figure 135).

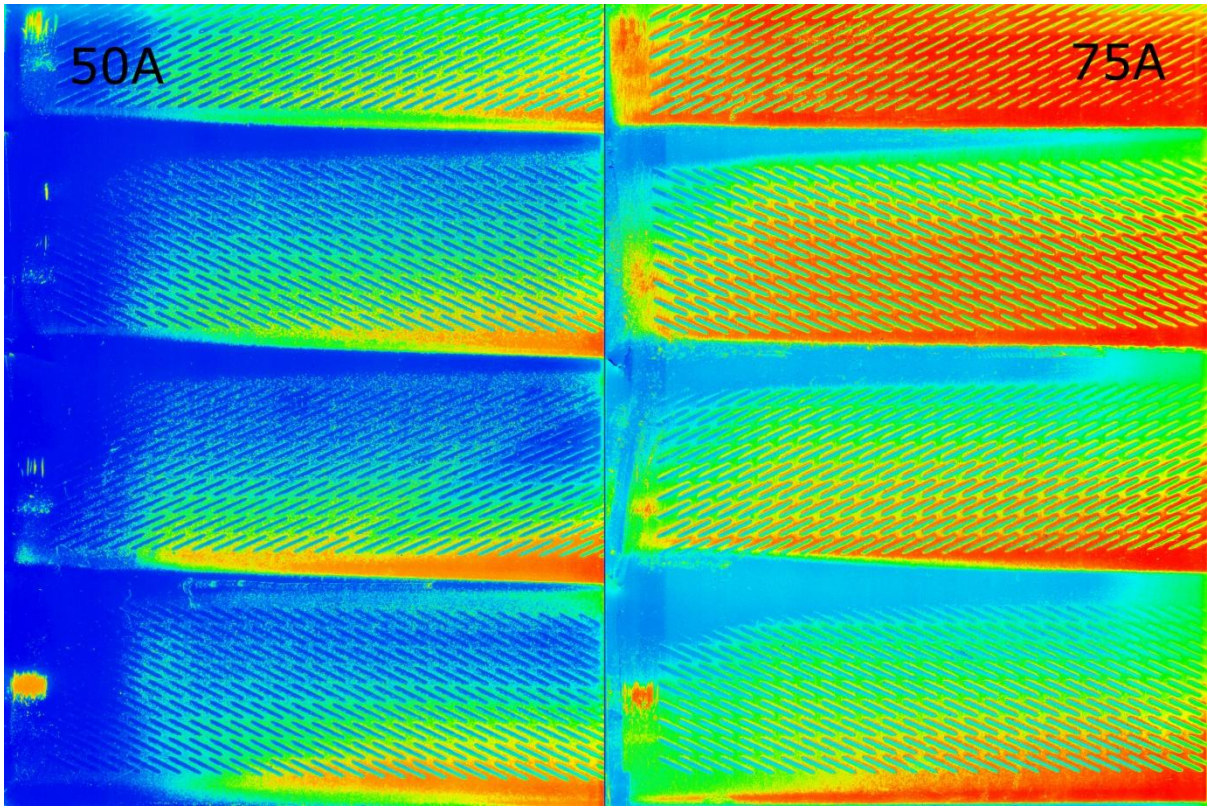

Figure 135 Pressure density comparison at inlet between 50A and 75A

The pressure against the screen is seen to be much lower when the loading is reduced. This is a sensible result as the loading is based on the fill of the chamber (a higher rice flow rate means a higher loading). It's interesting that the screen section

experiencing the highest pressure is different between the two cases. In the case of 50A loading, it is the second from top portion of the screen when running which indicates the highest pressure (second from bottom in the image) and in the 75A loading it is the bottom section (top in the image). The true cause of this is unknown however it is most likely related to the density of the grains altering the fill of the feed screw which in turn changes the way in which the grains flow into the chamber.

One of the main drawbacks in the pressure paper system is that it relies on not being contaminated by water. On contact with water, the paper becomes opaque and ceases to bleed colour with pressure, hence the previous tests had been run with no water misting in the polisher.
A test has been carried out using a polythene film as a barrier between the water misting and the pressure paper to determine how the pressure changes in the polisher with the addition of water (Figure 136).

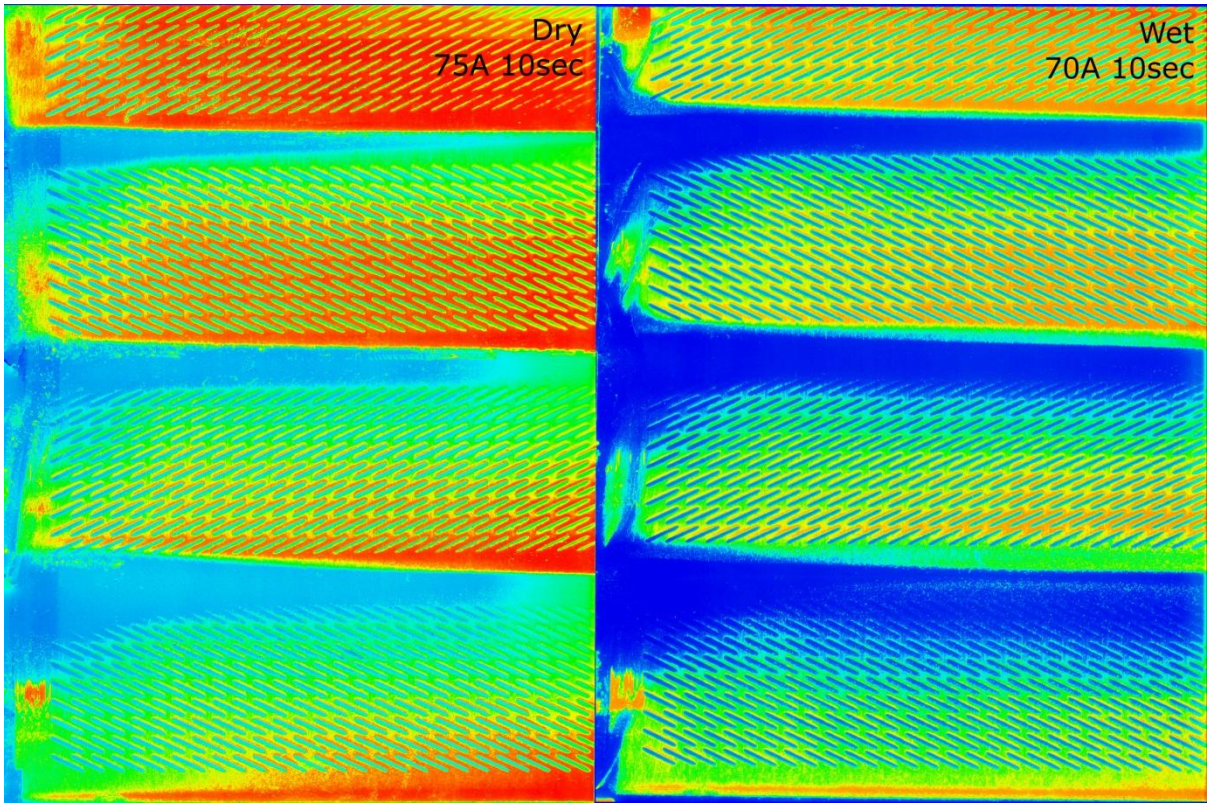

Figure 136 Pressure gradient map comparison between dry and wet test runs

The addition of water presented a problem in accurately running the machine at a load of 75A since control of both rice flow, loading, and water addition require the running and monitoring over time to ensure the quality of the product exiting the chamber is correct. Since the test durations were 10 seconds at load, it was not possible to accurately load the machine in this way. In the test run above, a loading of 70A was achieved for 10 seconds with a water flow rate of 40l/hr.

The result shows a reduction in pressure when the machine was running with water misting, however this goes against the previous evidence of an increase in wear rate with the addition of water. There are two possible reasons to why this result may not be reliable. Running the test at 70A rather than 75A may be a sufficient reduction in loading to reduce the pressure in the chamber. Secondly, the introduction of the polythene film may absorb and spread the impact of the grain across a larger area, thus reducing the observable pressure.
In order to accurately determine the effect of water flow rate on the wear of the screen by rice pressure, it would be necessary to run all trials using the polythene film as an intermediate barrier.

Since pressure has been seen to be responsible for the wear of the screens, and it has been hypothesised that the majority of the polishing work done to the grains is by grain-grain contact, the screen life should be extended by attempting to design in a way which promotes an even pressure distribution whilst still rotating grains for efficient polishing.

8.4 Screen Mechanics

The wear observations highlight the necessity of understanding fully the mechanics of the polisher screen. This includes both the material properties (principally hardness) and how the screen moves and behaves. Hardness has been measured for various screen materials and the screen dynamics observed in operation.

8.4.1 Hardness

Three different screen materials currently in use have been tested using a microhardness indent test. A 1kg load was applied using a diamond tip and the resulting indentation measured to determine the Vickers hardness (results shown in table 11).

	Max (HV)	Min (HV)	Avg (HV)
Cobramax	325	288	299
Nitriert	1247	956	1080
Nitro-carburised	1337	1207	1282

Table 11 Maximum, minimum and average measured hardness values of microhardness for various screen materials

The hardness is important as many studies have shown that it relates to wear rate in abrasive situations. The results above therefore suggest that the nitro-carburised screens are more likely to be the most resistant of the three to abrasive wear, having as it does the highest micro-hardness.

8.4.2 Screen Vibration

The vibration of the polisher can cause high levels of noise and suggests an inefficiency in the polishing process. It is also possible that the vibrations in the screen are of a harmonic which creates a node-antinode pattern of vibration which could help explain the uneven wear pattern seen in the paint test. The noise created by the vibrations has been noted to increase with increased loading and is also dependent on the product being processed. It is thought therefore that observing the vibrations in detail could help to reveal information about the efficiency of the polishing process. Ideally there would be zero vibrations around the polisher screen.

8.4.2.1 Measurements Using Dial gauge

As a pre-assessment tool, a dial gauge has been placed at various locations around the screen of the lab scale polisher with the intention of observing the magnitude of the vibrations (see Figure 137).

Figure 137 Dial gauge positioning

The high and low displacement were recorded at locations around the chamber. The test was run three times and the eight screen sections were measured each three times per test. Screen sections have been numbered progressively as follows in Figure 138:

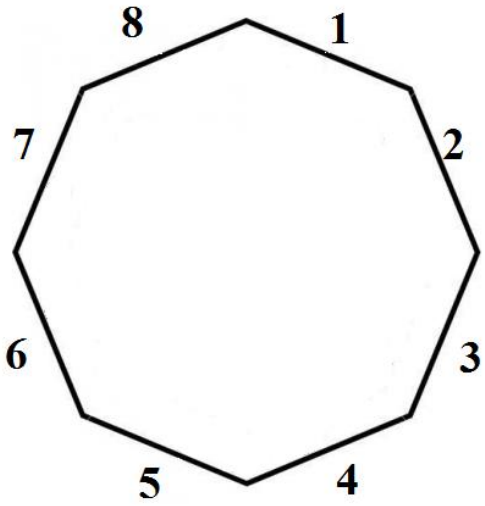

Figure 138 Dial gauge positionings around screen (1-8 followed by 9-16 then 17-24)

The results from the test are shown below in Figure 139:

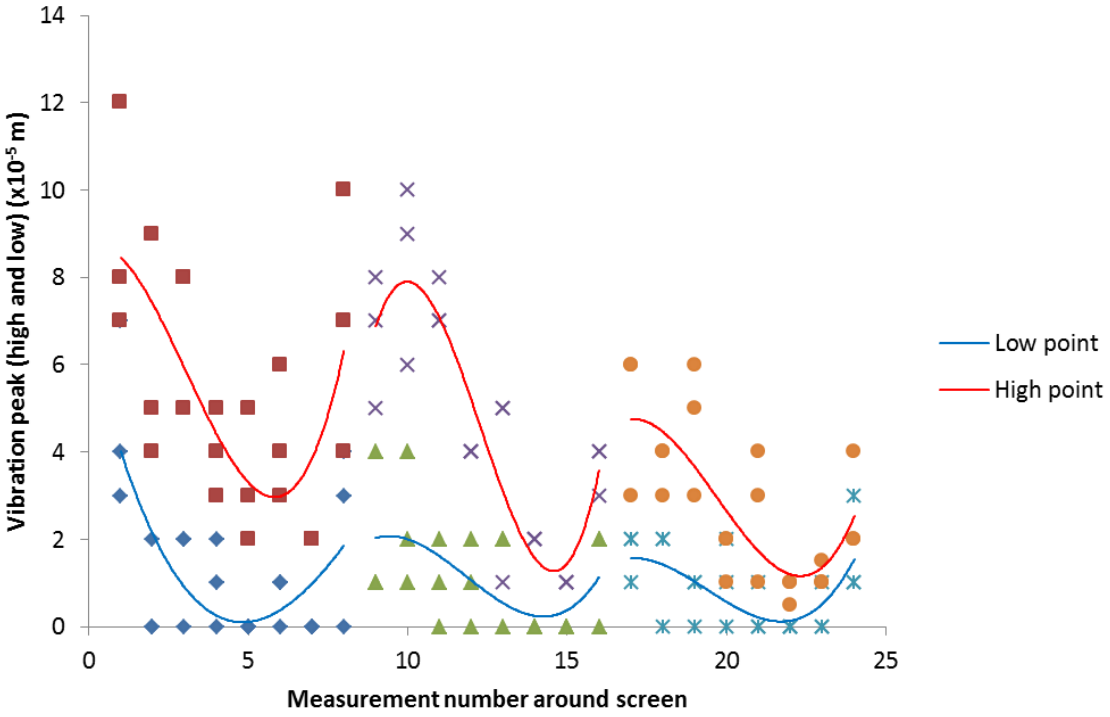

Figure 139 Vibrations in different locations around the screen

The results show that the magnitude of the vibrations varied dependant on location around the chamber. It is thought that this effect is due to the initial condition of the rice sitting at the bottom of the chamber.

Since between the three sets of measurements per test, the rice was not refreshed, the test also reveals a decrease in the magnitude of vibrations as the grains become

more rounded and polished. This is something that has been noted by millers in practise but has not been actively studied. Similarly, longer grain structures are known to create higher vibration magnitudes than short grains.

8.4.2.2 Measurements Using Laser Vibrometer on Lab Scale Polisher

A more accurate method of measuring the vibrations in the polisher chamber has been developed and involves the use of a laser vibrometer to capture the vibration data.

The vibrometer works by sending a continuous beam from the transmitter and recording its return, reflected position on a sensor. As the target surface moves closer and further away the position of the reflection on the detector changes. This is then recorded as a voltage relative to the position giving a high resolution over a small range of displacements.

The vibrometer was first set up on the lab polisher using clamp stand and an oscilloscope to observe the vibration data. A protective screen has been used to reduce the amount of dust expelled by the machine as seen in Figure 140.

Figure 140 Laser vibrometer equipment

A data acquisition box feeds the signal to the oscilloscope where the signal can be processed and read (Figure 141).

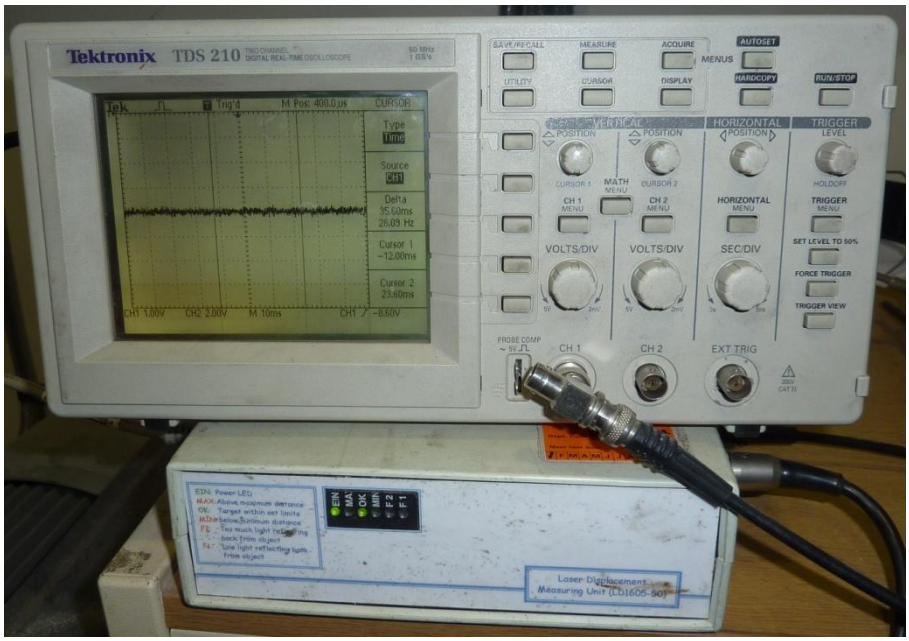

Figure 141 Oscilloscope and data acquisition box for laser vibrometer

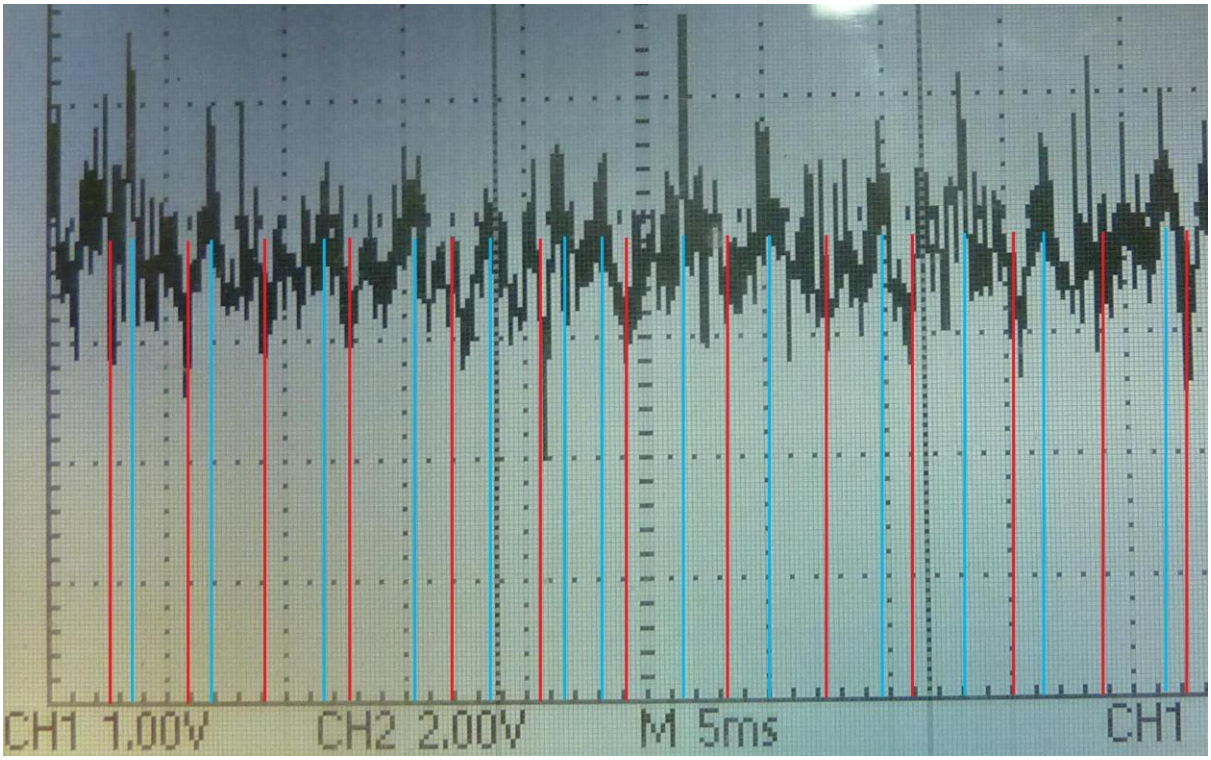

Figure 142 Oscilloscope plot of screen vibrations showing peaks (blue) and troughs (red)

The fundamental frequency of the polisher vibrations can be easily measured in this way (Figure 142) and are seen to match up with cam roll blade passes. The data can then be collected using Labview so that it can be processed and the frequencies analysed.

Having confirmed that the process gives satisfactory readings using the lab polisher, a full scale test was undertaken to investigate the vibrations at outlet of a polisher in practice.

8.4.2.3 Laser Vibrometer Measurements of Full Scale Polisher

Three test runs have been observed with different operating conditions. In the first instance (Figure 143), the polisher was run to capacity with dry rice grains released for 10 seconds. The current peaked up to 74A which is comparable with normal operating conditions.
In the second case (Figure 144), an error resulted in the over hydration of the grains which caused a blockage in the machine with the current spiking at 100A.
In the third case (Figure 145), water was misted into the chamber at a rate 40l/hr. Grains were released for 10 seconds and the current climbed to 75A.

The location of the vibrometer remained the same in each case and was secured to the polisher supports so that the vibration of the screen relative to the casing could be observed.

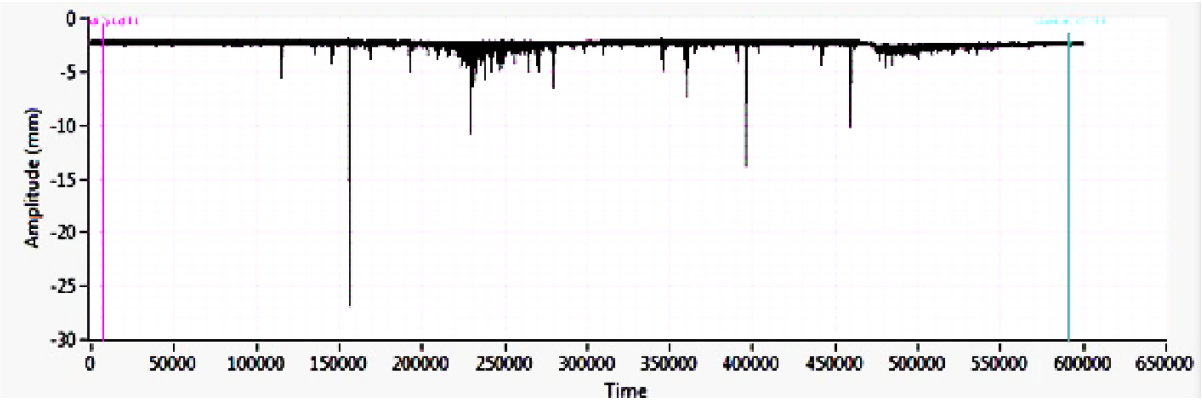

Figure 143 Vibrometer data first run

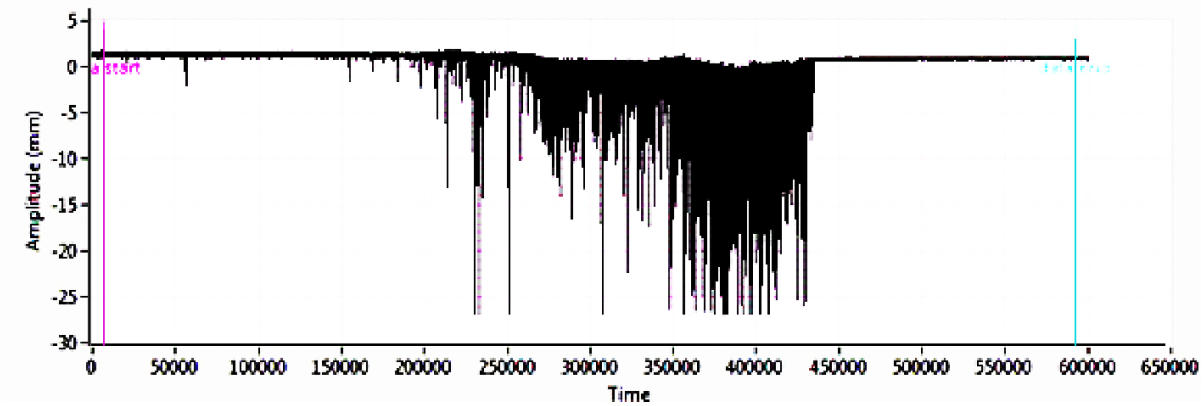

Figure 144 Vibrometer data second run

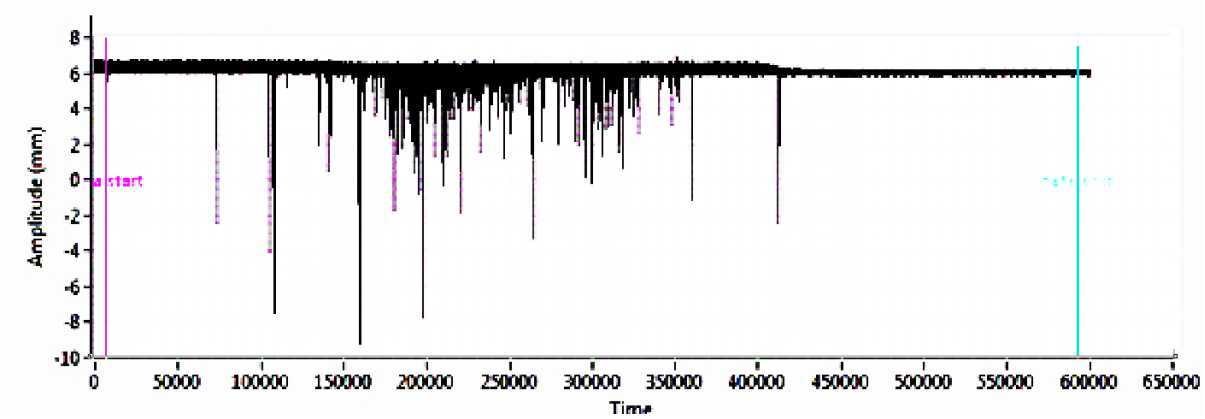

Figure 145 Vibrometer data third run

The raw data has then been split up into one second intervals, and a Fourier transform taken which allows the harmonic modes to be seen clearly. By separating into one second intervals it is possible to observe how the fundamental frequencies change during the course of the test and allows a useful means of comparison of the data. The lowest frequencies have been omitted as they do not give useful information to the nature of the vibrations and would otherwise constitute the majority of the data.

The first test results are shown below in Figure 146:

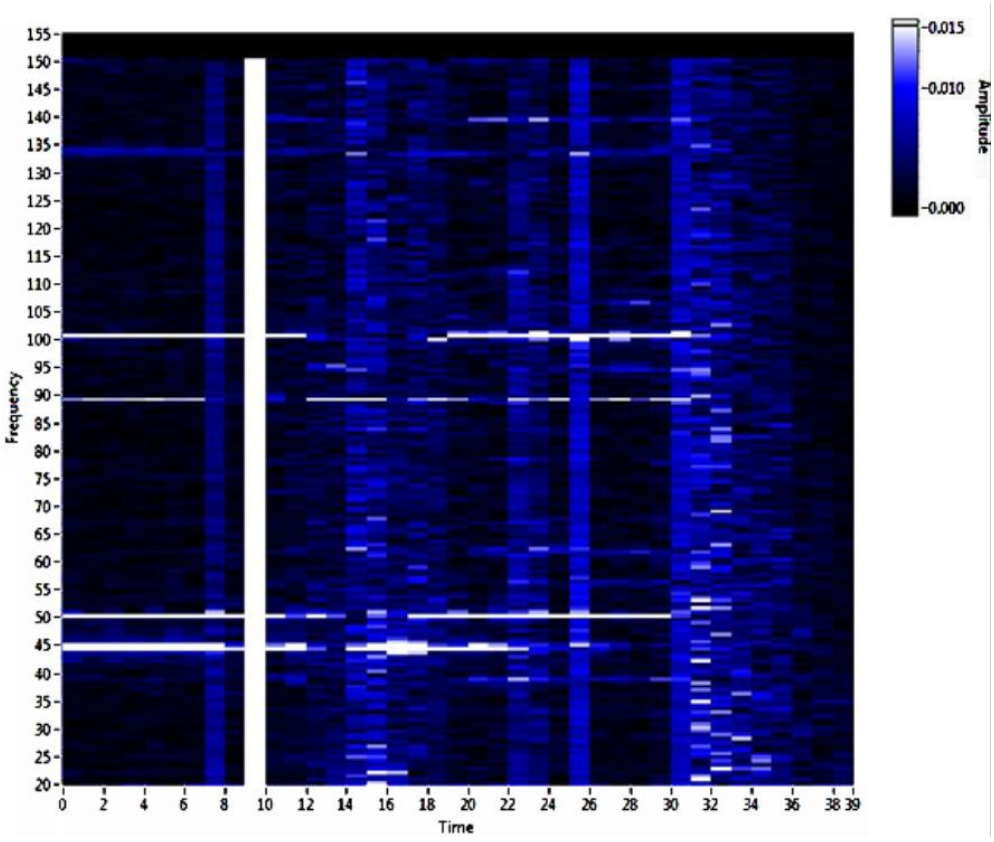

Figure 146 Fourier transform intensity for first run

The test shows a spike in intensity at the nine second mark which is the point at which the grains were released into the polisher. Between 14 and 18 seconds the polisher is operating at capacity and experiences a higher vibration intensity at all frequencies. At 18 seconds the rice flow is halted and at 30 seconds the cam roll is decelerated to rest.
The high intensity of the frequencies at 45Hz and 50Hz are the fundamental frequency of the polisher and correspond to the rotation of the cam roll. The elevated intensities at multiples of these frequencies are the harmonics resonances to the fundamental frequencies. As the machine moves to capacity the vibrations of the fundamental frequencies are partially interrupted.

In the second test run, the over-addition of water resulted in a fusing of the grains resulting in much higher machine loading and hence much higher magnitude vibrations (as seen in Figure 147).

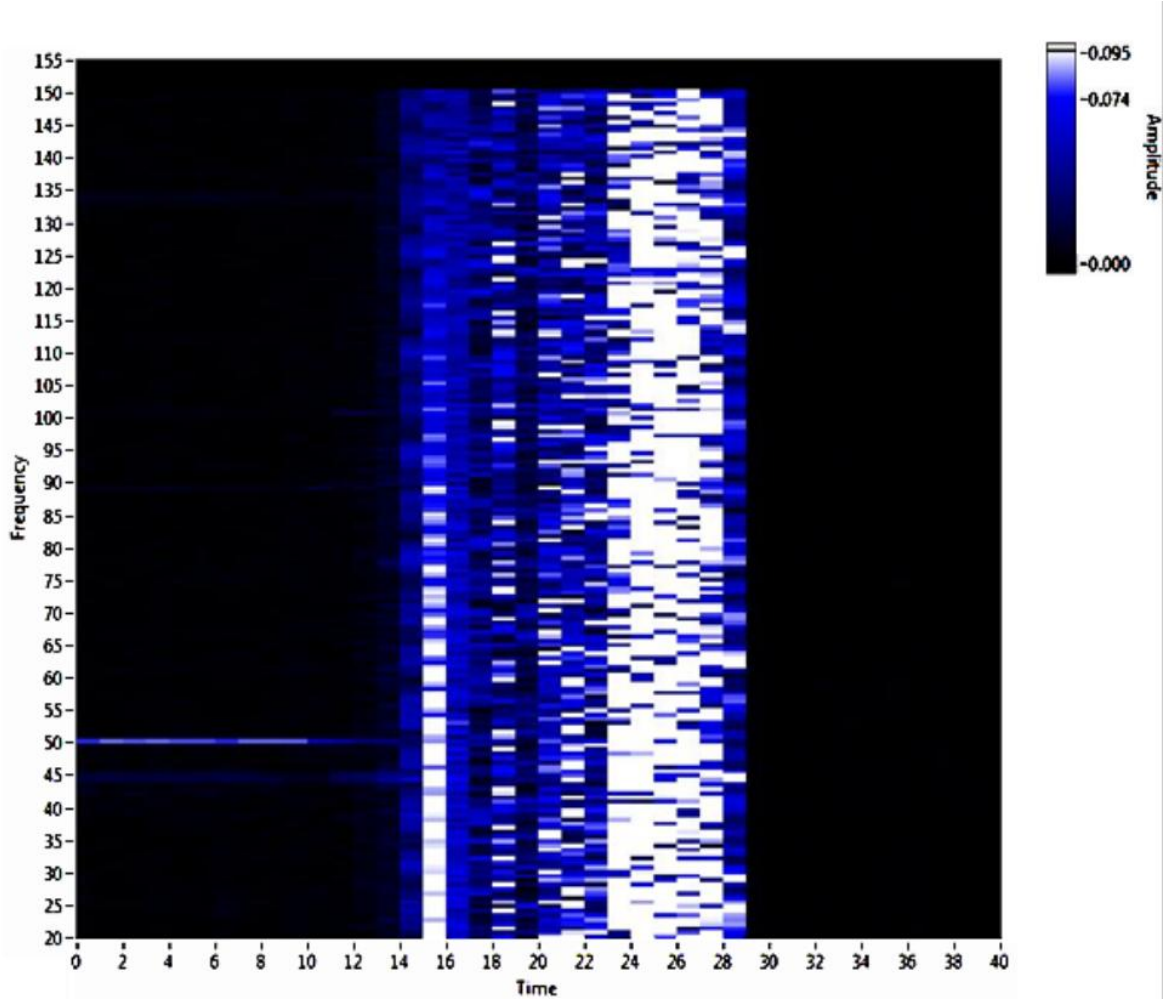

Figure 147 Fourier transform intensity for second run

Whilst the same fundamental frequencies are present prior to rice entrance into the machine, the magnitudes are completely overshadowed by the intensity of the vibrations as the grains begin to fuse together. The test was stopped abruptly at 29 seconds to prevent machine damage. Figure 148 shows the Fourier transform from a 10 second grain release. The fundamental frequencies are present throughout the run however further high magnitude frequencies are observed on grain release.

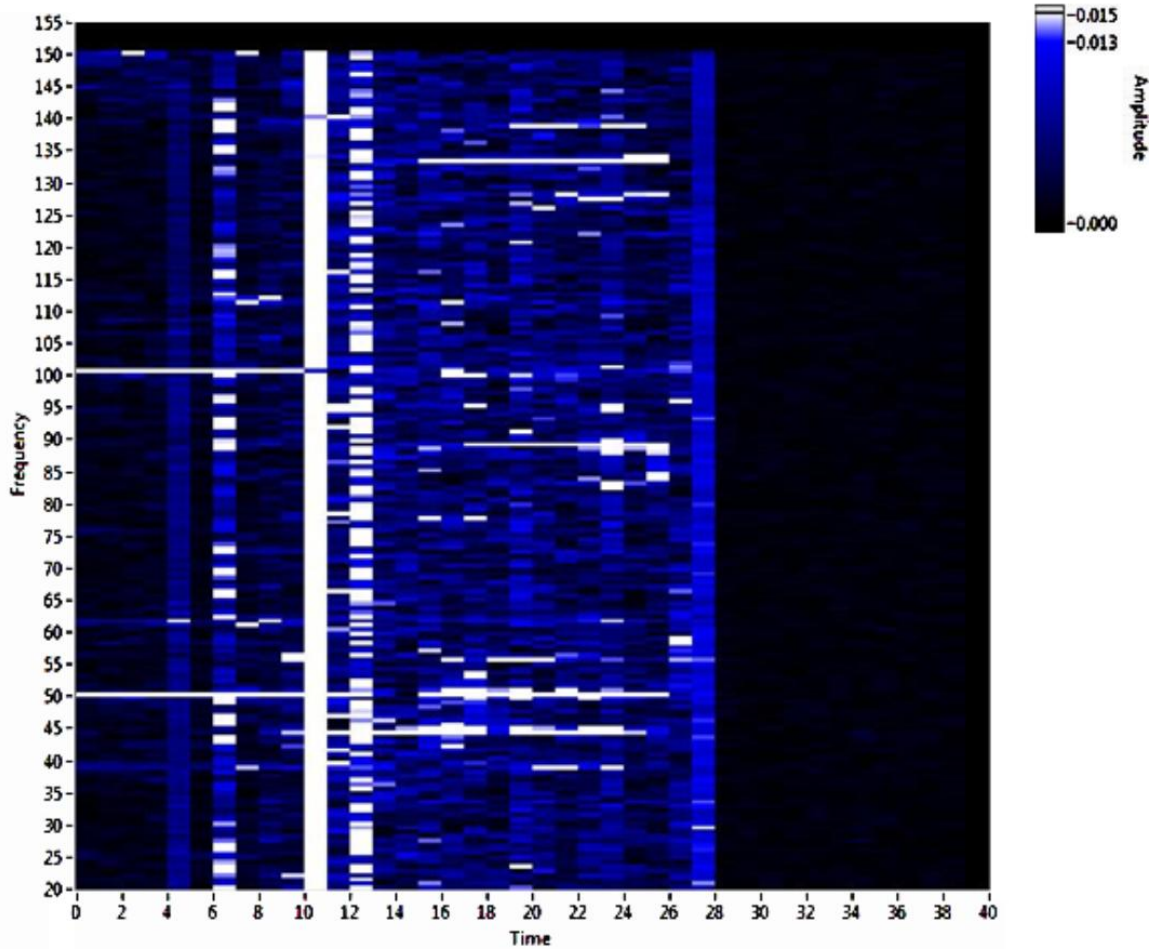

Figure 148 Fourier transform intensity for third run

8.4.3 Vibration as a form of automatic feed control

It has been shown that the magnitude of the vibration of the polisher directly corresponds to the load. It is therefore suggested that this could be utilised to automatically regulate the flow control of the polisher.

The machine vibrations correspond to the bulk flow of the grains meaning that by observing the Fourier transform intensities can reveal information on the evenness in polisher fill between blades. Using this information, it may be possible to develop a system by which grains are fed into the polishing chamber at different locations and at different rates in order to balance the machine which would have the overall effect

of reducing vibration and potential improvement of the uniformity of the product by ensuring the consistent work rate of the polisher.

8.5 Particle Simulation

8.5.1 Introduction

It is very difficult to model the behaviour of particles analytically. Predicting the motion of bulk flow is difficult since particles sometimes behave as a fluid or gas and sometimes behave as a solid. Granular materials can also exhibit a range of properties and pattern forming behaviours which are unique.

With the increasing trend in computing power comes the potential for carrying out more and more realistic simulations based on individual interactions of particles thus eliminating the need to model the granular material as a single body. Since the relative positions of particles can be monitored and the resulting motion from impact of each sphere calculated rapidly, there is a good potential for undertaking complex simulations with large numbers of particles.

Several studies have used discrete elements to understand the behaviour of granular flow in certain situations[73]. For instance, in 1995 Langston et al.[74] released a paper in which they carried out simulations with Newtonian dynamics of 2D disks and 3D spheres in model hoppers. Various aspects of hopper filling and discharge were examined and the interactions between particles improved upon until results gave good agreement with established literature empirical predictions. There are various drawbacks to particle simulation. The most notable is that results can look believable regardless of consistency with real situations. It is therefore important that the results collected by simulation be validated.

“Particle Flow Code” or PFC3D particle simulation software has been used to model the movement of rice grains in a polisher. If results from simulations can be shown to be comparable to the real flow of rice in the polishing chamber then particle simulation could be used to develop polisher design.

PFC3D uses a discrete element method of modelling spherical particle movements and interactions, whereby calculations are performed over a series of time steps. The simulation first develops a model outline using schematics of the polishing chamber. Particles are then generated randomly around the chamber and the central cam roll is rotated. Boundary conditions are applied such that the particles are not free to move beyond each other or walls without interacting.

A limited section of the polisher has been modeled to reduce the simulation run time although grains are free to move axially with the inclusion of a periodic boundary

condition, applied to the axial limits of the model. It was felt this represents a reasonable model of the middle section of the polisher. Gravity is applied vertically (at 9.81m/s²) and contacts are assumed to be perfect between spheres (with coefficient of restitution specified). At each time step, data is collected at any contact and the resulting motion for the following time step calculated. Any contacts with the specified wall are recorded and force and time data stored.

This data, once collected has then been post-processed (in Matlab) to distinguish between the number of sliding type contacts and impact type contacts. The properties of the polisher and the rice particles have been determined from some small scale experiments.

8.5.2 Model Inputs

Material inputs into the model are detailed below in table 12:

Rice-Rice Coefficient of Friction	0.7
Cam Coefficient of Friction	0.6
Screen Coefficient of Friction	0.6
Wall Coefficient of Restitution	0.5
Rice Coefficient of Restitution	0.2

Table 12 Rice/Wall properties for polisher model

The coefficients of friction for the various surfaces have been determined by experiment (see Chapter 4.3 and 8.4). Coefficients of restitution of rice and wall are from Camacho's "A Study of Erosion and Abrasion Wear Processes Caused During Food Processing"[75].

8.5.3 Modeling Constraints

The software used is limited to using spheres which can be fixed relative to other spheres as a cluster. Initial testing suggested that it is better to model rice grains as individual spheres rather than clusters of spheres as it was thought that although clusters resemble the shape of grains better, they result in grains interlocking between sphere boundaries and hence the appearance of an unnaturally high friction between particles. It is thought that spheres provide a more realistic solution and also cut down on simulation time.

A boundary condition has been applied such that particles are free to move along the axis of the machine. This means that a smaller section of the chamber can be modelled, significantly reducing computation run time. Since each simulation run of the full polishing chamber rotating the cam roll more than once would take several days this is a preferable solution.

It should be noted that the results presented are non-dimensionalised units of force.

Simulations have been run at two different cam roll rotational speeds; a low speed of 40.8rad/s and a high speed of 88rad/s. Conclusions can then be drawn by comparing the chamber operating speeds.

8.5.4 Current Buhler-Sortex Polisher Geometry

A section of the current Buhler-Sortex polisher geometry is shown diagrammatically in Figure 149. The results presented here are from the surface of the mesh screen labeled S1. In all the presented results the X axis is circumferential from the bottom of the polisher and the Z direction is axially along the polisher. The model was created as a section of the polisher with periodic boundary conditions on the Z axis.

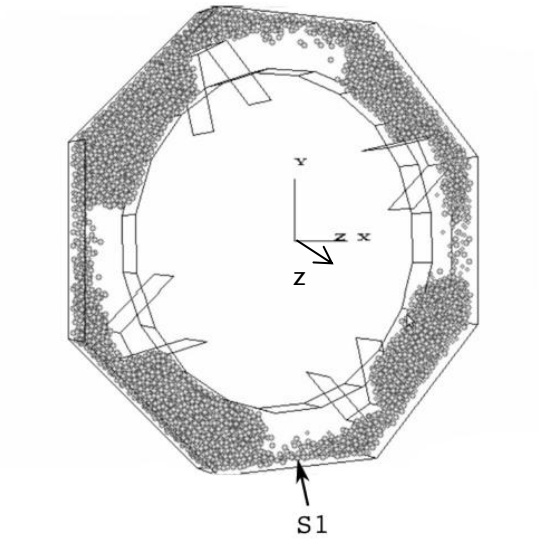

Figure 149 Simulation geometry and fill are for the labeled surface

The geometry considered is shown in Figure 149. The results presented here are taken from the surface labeled S1 in the figure. The simulation has been run for rotational speeds of 40.8 rad/s and 88 rad/s.

8.5.5 Simulation Results

A critical time for each sphere to be away from the wall was specified in order to separate ball contacts (above this critical time and the contact was considered to be new). This allowed the start time and end time of each full contact and hence the Euclidean sliding distance to be determined.
Figure 150 shows the distribution of contact distances for the geometry.

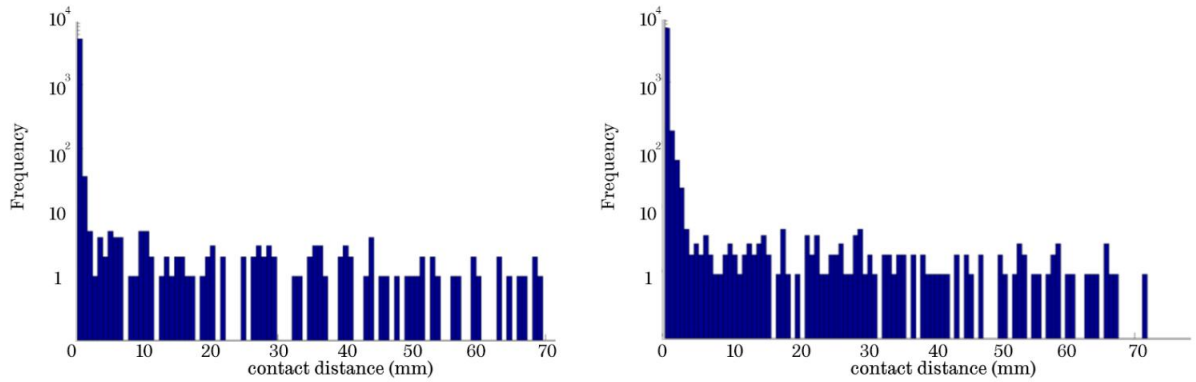

Figure 150 Histogram of contact distance at speeds (a) 40.8rad/s and (b) 88rad/s

Both distributions are similar and it is clear that the vast majority of contacts slide less than 1mm and could therefore be considered as impacts.

Figure 151 shows the contact positions over time for the slow and fast models respectively coloured by the normal force of each contact.

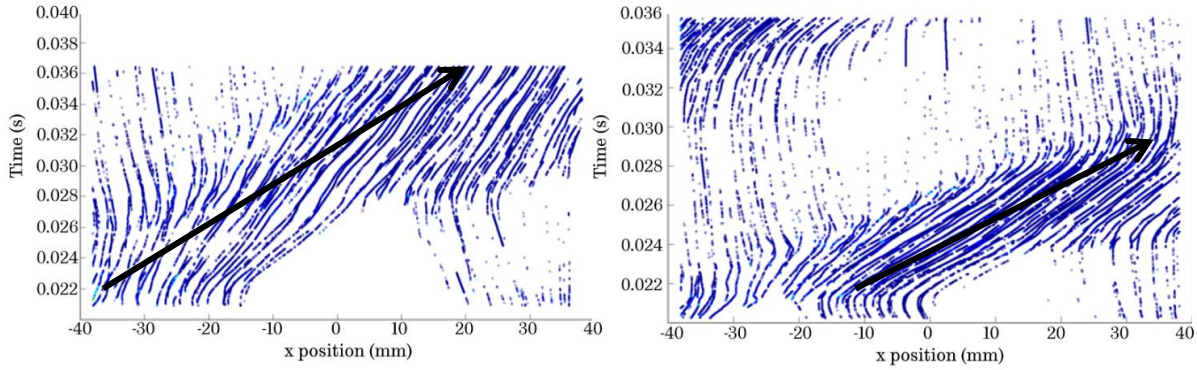

Figure 151 Contact positions over time at speeds (a) 40.8 rad/s and (b) 88rad/s with arrow showing blade tip position

Sliding contact can be seen by the long tracks of points which migrate from left to right with the passing of the cam. Impact collisions are visible also where there are only very short regions of contact. The vertical lines of contact points (seen top left and bottom right) are between the cam blade passes and demonstrate that the particles remain stationary between cam passes. The passes of the cams are obvious, and there is very little difference in the location of the large values of normal force.

Figure 152 shows the distribution of the position of the contacts for the slow and fast rotational speeds respectively, it can be seen that the distribution is very slightly more even in the fast rotational model.

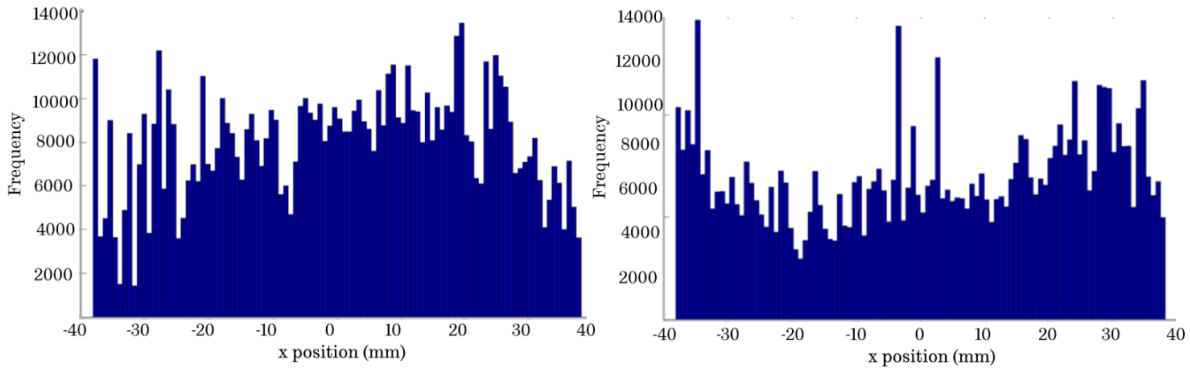

Figure 152 Distribution of contacts at speeds of (a) 40.8rad/s and (b) 88rad/s

In the slow case, the maximum number of collisions occurs towards the end of the surface, and then tails off. The fast rotation increases in frequency along the surface with a dip towards the start. Since the number of cam passes is low, it is likely that this result is affected by the start and end positions of the cam blade.
Figure 153 show the distribution of normal force along the surface.

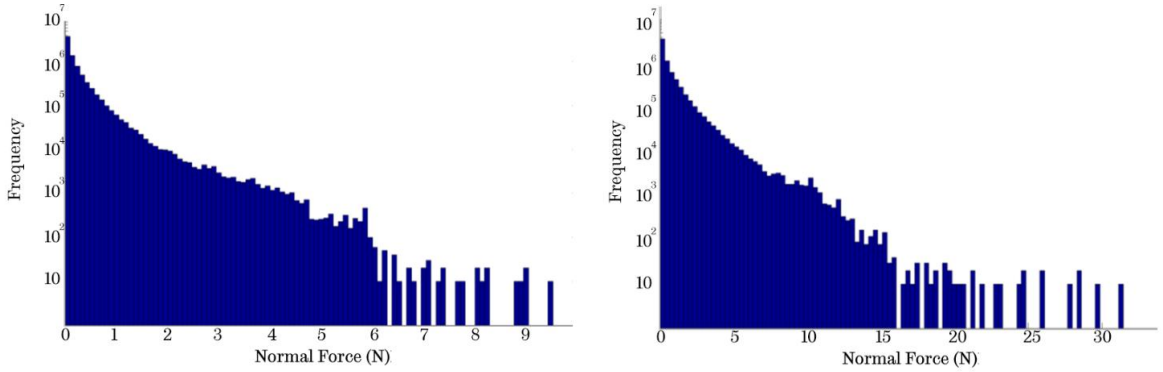

Figure 153 Distribution of normal force at speeds of (a) 40.8rad/s and (b) 88rad/s

The distribution of normal force is similar at both speeds although the slower speed generally takes around a third of the normal force. The majority of contacts have low normal force and relatively few are over 5N in the slow case and 10N in the fast case.
Figure 154 shows the normal force vs the x position. Both show a similar distribution with the larger normal forces towards the start of the surface. Spheres have been given different colours so that contacts can be seen.

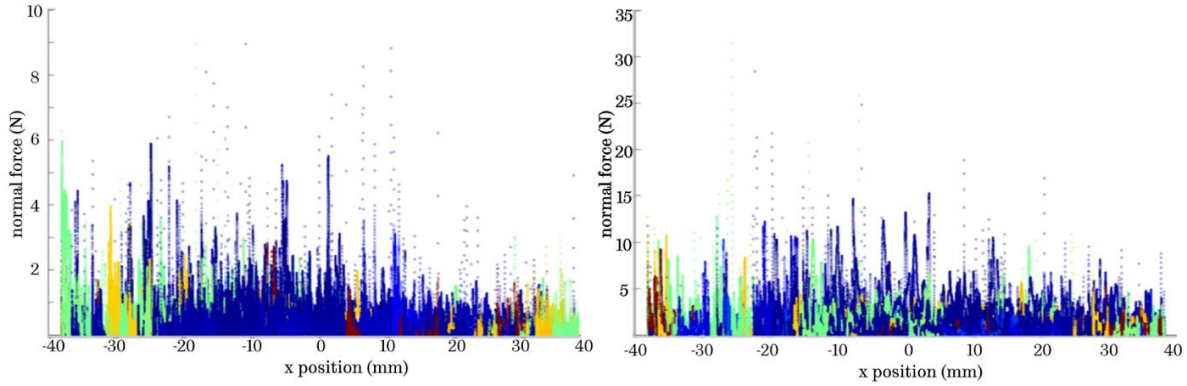

Figure 154 Contact normal force vs position at speeds of (a) 40.8rad/s and (b) 88rad/s

The larger normal forces on the left of the surface show a good correlation with the wear seen on the polisher screens.

8.5.6 Buhler-Sortex Proposed High Capacity Polisher Geometry

A second polisher geometry has been studied and has been designed to achieve a higher throughput of rice. There is a great interest in understanding how the two geometries compare in terms of performance before the high capacity geometry goes into production.

A section of the high capacity geometry is shown diagrammatically in Figure 155. This geometry has been specified by Sortex and represents the new potential polisher design. The results presented here are from the surfaces of the mesh screen labelled S1 and S2. As for geometry 1, in the presented results the X axis is circumferential from the bottom of the polisher and the Z direction is axially along the polisher. The model was created as a section of the polisher with periodic boundary conditions on the Z axis.

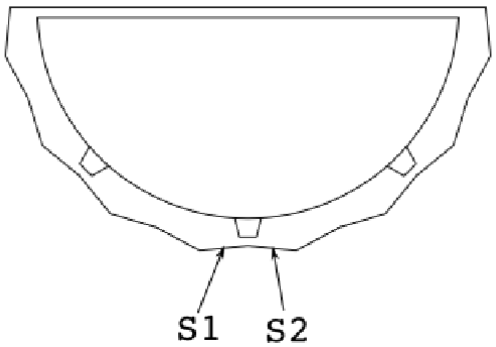

Figure 155 Geometry supplied by Sortex. Results presented are from the two labeled surfaces

8.5.6.1 Low Speed

Figure 156 shows the fill of the model during a run at the 40.8 rad/s. It is noticeable that not all the sections between cams has an equal fill, it is believed this is due to the starting condition (but has also been seen in the high speed videos produced by Sortex).

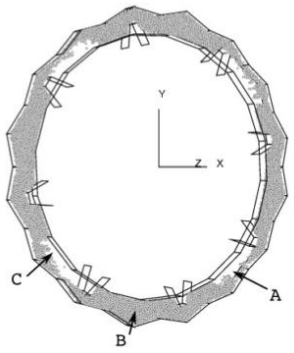

Figure 156 Showing the model with spheres during the simulation. The labelled sections show different section fills

Individual contacts with the surfaces S1 and S2 have been recorded and the data manipulated to determine the number of sliding type contacts and impact type contacts. (Figure 157)

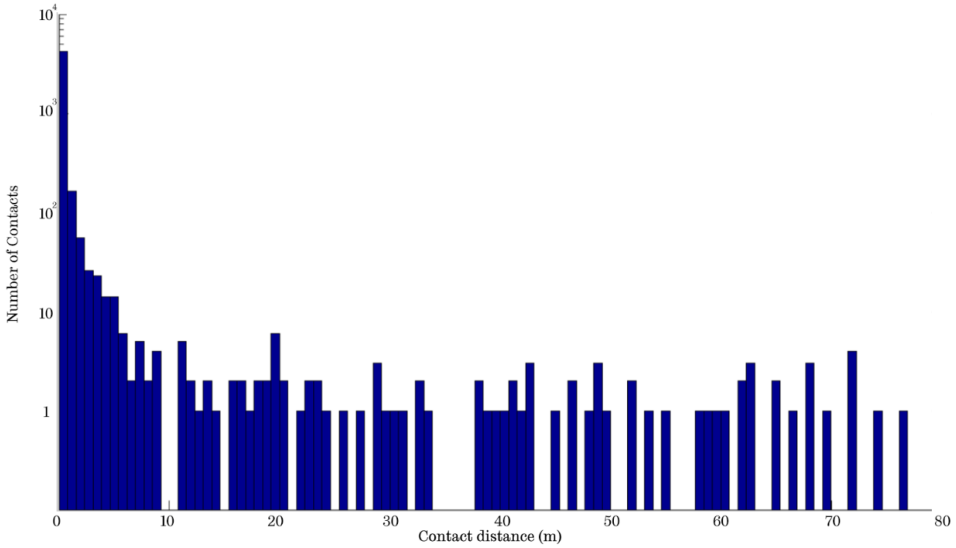

Figure 157 Contact distance along screen for individual contacts. Note log scale on Y axis

It is clear from this that the vast majority of contacts slide less than 1mm and could therefore be considered as impacts.

Figure 158 shows the position of the contacts between spheres and the walls over time, coloured by the magnitude of the normal forces. The passes of the cam can be seen in the density of contacts that steadily moves across the figure from the lower left corner. The figure shows the passing of a cam section, with varying fills, as seen in Figure 156. The join between the two surfaces S1 and S2 is also apparent with the number of contacts (individual) increasing on the counter rotational side of the boundary and being vastly decreased on the rotational side, as is expected with the two surfaces joining in a convex fashion.

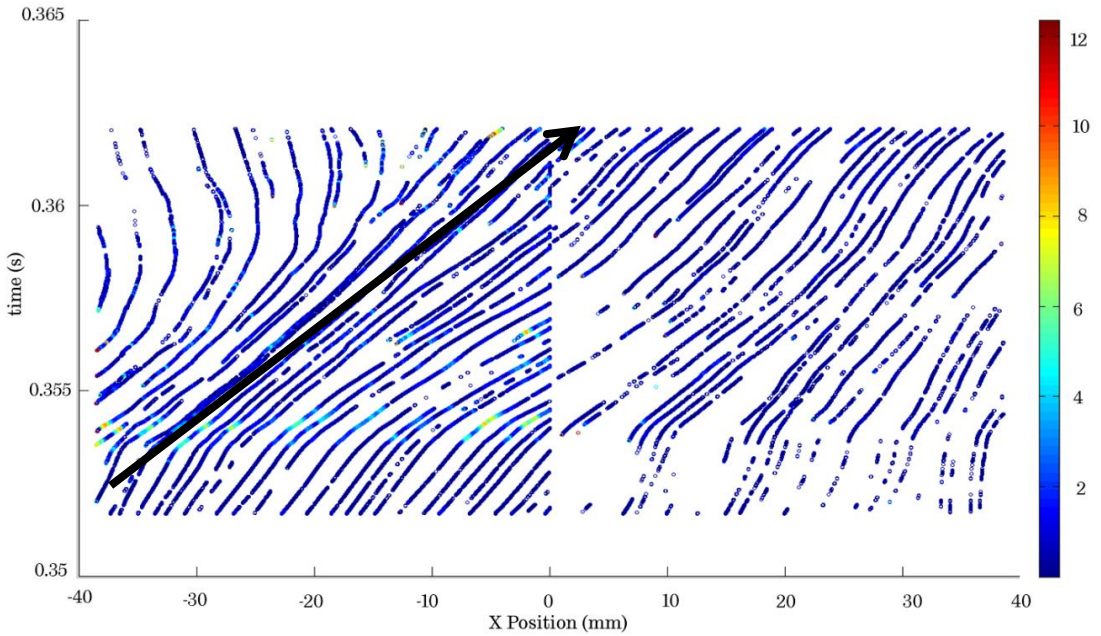

Figure 158 The points of contact along surfaces S1 and S2 over time coloured by normal force

Sliding contacts are, as with geometry 1, easy to see by the long tracks of points which migrate from left to right with the passing of the cam. Impacts are also visible where there are only very short regions of contact. The maximum normal force can be seen to occur on the leading surface (S1) at the time when the cam blade passes.

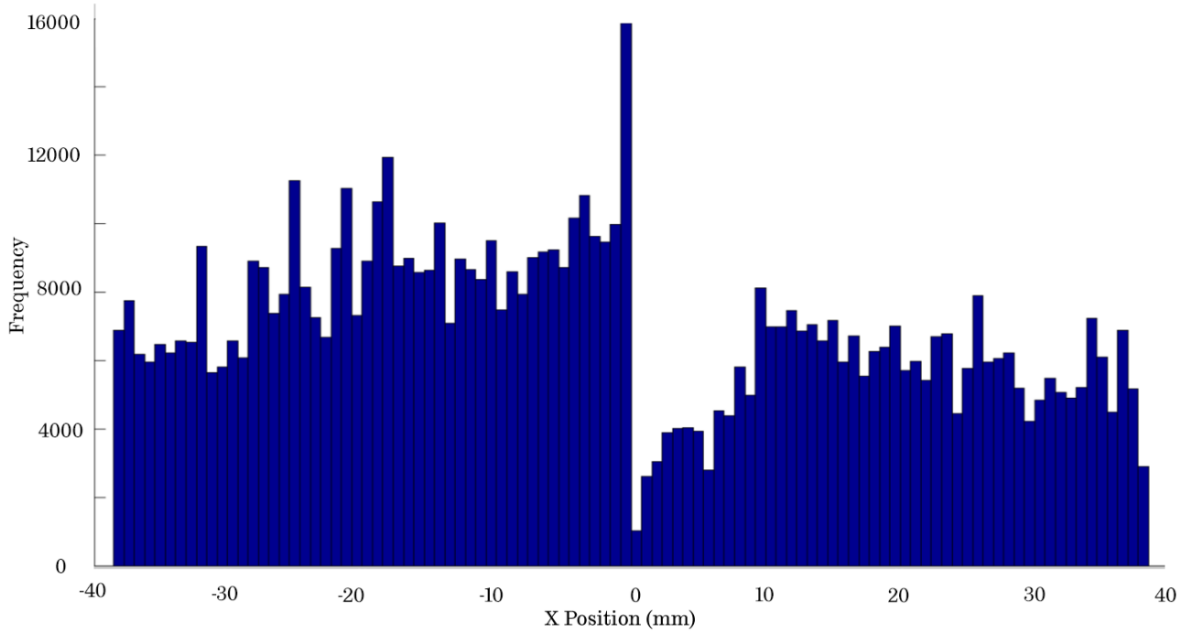

Figure 159 Histogram of the location of the contact positions along the length of surfaces S1 and S2

Figure 159 shows a histogram of the frequency of contacts on surfaces S1 and S2, again the border between the two surfaces is marked. Also the greatest number of contacts occurs at the end of surface S1, steadily increasing from the start until the

junction with surface S2 (X=0). After which the number of contacts rises steadily on surface S2, droping off again as you get close to the end of surface S2.

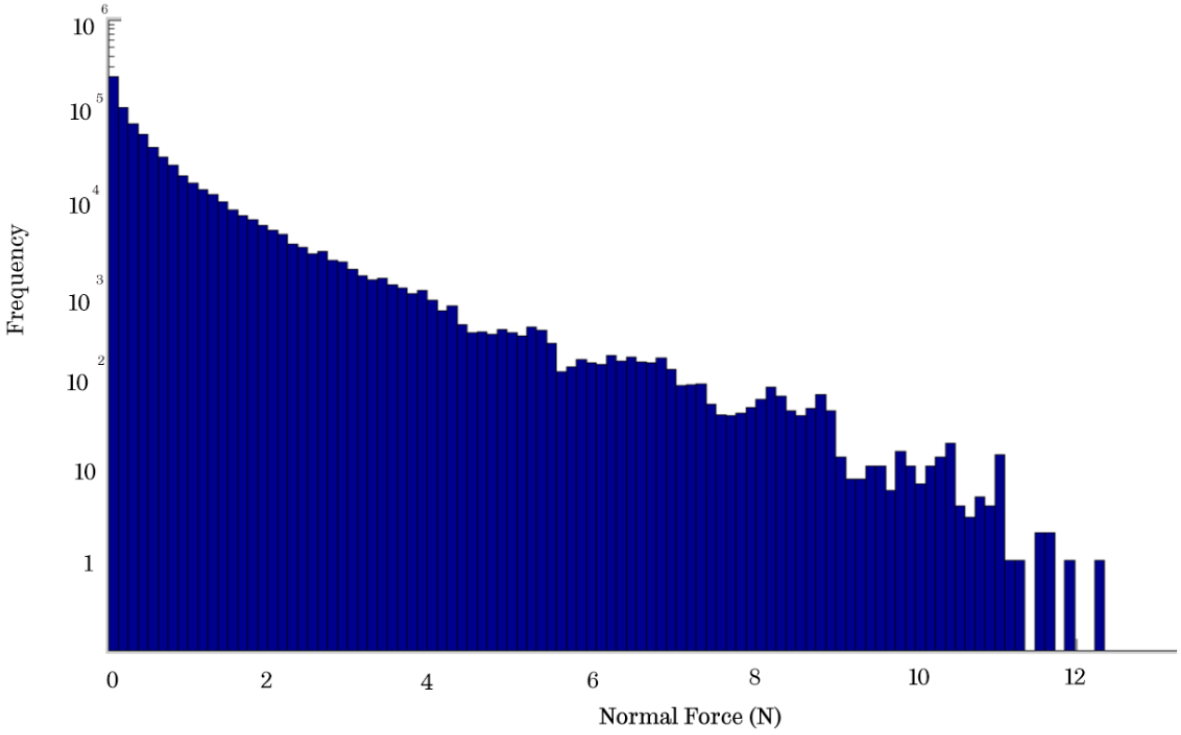

Figure 160 Distribution of contact normal force (log Y scale)

Figure 160 shows the distribution of normal force. It shows that the majority of contacts have low normal force and relatively few have over 10N, the maximum being around 12N.

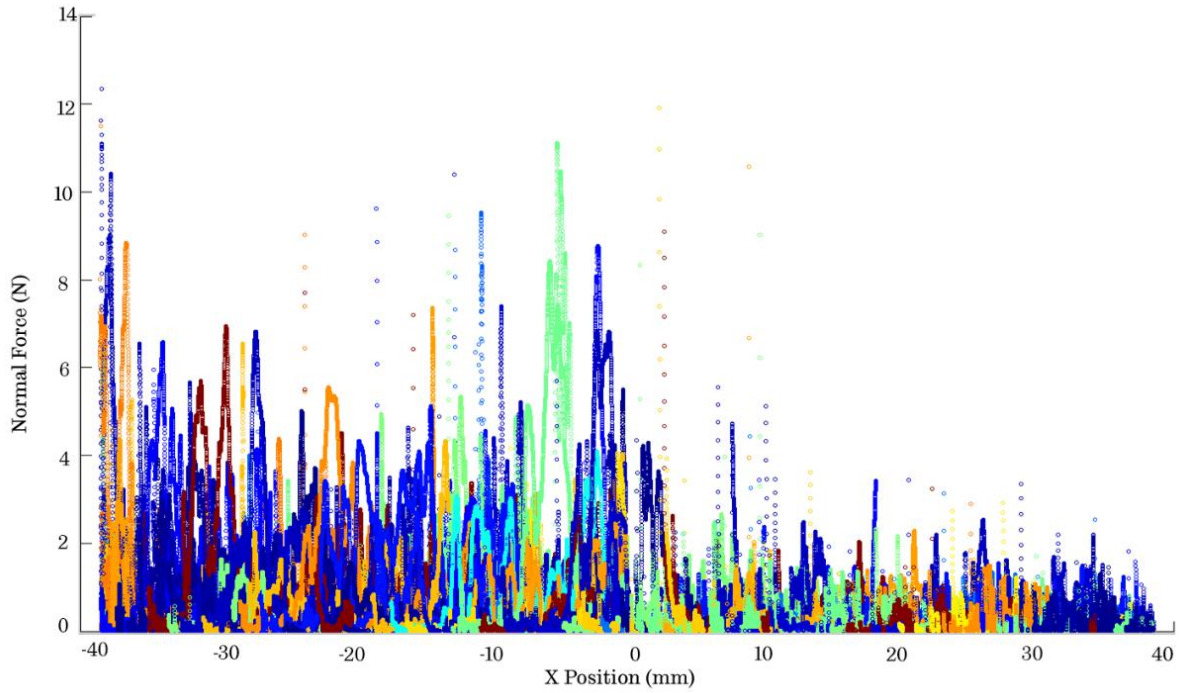

Figure 161 x position vs normal force coloured by different spheres

Figure 161 shows normal force at the position of the contacts. The change in normal force during sliding can be seen in individual spheres. It is also apparent that not only are there more contacts on the leading S1 surface (see also Figure 159), but also the normal force they exert is generally higher than on S2.

8.5.6.2 High Speed

The figures presented here are for the high capacity geometry for a rotational speed of 88 rad/s and should be directly compared to the results presented in section 8.5.6.1.

Figure 162 shows how far each sphere moves before lifting from the surface for longer than the critical time discussed above (compare with Figure 157).

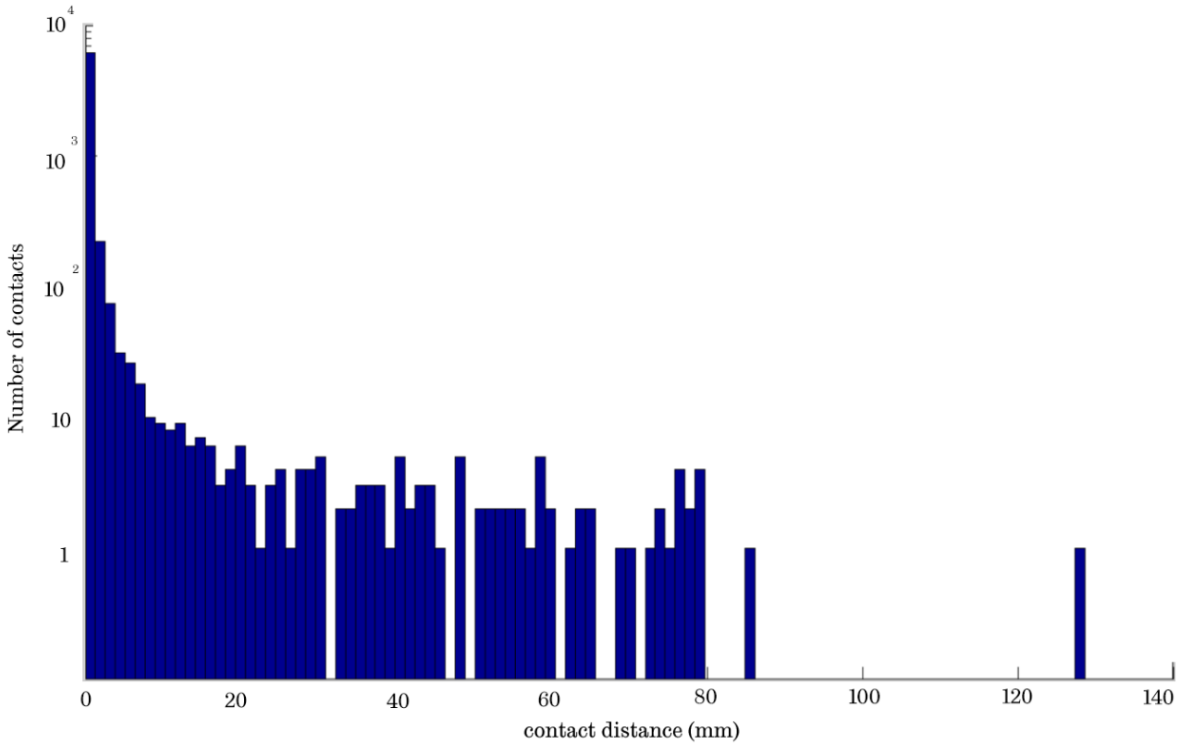

Figure 162 Contact distances along screen for individual contacts. (log Y scale)

Figure 163 shows the contact positions vs time coloured by magnitude of the normal force, to be compared with Figure 158. Here we can see two cam roll passes with uneven section fills.

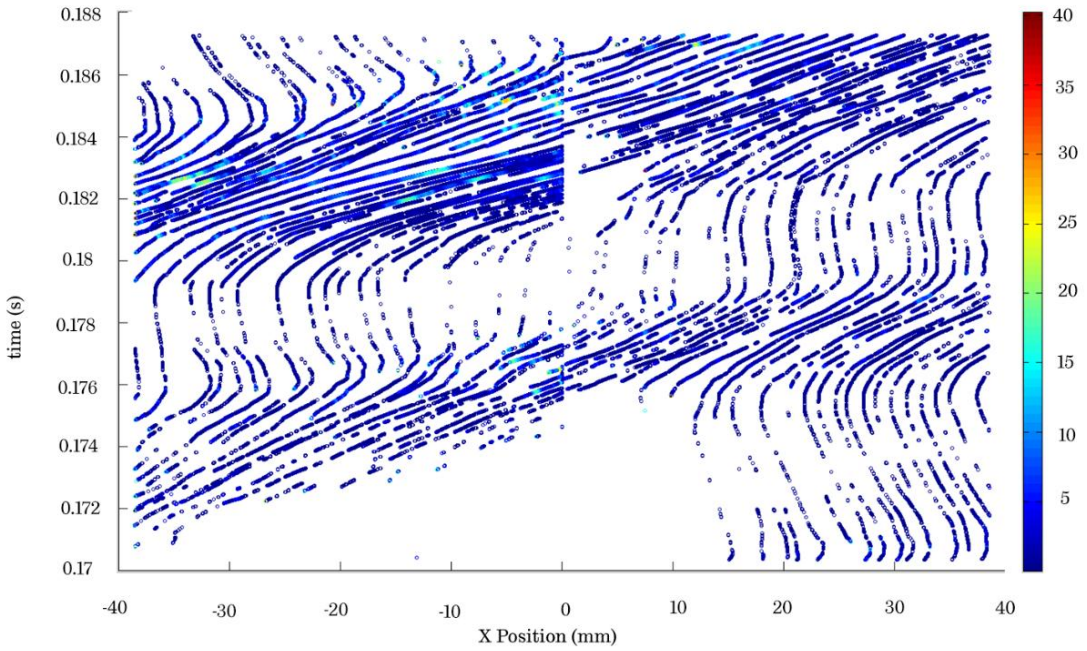

Figure 163 Contact positions coloured by normal force, for rotational speed of 88 rad/s

Figure 164 shows the distribution of contact X position. It shows a similar difference between the number of contacts on the upward facing surface S1 and downward facing S2 to the slow case, Figure 159.

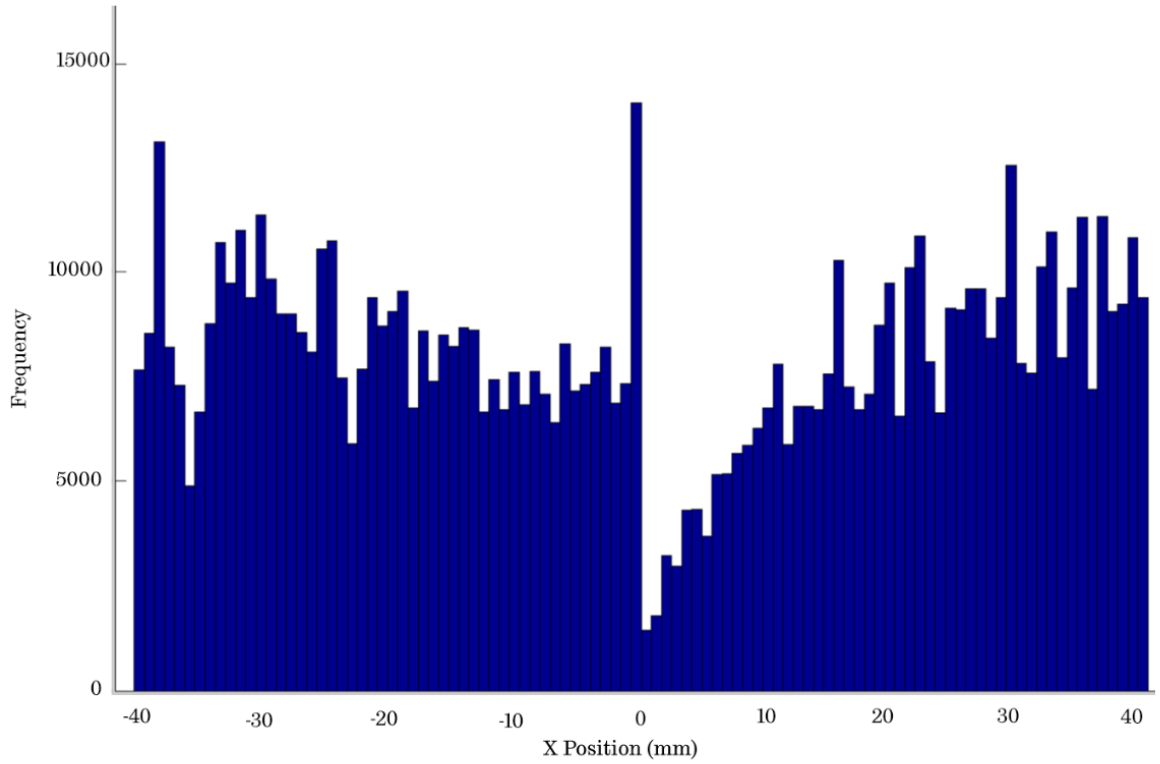

Figure 164 Histogram of the location of the contact positions along the length of surfaces S1 and S2

Figure 165 shows the distribution of normal forces for the contacts.

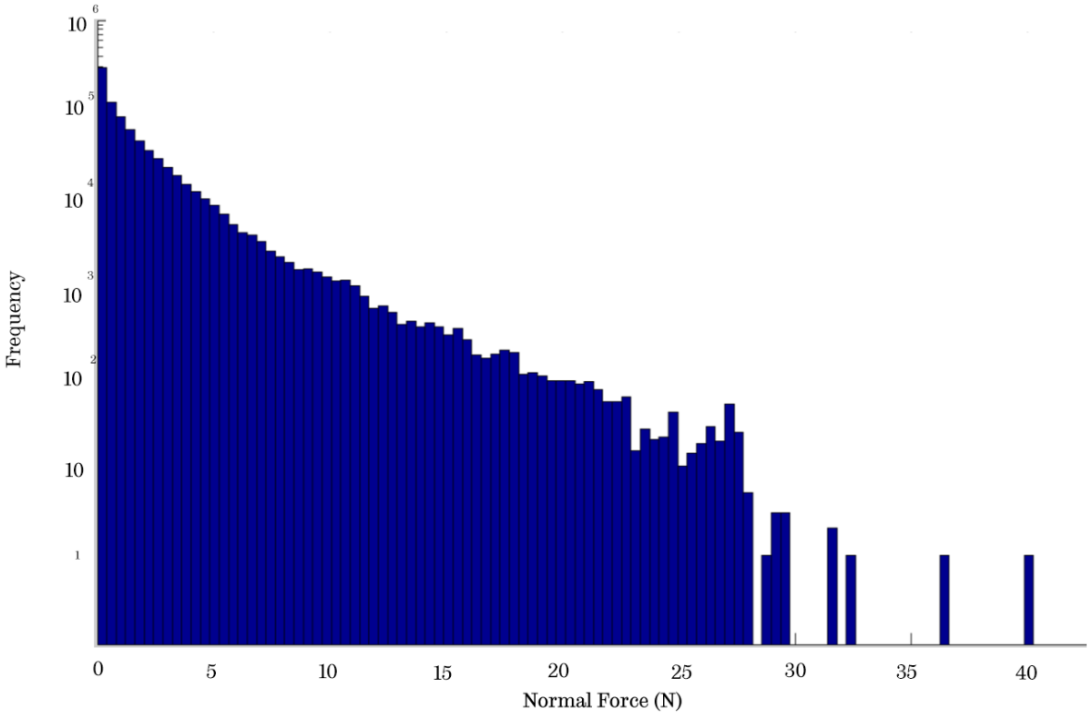

Figure 165 Distribution of contact normal forces, rotation 88 rad/s (log Y scale)

It can be seen that the contact normal forces are between two and four times the results obtained for the low speed run.

Figure 166 shows the normal force with respect to X position.

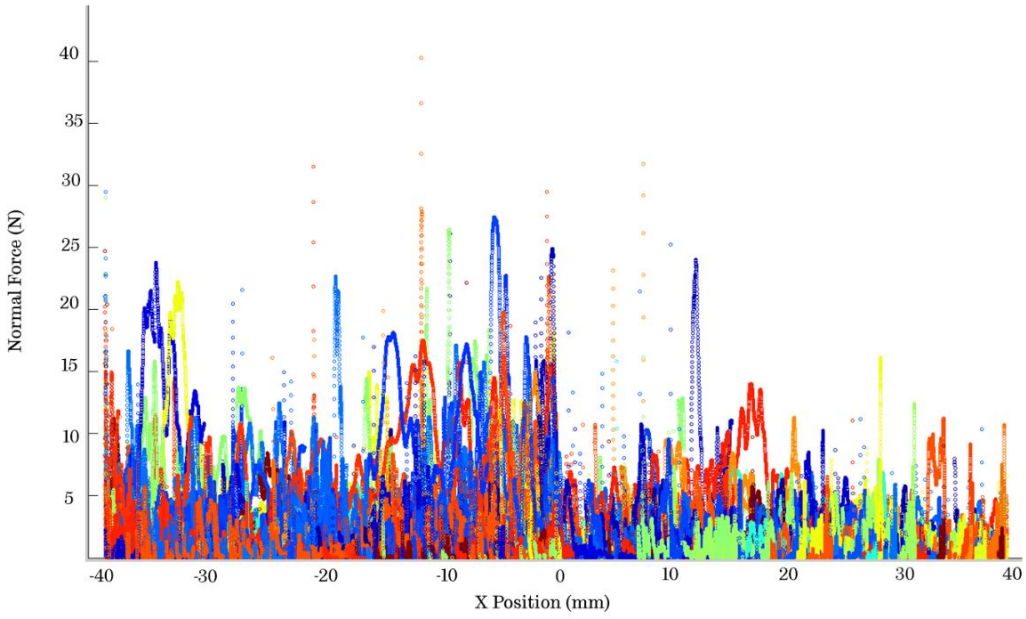

Figure 166 X position vs normal force coloured by different spheres

This result is comparable to the slow run with majority of high normal force impacts occurring on S1, though all forces are seen to be higher (as in Figure 161).

Comparing results for the old and new designs indicates a similar polishing performance for both. The distribution of normal forces is nominally higher at low speeds in the new geometry and comparable at high speed suggesting that the number of broken grains expected from the processing should be similar. One of the most notable differences is that there are a greater number of low distance contacts in the new design due to the shape of the screen. These distances are likely to result in a higher degree of mixing of the grains which could result in improved performance.

8.6 Fast Capture Imaging

Using the same fast capture imaging set up as that used to observe the husking mechanism, the lab polisher has been set up with a clear Perspex end panel in order that the internal rice motion be observed. The previous observations of the polisher screens have revealed how the rice interacts with the polishing chamber walls but not how the rice interacts with itself. Since rice-rice contact is the other aspect of the polishing mechanism, this method was developed as a means of understanding this interaction.
2kg of rice were placed into the chamber and the polisher run up to 750rpm. Some stills at various cam roll positions from the fast capture footage are shown below in Figure 167. Each represents a 45 degree turn from the previous image (top left, top right, bottom left, bottom right)

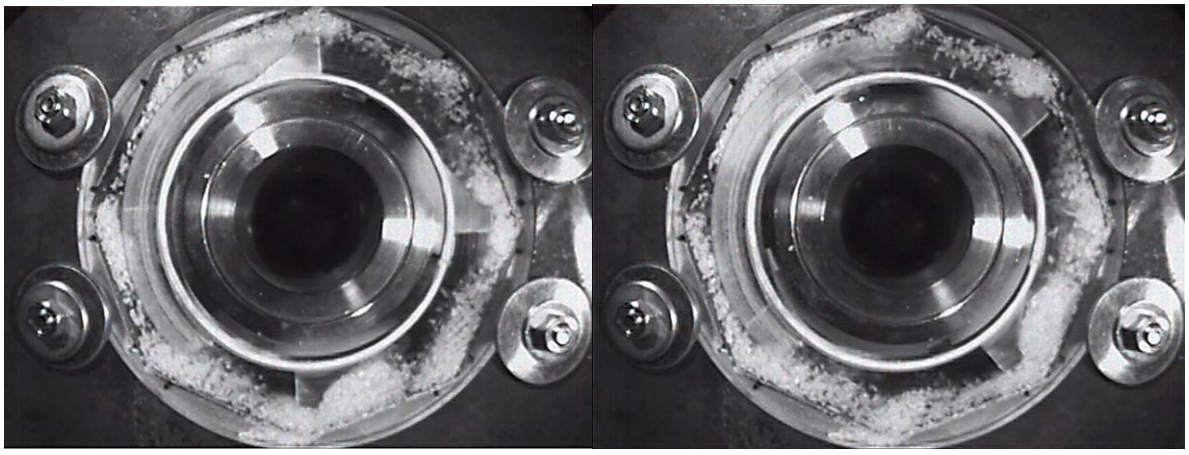

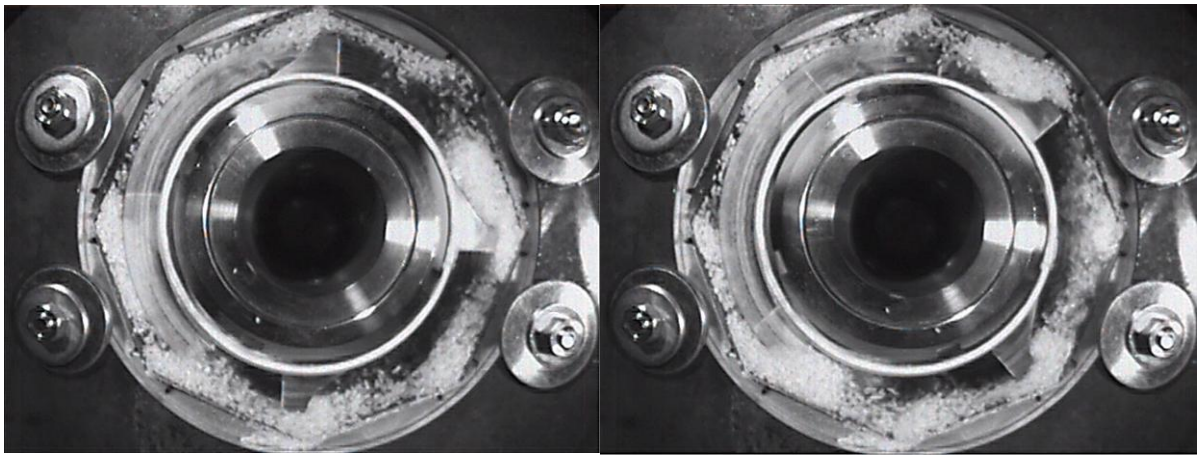

Figure 167 Fast capture stills from lab polisher trials – cam is rotating anti clockwise

The footage shows the grains as they move around the polishing chamber. Individual particles are observable as well as the bulk flow. The fill of the chamber has been revealed to be primarily distributed into two quarters (between cam roll blades). This means that the chamber fill is uneven which could lead to high levels of vibration as the bulk mass is redistributed by rotation.

Grain behaviour in the machine follows a distinct pattern. Where the screen is furthest from the central axis of the machine (i.e. the corners), grains can become trapped leading to an effective boundary layer. At these points, as the cam roll blades pass pushing grains ahead of them, the two bulk layers of grain move against each other. The resulting bran loss at these points will come from a combination of grain-grain impacts and grain-grain sliding abrasion.

Where the screen is closest to the central axis (i.e. the panel centres) the grains tend to slide against the screen wall. The cam blades have the effect of squeezing the grains through resulting in a long contact with the screen wall.

Figure 168 below shows the area of highest wear (just following a screen corner) during a cam blade pass.

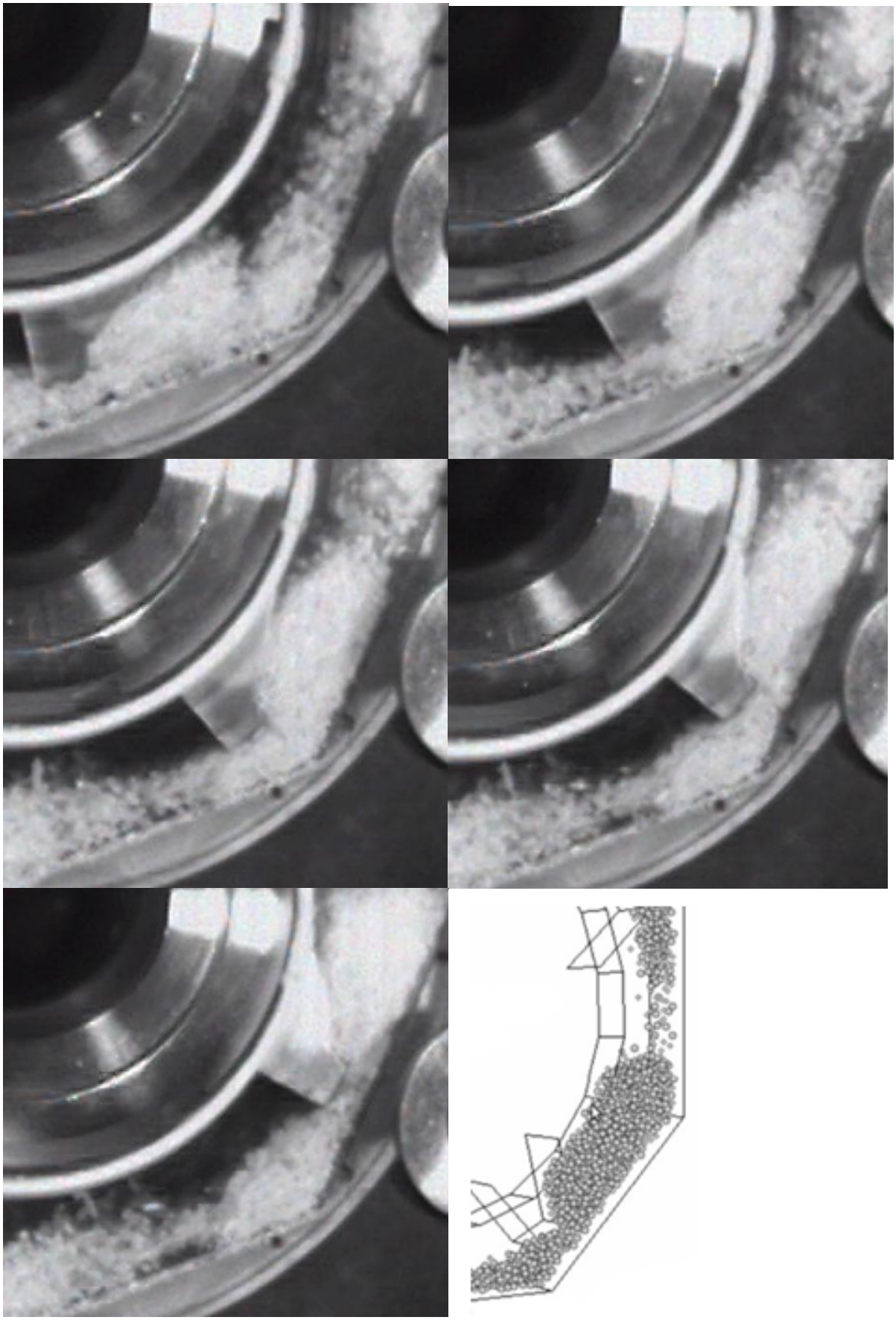

Figure 168 Fast capture stills showing rice progression at screen corners with simulation bottom right for comparison. Cam rotation is anti-clockwise

These images highlight the compression of the grain at various points of the screen. There are two main effects which could lead to the increased wear at the leading screen side. Firstly, the screen shape leads to a convergence and divergence in clearance between the blades and screen wall, leading to increased pressure at the narrowest sections. As the grains are forced towards a convergence (from a corner towards the middle of the screen) grains are likely to interlock (because of their shape) and effectively create a more rigid structure which then interacts with this part of the screen wall. As this begins to diverge (from centre of screen towards corner) the grains are freer to break up resulting in an overall lower pressure against the screen wall.
Secondly, the grains approaching a screen corner have greater freedom to follow the trajectory set by the cam roll and are therefore more likely to travel parallel to the screen. As such, grains travelling towards the screen corners must change direction in order to be carried onwards by the cam roll. This could lead to an increased wear rate by the part of the screen absorbing the momentum of the grains. This is shown schematically below in Figure 169.

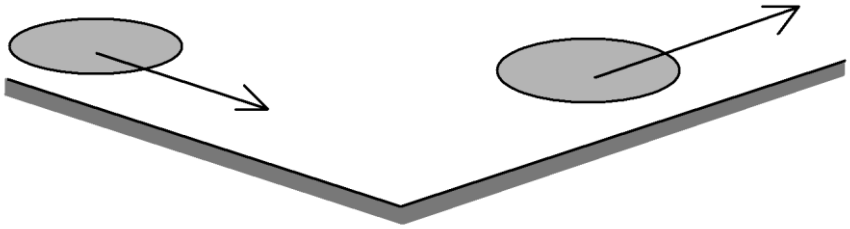

Figure 169 Grain direction of travel before and after screen corners

Whilst these actions ultimately lead to a higher wear rate in certain screen areas, it is likely that these are the same actions responsible for polishing the grains. It may be possible to reduce wear in these areas by screen redesign but polishing performance could well be affected. For instance, removing the screen corners altogether would eliminate the converging-diverging effect but would ultimately reduce performance since grains could not rotate, and bulk boundary layers of grains moving over grains would form less readily.

The fast capture images show a very good correspondence to the simulation data with two notable exceptions. Firstly, the chamber fill is different as the simulated grains are generated randomly leading to an even fill between all four cam roll blades. It is possible that given enough time and passes, the simulation would resemble the fill seen in the fast capture footage, however this would take enormous computing power and simulation time. Secondly, simulating grain shapes are not practical with the current software and so spheres have been used. This negates any grain interlocking meaning that in practise, pressures are likely to be higher than in the simulation.

8.7 Discussion of Polisher Wear

Various aspects of polishing and polisher wear have been observed and analysed. These observations have been made possible, primarily by the use of low throughput and zero throughput (lab) polishers.
Paint tests have revealed the areas of highest and lowest wear. Patterns in the worn region roughly correspond to twice the frequency of the cage support positions indicating either that the rice is entrained by the feedscrew in an uneven manner or that the screen is vibrating at a resonance caused by the cage spacing. Inlet wear has been observed to be more aggressive than further down the polisher. This effect is thought to be caused by the rapid scattering of the grains as they enter the polishing chamber from the feed screw. Inlet guide vanes have been suggested as a solution to this problem as it is thought that they would accelerate the rice more uniformly, potentially resulting in lower vibration magnitude, reduced noise and reduced wear in the inlet region.

Polisher operating pressure at various stages in the polishing chamber is thought to be directly linked to the corresponding wear rate, therefore an understanding of the effective pressure leads to the possibility of predicting wear.
Feed screw fill has been calculated based upon grain bulk densities and geometries. The result is interesting as it shows that the inlet is generally operating at around a 15% fill (corresponding to 7 tonnes/hr). The operators believed this to be much higher (by intuition) since the flow appears to be impeded when operating at high feed rates leading to the conclusion that this resistance is not due to the feed chamber being full but rather the friction and momentum of the grains.
Pressure sensitive paper has been used to determine contact pressure profiles for various stages and conditions in the polishing chamber. The method was first tested in the closed flow lab polisher and then on a full scale machine. The wear profiles and patterns observed suggest that the pressure on the polisher screen is much higher at inlet than outlet (around 20%) and that the leading screen corners have much higher pressure than the trailing corners. Further to this, a process has been developed to determine the effect of increased load (and hence increase in pressure) and the effect on pressure of water misting.

Screen mechanics have been observed and methods developed for monitoring the hardness of the screens and the vibrations during operation. Of the samples tested, the current nitro-carburised screens showed to be the hardest (and hence likely the most resilient to wear). To measure the motion of the screens in operation, a laser vibrometer has been used and three trial grain passes observed. The raw data has then been split up into one second intervals, and a Fourier transform taken which allows the harmonic modes to be seen clearly. By separating into one second intervals it is possible to observe how the fundamental frequencies change during

the course of the test and allows a useful means of comparison of the data. The fundamental frequencies of the cam roll are apparent and from the data it is possible to see changes in screen motion as grains are added, when the loading changes and when the grain flow is stopped.
The vibration of the polisher can cause high levels of noise and suggests an inefficiency in the polishing process. It is also possible that the vibrations in the screen are of a harmonic which creates a node-antinode pattern of vibration which could help explain the uneven wear pattern seen in the paint test.

Simulations have been run using PFC3d software to model the rice grains inside the polisher. Spheres have been used to model the grains whilst boundary conditions have been set in an attempt to both match the real world geometry and reduce computation run time. Two speeds and two geometries of polisher have been modeled in order that the resultant forces could be compared. Euclidean sliding distances were determined for each contact to determine whether the predominant mechanism was sliding or impact. The vast majority of contacts slid less than 1mm in all scenarios and could therefore be considered as impacts. The number of contacts increased dramatically as the fins passed by the wall location and contact normal force increased at the same point as the grains are effectively squeezed between cam roll and wall. The wall locations with the highest normal force are comparable with the wear observed on polisher screens in practice. Distribution of normal force was seen to be the same regardless of speed, however magnitude increased with increasing speed. A proposed future geometry provides a split surface by which impacts occur at two different angles. The distribution of impacts and forces is reflected by this as the grains impact with higher force towards the narrowest gap between cam roll and screen. This indicates that this area of the screen is likely to do more polishing work and hence wear more rapidly than other areas of the screen, particularly the trailing side.
It should be again noted that whilst these results show some useful and interesting aspects of the polishing process; they require good validation with experimental data. However with suitable calibration and some further investigation of the properties of rice/bran, it shows the potential of this method to give increasing insight into the dynamics of rice particles in commercial rice polishers, and the potential to use this method to assist with polisher design.

Fast capture imaging has been used to gather further real world information about grain movements inside the polishing chamber. These images highlight the compression of the grain at various points of the screen. There are two main effects which could lead to the increased wear at the leading screen side, firstly the effective convergence and divergence of the cam roll and screen creating grain compressions at the areas noted to have a higher pressure from the pressure tests. Secondly, the

grains approaching a screen corner have greater freedom of motion allowing them to gain momentum with which they impact the following screen segment, again at the area of higher pressure.
This fast capture footage show a very good correspondence to the motion of the particles when simulated, with the exception of particle fill (as a result of the random generation of simulation particles) and with grain interlocking which is not accounted for in the simulations.

9 CONCLUSIONS

This chapter covers conclusions drawn on the wear of major components in the rice milling process that have been investigated. It covers material properties measured for both grain and machine components, wear observations made, small scale testing and determination of wear mechanisms and other tribological aspects of rice husking and polishing. It then goes on to cover the potential for industrial application of the techniques and findings along with further work which has been opened up as a result of this thesis.

9.1 Measured properties

Initially, various properties of rice grains (paddy, brown and polished) have been measured and observed.

- Grain dimensions
- SEM images
- Mass change during polishing/bulk density
- Grain profiles
- Coefficient of friction
- Grain hardness
- Compressive strength

These properties give a good overview of grains and grain variation. It can be concluded from this data that general observations to cover all grain varieties are very difficult to make. The organic nature of the grains means that even within the same variety, different grains can have substantially different properties.

9.2 Wear observations

Wear characteristics have been observed and compared to known wear mechanisms. Particular attention has been paid to research into other milling operations such as sugar and wheat because of their similarities with rubber roll husking.

Husking roller wear has been observed and categorised. Rollers typically begin to show signs of wear from 10 to 30 tonnes processed depending on how the machine is operated and the variety of grain. The wear is visually typical of erosive wear with pitting leading to material removal.

Polisher wear studies have concentrated on the octagonal mesh screens which are the major replaceable component of the polishing machine. Wear of the screens can lead to catastrophic failure if they then become too weakened to support the pressure of the grains inside. Microscopy has been used to look at the degradation of the slots. Profilometry too has shown the increased wear rate of the slot edges as position moves towards the inlet. Further, the trailing slot edge (by direction of grain flow) experiences a higher wear rate leading to a more rapid surface removal and slot rounding. Scratch angles measured against the machine axis have shown the direction of motion of the grains and how it changes along the length of the machine. The measurements indicate that the motion of the grains becomes more turbulent the further down the polishing chamber. This is most likely an effect of pressure variation down the polisher.

9.3 Small Scale testing

Producing and testing full scale rubber rollers and polishing machines is expensive and time consuming, therefore a series of small scale tests have been developed as a way to identify the mechanisms involved in polishing and husking and associated wear regimes.
Small scale "lab" versions of the husking rollers and polisher have also been used in order that the various mechanisms of husking and polishing be tested in a controlled but more comparable way to the full scale machines than coupon testing allows. Further to this, full sized polishers with a limited feed supply have been used to give real world applicable results.

9.3.1 Small scale husking

Rubber properties have been measured (friction coefficients ranging from 0.5 to 1.8 and modulus ranging from 3.5GPa to 54GPa). Combined with husking tests to determine husked ratio for the various samples, a relationship has been established between shear stress and husked ratio. It has been found that the shear stress required to achieve a given husked ratio is constant (1.9MPa for 80% husked ratio, 1.4MPa for 20% husked ratio). Therefore a harder rubber with the same coefficient of friction as a softer rubber will husk more efficiently. Further, the shear stress to achieve a given husked ratio increases linearly with that desired husked ratio. Limitations to this relationship follow that a maximum point is reached whereby the grains are either engulfed by the rubber or are crushed as the compressive yield is reached. One drawback to using this method is that in husking a single grain at a time, husking sufficient grains to reduce the error caused by grain property variation is very time consuming.
Fast capture camera footage during these husking experiments has been used to show that grains rotate between rubber counterfaces before husking effectively creating a high pressure region at either end of the grain (though on opposing sides).

Fast capture footage has also been used to observe grain motion through the lab husker. It showed that grains maintain their initial contact with the slow roller throughout whilst sliding against the fast roller once husked. This observation has been backed up by inking of grains to measure the contact with the rollers, showing that the contact region of the fast roller is larger than that of the slow roller regardless of separation. It is thought that this is an effect of friction (dynamic and static) and grain acceleration. On initial contact, the grains are accelerated to the speed of the slow roller and thus the contact is governed by static coefficient of friction, whilst the fast roller still rotates past the grain (contact governed by dynamic coefficient of friction). Since the static coefficient is higher than the

dynamic, the grain remains stuck to the slow roller whilst sliding against the fast roller.
Husking efficiency of the lab husker has been determined relative to roller separation and shows that as roller separation decreases, efficiency increases up to a maximum of around 70%. This has been compared to the coupon test using Hertzian contact theory. The results are comparable for larger equivalent separations, however smaller separations show the coupon test to have a higher effective efficiency. This is most likely due to the difference between the two materials and the relative efficiency of a cylindrical roller against a flat coupon.
Since the grains sticking to the slow roller and slipping against the fast roller is thought to cause the uneven wear of the rollers a test was developed to introduce axial movement into the slow roller (so that both rollers operate under dynamic coefficient of friction). A secondary, but not insignificant effect is thought to be that due to the structure of the husk (being in two halves) there is likely to be an orientation of the grain which requires lower energy to break the bond of the husk. By introducing axial movement, grains are allowed to rotate and will husk more freely when oriented to a lower energy fracture. Experiments were carried out and it was found that the introduction of axial vibrations increased husking efficiency for small roller spacings.

9.3.2 Small scale polishing

Polishing mechanisms have been identified and categorised as grain-grain contacts or grain-machine contacts. The grain-machine contacts can be further split into impact and sliding type. These contacts ultimately lead to the deterioration (via various tribological mechanisms) of the polisher screens.

Low throughput wear testing initially revealed the locations of highest wear. This was achieved by painting the screen thinly and evenly, running at capacity for 20 seconds and observing the areas where the paint had been removed. The areas of highest and lowest wear have therefore been observed revealing patterns suggesting an uneven entraining of grains by the feedscrew or a resonance of the screens caused by the cage spacing. High wear was seen at the polisher inlet which is thought to be caused by the rapid scattering of grains as they enter the polishing chamber from the feedscrew. Feedscrew fill has been calculated at 15% (for 7 tonnes/hr flow rate) which is lower than thought intuitively by the operators.
Pressure sensitive paper has been used to determine contact pressure profiles for various stages and conditions in the polishing chamber. The wear profiles and patterns observed suggest that the pressure on the polisher screen is much higher at inlet than outlet (around 20%) and that the leading screen corners have much higher pressure than the trailing corners. Further to this, a process has been developed to

determine the effect of increased load (and hence increase in pressure) and the effect on pressure of water misting.
A laser vibrometer has been used to observe vibrations in the screens during operation. The raw data has then been split up into one second intervals, and a Fourier transform taken which allows the harmonic modes to be seen clearly. By separating into one second intervals it is possible to observe how the fundamental frequencies change during the course of the test and allows a useful means of comparison of the data. The fundamental frequencies of the cam roll are apparent and from the data it is possible to see changes in screen motion as grains are added, when the loading changes and when the grain flow is stopped.
The vibration of the polisher can cause high levels of noise and suggests an inefficiency in the polishing process. It is also possible that the vibrations in the screen are of a harmonic which creates a node-antinode pattern of vibration which could help explain the uneven wear pattern seen in the paint test.

PFC3d software has been used to simulate grain flow around the polishing chamber. Two speeds (40.8rad/s and 88rad/s) and two geometries have been modelled in order that resultant forces can be compared. Further, Euclidean sliding distances were determined for each contact.
The number of contacts increased dramatically as the fins passed by the wall location and normal force increased as grains were effectively squeezed between the fin and the screen wall. The wall locations with the highest normal force are comparable with the wear observed on polisher screens in practice. Distribution of normal force was seen to be the same regardless of speed, however magnitude increased with increasing speed.

Fast capture imaging of the grain motion in the polisher has revealed that there are two main effects which could lead to increased screen wear. The grains are converged by the cam roll creating a highly compressive effect at the areas noted to have a higher pressure from the pressure tests. Grains also have a greater freedom of motion close to screen corners allowing them to gain momentum with which they impact the proceeding screen segment. This too corresponds to the areas of higher pressure. The fast capture footage gives a good correspondence with the motion of the particles in the simulations.

9.4 Industrial Implementation

Whilst this thesis has concentrated on the fundamental understanding of wear processes during rice milling, various aspects can be readily adopted as tools for the machine design process. These tools include pressure sensitive paper as a method for determining polisher pressure, particle simulations to predict grain motion, the

use of a laser vibrometer to monitor machine vibration and fast capture imaging to observe particle movement.

Both husker rubber and polisher screen material properties have been studied in detail. In both cases, harder materials have been found to be more appropriate for practical purposes. For husking rubbers, it has been found that harder samples and samples with higher coefficient of friction perform more efficiently. Whilst no limit has been found, it is likely that rubber samples which are too hard will result in a higher percentage of broken grains. Further to increases in efficiency, the use of harder rubbers is likely to improve the wear life of the rollers.
For polisher screens, surface treatments can result in a dramatically improved wear life. Whilst a small selection have been tested, the methods used (micro hardness and profilometry/microscopy of worn screens) could be implemented for other materials/surface treatments.

Inlet guide vanes have been suggested as a solution to the uneven filling of the polishing chamber. It is thought that this could result in decreased machine vibration and a reduced inlet wear.

Axial vibrations have shown in small scale experiments to improve husking efficiency. With further testing this could potentially be used in practise to improve the husked ratio, lower the energy requirements of husking and improve roller wear life. It may also be effective at improving the even-ness of the roller wear, potentially allowing a wider roller (hence improving machine capacity).

9.5 Further Work

The major requirement further to this thesis is the need to observe the behaviour of other varieties of rice. It is known that performance and wear are affected by variety throughout the milling process. Whilst it would have been impractical to study multiple varieties for this thesis, in order to extend the reach of the findings it would be necessary to note the effects of grain properties on wear and performance. This would require a test matrix of comparable grain properties such as grain size, grain shape, hardness etc.

The rubber properties required to increase husked ratio have been determined. It would be useful to take this a stage further and produce rubber samples to this specification and run the same coupon test to confirm the findings.
Whilst polishing actions have been discussed in detail, Satake[3] states some unsubstantiated figures on speeds at which polishing action changes. A detailed study of these actions in a precise and controlled way (rather than in a single polisher) may reveal further information on the tribology of polishing.

Further studies on the effect of water misting are required for confirmation of pressure change. Following the procedure set out for determining pressure using pressure sensitive paper and altering water misting level should be sufficient to monitor the changes in pressure profile. It would also be useful to conduct a microscopic analysis of the polisher screen surface treatments to identify the stress distribution occurring from grain impacts. This would help to determine the effectiveness of the surface treatment and whether the thickness is sufficient for the stresses involved.

Further studies are required on the effect of roller axial vibration on husking efficiency. Whilst the initial results are promising, further work is required to confirm the findings and to implement industrial trials.

Whilst it is difficult to access full scale machines due to the required throughput, ultimately any design changes based on the research above need to be observed in a real world situation before being put into service.

10 REFERENCES

[1] E. T. Champagne, *Rice: chemistry and technology*, 3rd ed. American Association of Cereal Chemists Inc, 2004.

[2] B. S. Luh, *Rice: Utilization*, 2nd ed. 1991.

[3] T. Satake, *Modern Rice Milling Technology*. Tokyo: Tokyo Press, 1990, pp. 40–46.

[4] Intergovernmental Group on Rice, *Recommended Model Grading System for Rice in International Trade*. 1972, pp. 1–13.

[5] K. Esau, *Anatomy of Seed Plants*, 2nd ed. 1977.

[6] F. Garibaldi, *Rice Milling Equipment Operation and Maintenance*. Rome, 1981.

[7] World Bank, "World Development Indicators," 2011. [Online]. Available: http://data.worldbank.org/data-catalog/world-development-indicators?cid=GPD_WDI. [Accessed: 18-Apr-2012].

[8] International Rice Research Institute, "Rice Production and Processing," 2009. [Online]. Available: http://irri.org/about-rice/rice-facts/rice-production-and-processing. [Accessed: 18-Apr-2012].

[9] IRRI, "How many rice varieties are there?," 2006. [Online]. Available: http://irri.org/index.php?option=com_k2&view=item&id=10341:how-many-rice-varieties-are-there?&lang=en. [Accessed: 04-Feb-2013].

[10] IRRI, "The International Rice Genebank - conserving rice." [Online]. Available: http://irri.org/index.php?option=com_k2&view=item&id=9960&lang=en. [Accessed: 04-Feb-2013].

[11] DHM Rice Mill, "Paddy To Rice." [Online]. Available: http://dhmricemill.com/?Process.html. [Accessed: 11-Nov-2013].

[12] M. Gummert, J. Rickman, and M. Bell, "Paddy Drying Systems," 2004.

[13] S. N. Rhaghavendra Rao and B. O. Juliano, "Effect of Parboiling on Some Physicochemical Properties of Rice," *J. Agric. Food Chem.*, vol. 18, no. 2, pp. 289–294, 1970.

[14] A. K. Miah, A. Haque, P. Douglass, and B. Clarke, "Parboiling of Rice Part 1: Effect of Hot Soaking Time on Quality of Milled Rice," *Int. J. Food Sci. Technol.*, vol. 37, no. 5, pp. 527–537, 2002.

[15] A. B. Chhetri and M. Rafiqul Islam, *Inherently Sustainable Technology Developments*. 2008, pp. 257–258.

[16] T. Massumoto, “Impact Rice Huller,” 48008101987.

[17] K. Takekura, S. Kawamura, and K. Ito, “Influence of Difference in Hulling Systems on Quality of Brown Rice after Storage,” *J. Japanese Soc. Agric. Mach.*, vol. 66, no. 3, pp. 51–58, 2004.

[18] Buhler Sortex, “Tophusk Huller and Separator.” [Online]. Available: http://www.maxtex.net/products/rc/tophusk/DRHC-DRSC 6 Pgs Eng.pdf. [Accessed: 21-Dec-2012].

[19] A. J. H. Latham, “From Competition to Constraint : The International Rice Trade in the Nineteenth and Twentieth Centuries,” *Business*, no. c, pp. 91–102, 1988.

[20] Buhler Sortex, “Highpoly Polisher DRPF.” [Online]. Available: http://ricemill.net/sites/default/files/brochures/DRPF_en.pdf. [Accessed: 22-Dec-2012].

[21] Kett, “Instant rice whiteness tester.” [Online]. Available: http://www.kett.com/files/brc600.pdf. [Accessed: 04-Feb-2013].

[22] D. Pye, *Practical Nitriding and Ferritic Nitrocarburizing*. 2003, pp. 1–11.

[23] L.-H. Chiu, W. Chang-Hui, and C. Heng, “Wear behavior of nitrocarburized JIS SKD61 tool steel,” *Wear*, vol. 253, no. 7–8, pp. 778–786, 2002.

[24] Buhler Sortex, “TopWhite II Whitener.” [Online]. Available: http://www.buhlergroup.com/northamerica/downloads/BSPB_TopWhite_Whitener_RC28004_en.pdf. [Accessed: 21-Dec-2012].

[25] Tribology.co.uk, “Gear Failures.” [Online]. Available: http://www.tribology.co.uk/services/investigate/g08-0.htm. [Accessed: 01-Feb-2013].

[26] Wear-Management, “Wear Mechanisms.” [Online]. Available: http://www.wear-management.ch/?path=root+coatings&lang=en. [Accessed: 01-Feb-2013].

[27] E. Brakes, “Surface crazing or cracking on brake discs.” [Online]. Available: http://www.ebcbrakes.com/ebc_brakes_technical_articles/car_brake_technical_articles/surface_crazing_or_cracking_on_brake_discs.shtml. [Accessed: 01-Feb-2013].

[28] NSK, “Wear.” [Online]. Available: http://www.nskamericas.com/cps/rde/xchg/na_en/hs.xsl/wear.html. [Accessed: 01-Feb-2013].

[29] Neale Consulting Engineering, “Plain Bearing Failure.” [Online]. Available: http://www.tribology.co.uk/services/investigate/pb02-2.htm. [Accessed: 01-Feb-2013].

[30] I. M. Hutchings, *Tribology: Friction and Wear of Engineering Materials*. London: Edward Arnold, 1992.

[31] OilCheck, “Delamination Wear.” [Online]. Available: http://www.oilcheck.com.au/Tutorial/17_delamination_wear.htm. [Accessed: 12-Nov-2013].

[32] cat.com, “Reusability of Drive Train Gears:Abnormal Wear.” [Online]. Available: http://catreuseguidelines.blogspot.co.uk/2012/12/reusability-of-drive-train_616.html. [Accessed: 05-Feb-2013].

[33] J. Duran, *Sands, powders and grains - an introduction to the physics of granular materials*. 2012.

[34] W. Losert, “Granular Materials,” *Encyclopedia of non-linear science*. pp. 381–383, 2004.

[35] H. P. Zhu, Z. Y. Zhou, R. Y. Yang, and A. B. Yu, “Discrete particle simulation of particulate systems: Theoretical developments,” *Chem. Eng. Sci.*, vol. 62, no. 13, pp. 3378–3396, 2007.

[36] Plasma Coatings, “Pump Repair.” [Online]. Available: http://www.plasmacoatings.com/pumprepair.html. [Accessed: 01-Feb-2013].

[37] M. S. Eltobgy, E. Ng, and M. A. Elbastawi, “Finite element modelling of erosive wear,” *Int. J. Mach. Tools Manuf.*, vol. 45, no. 11, pp. 1337–1346, 2005.

[38] I. Finnie, “Some observations on the erosion of ductile metals,” *Wear*, vol. 19, no. 1, pp. 81–90, 1972.

[39] D. Tabor, “Mohs’s Hardness Scale - A Physical Interpretation,” *Proc. Phys. Soc.*, vol. 67, no. 3, p. 249, 1954.

[40] A. Misra and I. Finnie, “On the Size Effect in Abrasive and Erosive Wear,” *Wear*, vol. 65, no. 3, 1981.

[41] J. J. Coronado, “Effect of Abrasive Size on Wear,” in in *Abrasion Resistance of Materials*, 2012, pp. 167–182.

[42] E. Rabinowicz and A. Mutis, “Effect of abrasive particle size on wear,” *Wear*, vol. 8, no. 5, pp. 381–390, 1965.

[43] I. Finnie, “Some reflections on the past and future of erosion,” *Wear*, vol. 186–187, pp. 1–10, 1995.

[44] I. Finnie, “Erosion of surfaces by solid particles,” *Wear*, vol. 3, no. 2, pp. 87–103, 1960.

[45] M. Buijs, “Erosion of glass as modelled by indentation theory,” *Commun. Am. Soc.*, vol. 77, no. 6, 1976.

[46] S. Ogawa, A. Umemura, N. Oshima, and I. Physics, “On the Equations of Fully Fluidized Granular Materials,” *J. Appl. Math.*, vol. 31, 1980.

[47] H. H. Shen and N. L. Ackermann, “Constitutive Relationships for Fluid-Solid Mixtures,” *J. Eng. Mech.*, vol. 108, no. 5, 1982.

[48] S. B. Savage and D. J. Jeffrey, “The stress tensor in a granular flow at high shear rates,” *J. Fluid Mech.*, vol. 110, no. -1, pp. 255–272, 1981.

[49] J. T. Jenkins and S. B. Savage, “A theory for the rapid flow of identical, smooth, nearly elastic, spherical particles,” *J. Fluid Mech.*, vol. 130, no. MAY, pp. 187–202, 1983.

[50] S. Chapman and T. G. Cowling, *The Mathematical Theory of Non-Uniform Gases*. Cambridge University Press, 1970, p. 448.

[51] C. K. K. Lun, S. B. Savage, D. J. Jeffrey, and N. Chepurniy, “Kinetic theories for granular flow: inelastic particles in Couette flow and slightly inelastic particles in a general flowfield,” *J. Fluid Mech.*, vol. 140, no. -1, pp. 223–256, 1984.

[52] National Center for Earth-surface Dynamics, “A History of Saint Anthony Falls.” [Online]. Available: http://www.geo.umn.edu/courses/1001/1001_kirkby/SAFL/WEBSITEPAGES/6.html. [Accessed: 07-Feb-2013].

[53] B. F. Yousif, T. A. Jensen, and J. M. Al-Sandooq, “Tribological Loading in Roller Mill Machine,” *Proc. ASME 2011 Int. Mech. Eng. Congr. Expo.*, 2011.

[54] Q. Luo and J. Xie, “Investigation of the wear failure mechanism of a flour milling roller,” *Wear*, vol. 161, pp. 11–16, 1993.

[55] K. Ping Zhang, J. Long Huang, and J. Feng Wu, “Experiment of Gray Iron Abrasive Wear for Wheat Grain Powder,” *Adv. Mater. Res.*, vol. 328–330, pp. 1228–1231, 2011.

[56] L. C. Seabra and A. M. Baptista, “Tribological behaviour of food grade polymers against stainless steel in dry sliding and with sugar,” *Wear*, vol. 253, no. 3–4, pp. 394–402, Aug. 2002.

[57] F. Casanova and Y. Aguilar, “A study on the wear of sugar cane rolls,” *Wear*, vol. 265, no. 1–2, pp. 236–243, 2008.

[58] A. Mehta and G. C. Barker, “The Dynamics of Sand,” *Reports Prog. Phys.*, vol. 57, no. 4, p. 383, 1994.

[59] H. Kibar, T. Ozturk, and B. Esen, “The effect of moisture content on physical and mechanical properties of rice,” *Spanish J. Agric. Res.*, vol. 8, no. 3, pp. 741–749, 2010.

[60] Q. Qu, S. C. Negi, and J. J. C, “Storage of cohesive material in silos - Part 2: Parametic study,” *Power Handl. Process.*, vol. 13, pp. 27–30, 2001.

[61] C. Heirloom, “Heirloomrice’s Blog,” 2012. [Online]. Available: http://heirloomrice.wordpress.com/page/2/. [Accessed: 22-Mar-2013].

[62] D. Shitanda, Y. Nishiyana, and K. S, “Husking Characteristics of Short and Long Grain Rice by Rubber Roll Husker (Part 1),” *J. Japanese Soc. Agric. Mach.*, vol. 63, no. 1, pp. 55–63, 2001.

[63] G. Brandt, “Flank and crater wear mechanisms of Alumina-based cutting tools when machining steel,” *Wear*, vol. 112, pp. 39–56, 1986.

[64] G. Bocco, “Gully Erosion: Processes and Models,” *Prog. Phys. Geogr.*, vol. 15, no. 4, pp. 392–406, 1991.

[65] Materials Engineering Research Laboratory Ltd, “Rubber Selection - A Guide to Outline Properties.” [Online]. Available: www.merl-ltd.co.uk/2003_materials/rubber12.shtml. [Accessed: 27-Jul-2009].

[66] D. Shitanda, “Compressive strength properties of rough rice considering variation of contact area,” *J. Food Eng.*, vol. 53, pp. 53–58, 2002.

[67] G. Kamst, C. Bonazzi, J. Vasseur, and J. Bimbenet, “Effect of deformation rate and moisture content on the mechanical properties of rice grains,” *Trans. Am. Soc. Agric. Eng.*, vol. 45, no. 1, pp. 145–152, 2002.

[68] T. E. Toolbox, “Poisson’s Ratio: The Engineering Toolbox.” [Online]. Available: http://www.engineeringtoolbox.com/poissons-ratio-d_1224.html. [Accessed: 27-Jul-2009].

[69] K. L. Johnson, *Contact Mechanics*. Cambridge: Cambridge University Press, 2008, pp. 427–428.

[70] D. Shitanda and Y. Nishiyama, “Performance Analysis of Impeller and Rubber Roll Husker Using Different Varieties of Rice,” *CIGR J. Sci. Res. Dev.*, vol. 3, no. 1, pp. 195–203, 2001.

[71] AJP Automotive, “Pressure Sensitive Paper Applications.” [Online]. Available: http://www.ajpautomotive.co.uk/html/applications.html. [Accessed: 28-Dec-2012].

[72] AJP Automotive, “Pressure Sensitive Paper.” [Online]. Available: http://www.ajpautomotive.co.uk/html/product_spec.html. [Accessed: 28-Dec-2012].

[73] H. Konietzky, *Numerical modelling in micromechanics via particle methods*. 2003, pp. 1 – 56.

[74] P. A. Langston, U. Tuzun, and D. M. Heyes, “Discrete element simulation of granular flow in 2D and 3D hoppers: Dependence of discharge rate and wall stress on particle interactions,” *Chem. Eng. Sci.*, vol. 50, pp. 967–987, 1995.

[75] J. R. L. Camacho, “A Study of Erosion and Abrasion Wear Processes caused during Food Processing,” The University of Sheffield, 2009.